Impacts of vegetation on climate and the global water and carbon cycles

Claire M. Zarakas

A dissertation
submitted in partial fulfillment of the
requirements for the degree of

Doctor of Philosophy

University of Washington

2024

Reading Committee:

Abigail L. S. Swann, Chair

David S. Battisti

Cecilia Bitz

Program Authorized to Offer Degree:
Atmospheric Sciences

University of Washington

Abstract

Impacts of vegetation on climate and
the global water and carbon cycles

Claire M. Zarakas

Chair of the Supervisory Committee:
Abigail L. S. Swann
Department of Atmospheric Sciences, Department of Biology

It is widely recognized that climate influences the terrestrial water and carbon cycles, but land processes also exert a strong control on climate by modifying land-to-atmosphere fluxes of water, energy, and momentum. This dissertation focuses on feedbacks between vegetation, climate, and the global water and carbon cycles through a series of modeling studies that address how climate impacts vegetation (Chapter 2), how land parameter uncertainty impacts climate (Chapter 3), and how atmospheric feedbacks modulate changes in land processes (Chapter 4).

Chapter 1 introduces previous work in biosphere-atmosphere interactions, and outlines key outstanding questions in this area of research.

Chapter 2 focuses on how climate influences vegetation, disentangling how different atmospheric drivers contribute to observed declines in tropical forest photosynthesis under high temperatures. It is challenging to disentangle the impact of direct temperature effects vs. vapor pressure deficit (VPD) effects on vegetation because these quantities are tightly correlated. I use two terrestrial biosphere models and observational data to show that plant hydraulics and photosynthetic temperature acclimation govern the strength of temperature and VPD effects. This work identifies a novel source of compensating errors in models – models can match the observed apparent ecosystem-level photosynthesis response to temperature by excluding plant hydraulics and photosynthetic temperature acclimation (which yields stronger direct temperature effects) or by including both processes (which yields stronger VPD effects). However, these two sets of assumptions yield divergent predic-

tions of ecosystem resilience to warming, underscoring the importance of accurately representing these processes in models.

Chapter 3 focuses on the impact of land processes on climate, by evaluating the impact of land parameter uncertainty in a coupled Earth system model. Prior research has demonstrated that uncertainty in the representation of land processes drives uncertainty in land surface water, energy, and carbon fluxes. However, the influence of land process uncertainty on the climate system remains underexplored. I run an ensemble of simulations where I perturb 18 parameters governing land processes in a coupled Earth system model. Using this perturbed parameter ensemble (PPE), I demonstrate that land parameters generate biogeophysical feedbacks that substantially impact mean temperature and precipitation, primarily through parameters' influence on evapotranspiration. Notably, the spatial patterns of parameter-driven changes in precipitation and temperature differ from those due to radiatively-driven warming. My analysis demonstrates that land parameter uncertainty propagates to the entire Earth system, highlighting an underappreciated impact of land processes in determining the mean climate state and providing insights into where and how land process uncertainty influences climate.

Chapter 4 analyzes land-atmosphere interactions, quantifying how land-driven climate changes feed back on the global water and carbon cycles. I isolate the impact of atmospheric feedbacks by comparing the coupled PPE with a paired land-only PPE in which the atmosphere does not respond to changes in land surface properties. I find that atmospheric feedbacks dampen land-driven hydrologic changes in climatologically wet regions, but amplify hydrologic changes in some climatologically dry regions. I also identify several hot spots where atmospheric feedbacks have a regionally significant impact on photosynthesis. This analysis provides insights into where and how atmospheric feedbacks modulate terrestrial processes, posing a challenge to the widespread practice of developing and evaluating land models in an uncoupled configuration and then deploying them to understand and predict terrestrial processes in a coupled context.

Chapter 5 presents a discussion of the implications of the results in Chapters 2-4 as well as plans for future research.

TABLE OF CONTENTS

LIST OF FIGURES

ACKNOWLEDGMENTS

This research was made possible by countless mentors, colleagues, friends, and family who supported me throughout my PhD. I would like to thank my advisor, Abby Swann, for her exceptional mentorship, advising, and support. Thank you for being so generous with your time and ideas, for advocating for me, for always giving me a renewed enthusiasm for science during our meetings, and for being a role model of how to be an interdisciplinary scientist and compassionate mentor.

I also appreciate the guidance from my committee members – David Battisti, Cecilia Bitz, Alex Turner, Brian Harvey, and Rebecca Neumann – thank you for helpful discussions and feedback related to my graduate research. I feel incredibly lucky to have also collaborated with many scientists outside of the University of Washington throughout graduate school. Thank you to Charlie Koven, Jim Randerson, Gordon Bonan, Daniel Kennedy, Katie Dagon, Dave Lawrence, Marielle Smith, Tyeen Taylor, Danica Lombardozzi, Chris Still, and Gabe Kooperman, among others, for being great scientific collaborators as well as amazing mentors and advocates. And thank you to the NCAR Terrestrial Sciences Section and the broader land model and biogeochemistry working groups for being so welcoming and supportive throughout my PhD.

The department of Atmospheric Sciences and the Ecoclimate lab have also been welcoming and fun communities, with a truly collaborative research culture. Thank you to the many friends and colleagues who have worked to cultivate this culture, including my graduate student cohort and all of the Ecoclimate lab members (past and present) who I have overlapped with at UW. A special thanks to Greta Shum for going through every step of the graduate program with me - I could not have done this without you. I also want to thank my friends from outside of graduate school for supporting me throughout the ups and downs of graduate school. I particularly want to thank my housemate Lizzy for being an endless source of emotional support and solidarity throughout this whole adventure.

And finally, thank you to my family for their love and support. Thank you to my parents for

always supporting me and encouraging me to chart my own path. And thank you to my husband Doug for being my partner in this PhD journey and in life, going back to my first research project over ten years ago. Thank you for believing in me, for cooking me so many delicious meals, and for being my biggest supporter and cheerleader throughout it all.

Chapter 1

INTRODUCTION

It is widely recognized that climate influences terrestrial water and carbon cycles, but land processes also exert a strong control on climate by modifying land-to-atmosphere fluxes of water, energy, and carbon. This dissertation draws from perspectives in both atmospheric sciences and terrestrial biology to understand interactions between vegetation, climate, and the global water and carbon cycles.

1.1 Background on ecological climatology

Atmospheric CO_2 concentrations directly influence vegetation, and vegetation also influences atmospheric CO_2 concentrations by exchanging CO_2 with the atmosphere. Land's influence on the chemical composition of the atmosphere is referred to as land's biogeochemical effect on climate. Vegetation's influence on atmospheric CO_2 concentration is particularly critical for projecting future climate. Only about half of anthropogenic CO_2 emissions remain in the atmosphere - the land takes up about 31% of anthropogenic emissions and the ocean takes up about 23% (Friedlingstein et al. 2020). Comparing future emissions pathways to the past century, most CMIP6 Earth system models qualitatively project that terrestrial ecosystems will take up more carbon in absolute terms but that land will take up a smaller fraction of CO_2 emissions, leading to a larger airborne fraction of emissions (IPCC AR6). However, these projections are highly uncertain, reflecting uncertainties in both terrestrial ecosystems' response to increasing atmospheric CO_2 concentration (i.e., the carbon-concentration feedback) and ecosystems' response to increasing temperature (i.e., the carbon-climate feedback). Most Earth system models indicate that the carbon-concentration feedback is positive and the carbon-climate feedback is negative, but there is a large spread in the strength of these feedbacks across models (Arora et al. 2020, Friedlingstein et al. 2013, Friedlingstein et al. 2006). It is challenging to quantify the strength of these feedbacks because they emerge from the interaction of diverse terrestrial processes operating at multiple scales.

In the same way that vegetation both influences and is influenced by atmospheric CO_2 concentrations, vegetation also influences and is influenced by the water cycle. Plant transpiration constitutes about 60% of the total flux of water from the land to the atmosphere (Lian et al., 2018), so changes in vegetation cover, plant traits, or plant functioning can therefore substantially impact the overall flux of water from the land to the atmosphere, which propagates to influence other parts of the land water cycle.

The land-to-atmosphere water flux also impacts climate, because evapotranspiration (ET) is a key component of the surface energy budget which controls surface temperature. Changing evapotranspiration directly impacts land surface temperature due to evaporative cooling, and can further influence climate by driving atmospheric responses in precipitation (Kooperman et al., 2018; Saint-Lu et al., 2019) and cloud cover (Park et al., 2021; Zarakas et al., 2020). Land-atmosphere exchanges of energy and water are fundamentally governed by the surface energy budget, which requires that the net radiation absorbed at the surface (R_{net}) is balanced by the sum of the sensible heat flux (H), latent heat flux (λET) and ground storage (G, which is negligible over long timescales, but substantial on seasonal timescales), i.e., energy is conserved:

$$R_{net} = SW_{\downarrow} - SW_{\uparrow} + LW{\downarrow} - + LW{\uparrow} = H + \lambda ET + G \tag{1.1}$$

where $SW_{\downarrow}$ and $SW_{\uparrow}$ are downwelling and upwelling shortwave radiation, and $LW{\downarrow}$ and $LW{\uparrow}$ are downwelling and upwelling longwave radiation. Land processes can modify these land-atmosphere fluxes of energy and water, thereby influencing climate; this is referred to as land's biogeophysical effect on climate. Changes in the land surface can drive biogeophysical feedbacks by changing the land surface evaporative resistance, as well as by changing the land albedo, and the roughness of the land surface which influences the turbulent fluxes of sensible and latent heat.

Land therefore plays a critical role in the Earth's carbon, water, and energy cycles, and understanding the mechanisms through which land impacts climate is critical for understanding how the Earth works and how it will respond to anthropogenic change.

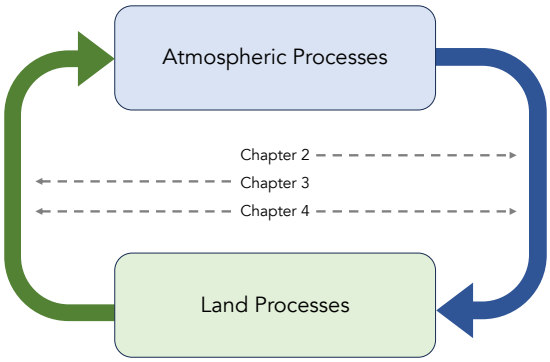

Figure 1.1: Schematic diagram of land-atmosphere interactions.

1.2 Outline of this dissertation

This dissertation treats the land and atmosphere as a coupled system (Figure 1.1), recognizing that changes in the atmosphere influence land, and that changes in land processes in turn influence the atmosphere. I conduct a series of studies to advance understanding of the mechanisms through which these interactions occur, drawing from perspectives in both atmospheric sciences and terrestrial ecology. I use Earth system models in creative ways to isolate different components of this coupled system: exploring how climate impacts vegetation (Chapter 2), how land processes influence the mean climate state through biogeophysical feedbacks (Chapter 3), and how atmospheric feedbacks modulate changes in land processes (Chapter 4).

Chapter 2 focuses on how climate influences vegetation, with implications for biogeochemical biosphere-atmosphere interactions under climate change. Tropical forests are arguably the dominant driver of inter-model variation in the strength of the carbon-climate feedback (Friedlingstein et al., 2006, 2013). Reducing this uncertainty is important for projecting future climate change, because the tropical forest carbon sink controls the airborne fraction of anthropogenic CO_2 emissions, and thereby influences how much the climate will warm under a given CO_2 emissions trajectory. Prior work has shown that much of the inter-model spread in tropical carbon uptake can be explained by differences in photosynthetic responses to warming (Mercado et al., 2018), making it critical to understand how and why increasing temperatures influence tropical forest photosynthe-

sis. This study focuses specifically on disentangling how different atmospheric drivers contribute to observed declines in tropical forest photosynthesis under high temperatures. It is challenging to disentangle the impact of direct temperature effects vs. vapor pressure deficit (VPD) effects on vegetation because these quantities are tightly correlated. I use two terrestrial biosphere models and observational data to show that plant hydraulics and photosynthetic temperature acclimation govern the strength of temperature and VPD effects. This work identifies a novel source of compensating errors in models – models can match the observed apparent ecosystem-level photosynthesis response to temperature by excluding photosynthetic temperature acclimation and plant hydraulics (which yields stronger direct temperature effects) or by including both photosynthetic temperature acclimation and plant hydraulics (which yields stronger VPD effects). However, these two sets of assumptions yield divergent predictions of ecosystem resilience to warming, underscoring the importance of accurately representing photosynthetic temperature acclimation and plant hydraulics in models.

Chapter 3 focuses on how land processes influence climate, by evaluating the biogeophysical impact of land parameter uncertainty. Prior research has demonstrated that parameter uncertainty drives uncertainty in land surface water, energy, and carbon fluxes. However, the influence of land process uncertainty on the climate system remains underexplored. I use an ensemble of simulations where I perturb 18 parameters governing land processes in a coupled Earth system model. Using this perturbed parameter ensemble (PPE), I demonstrate that land parameters generate biogeophysical feedbacks that substantially impact mean temperature and precipitation, primarily through parameters' influence on evapotranspiration. Notably, the spatial patterns of parameter-driven changes in precipitation and temperature differ from those due to radiatively-driven warming. My analysis demonstrates that land parameter uncertainty propagates to the entire Earth system, highlighting an underappreciated impact of land processes in determining the mean climate state and providing insights into where and how land process uncertainty influences climate. My analysis also highlights that processes typically evaluated in the context of biogeochemical rather than biogeophysical impacts (e.g. parametric controls of photosynthesis) can still generate large climate responses through biogeophysical pathways.

Chapter 4 analyzes land-atmosphere interactions, quantifying how land-driven climate changes feed back on the global water and carbon cycles. I isolate the impact of atmospheric feedbacks by

comparing the coupled PPE with a paired land-only PPE in which the atmosphere does not respond to changes in land surface properties. I find that atmospheric feedbacks dampen land-driven hydrologic changes in climatologically wet regions, but amplify hydrologic changes in climatologically dry regions. I also identify several hot spots where atmospheric feedbacks have a regionally significant impact on the carbon cycle. This analysis provides insights into where and how atmospheric feedbacks modulate terrestrial processes, posing a challenge to the widespread practice of developing and evaluating land models in an uncoupled configuration and then deploying them to understand and predict terrestrial processes in a coupled context. This study bridges biogeochemical and biogeophysical perspectives on biosphere-atmosphere interactions by showing how biogeophysical land-atmosphere feedbacks modulate biogeochemical process.

Chapter 5 presents a discussion of the implications of the results in Chapters 2-4 as well as plans for future research.

Chapter 2

DIFFERENT MODEL ASSUMPTIONS ABOUT PLANT HYDRAULICS AND PHOTOSYNTHETIC TEMPERATURE ACCLIMATION YIELD DIVERGING IMPLICATIONS FOR TROPICAL FOREST RESILIENCE

Abstract

Tropical forest photosynthesis can decline at high temperatures due to (1) biochemical responses to increasing temperature and (2) stomatal responses to increasing vapor pressure deficit (VPD), which is associated with increasing temperature. It is challenging to disentangle the influence of these two mechanisms on photosynthesis in observations, because temperature and VPD are tightly correlated in tropical forests. Nonetheless, quantifying the relative strength of these two mechanisms is essential for understanding how tropical gross primary productivity (GPP) will respond to climate change, because increasing atmospheric CO_2 concentration may partially offset VPD-driven stomatal responses, but is not expected to mitigate the effects of temperature-driven biochemical responses. We use two terrestrial biosphere models to quantify how physiological processes (photosynthetic temperature acclimation and plant hydraulic stress) and functional traits (e.g. maximum xylem conductivity) influence the relative strength of modeled temperature vs. VPD effects on light-saturated GPP at a tropical forest site in the Amazon, at a seasonally dry tropical forest site in Mexico, and at an experimental tropical forest mesocosm. By simulating idealized climate change scenarios, we quantify GPP changes under model configurations with stronger VPD effects compared to stronger direct temperature effects. Assumptions consistent with stronger direct temperature effects result in larger GPP declines under warming, while assumptions consistent with stronger VPD effects result in more resilient GPP under warming. Our findings underscore the importance of quantifying the role of direct temperature and indirect VPD effects for projecting the resilience of tropical forests in the future, and demonstrate that the relative strength of temperature vs. VPD effects in models is highly sensitive to plant functional parameters and structural

assumptions about photosynthetic temperature acclimation and plant hydraulics.

2.1 Introduction

Predicting how projected temperature increases will impact the tropical forest carbon sink requires understanding how tropical forest photosynthesis responds to increasing temperature. Photosynthesis, like most biological processes, is temperature dependent, with photosynthesis-temperature response curves exhibiting a temperature optimum above which photosynthetic rates decline. Some studies suggest that tropical forests may already be near their current optimum temperature (Doughty & Goulden, 2008; Mau et al., 2018; Huang et al., 2019; Duffy et al., 2021; Doughty et al., 2023), but this is a subject of ongoing debate (Lloyd & Farquhar, 2008; Tan et al., 2017). It remains unclear what processes drive ecosystem-level photosynthetic declines beyond forests' apparent temperature optima, and it is likewise unclear how photosynthetic rates will respond to further increases in air temperature due to climate change.

It is challenging to quantify tropical forests' direct photosynthetic response to temperature from observations because temperature is highly correlated with vapor pressure deficit (VPD), which also directly impacts photosynthesis. Observed photosynthetic declines associated with temperatures beyond a forest's thermal optimum can therefore result from two distinct mechanisms: (1) direct temperature effects on photosynthesis and (2) VPD effects on photosynthesis. VPD effects can also be considered indirect temperature effects because temperature directly controls the saturation vapor pressure of air, so increasing temperature increases VPD even if the water content of the air, or more conservatively the relative humidity, remains constant.

Direct temperature effects result from biochemical responses to high temperatures. Temperature controls enzymes' activity rates, and biochemical responses to increasing temperature beyond a plant's thermal optimum can lead to reversible downregulation of photosynthesis. Very high temperatures (e.g. leaf temperature greater than 40°C) can cause permanent damage to photosynthetic machinery, leading to longer-term suppression of photosynthetic capacity (Grossiord et al., 2020). Under sustained temperature increases, observations indicate that plants can acclimate to higher temperatures by shifting their photosynthetic thermal optima closer to ambient temperatures (Kattge & Knorr, 2007; Kumarathunge et al., 2019).

Meanwhile, changes in VPD cause reversible stomatal responses to atmospheric demand for water. Stomata close with increasing VPD in order to minimize water loss, and this stomatal closure reduces leaf-level photosynthesis. Increasing VPD reduces stomatal conductance even under well-watered conditions (Medlyn et al., 2011), and leaf water declines driven by plant hydraulic limitations on supplying water to leaves can further amplify VPD-driven stomatal conductance declines (Grossiord et al., 2020).

While it is challenging to disentangle these two mechanisms, it is nonetheless essential to do so in order to project how tropical gross primary productivity (GPP) will respond to climate change. Future relationships between temperature and VPD are expected to deviate from present day temperature-VPD relationships because global warming tends to decrease relative humidity over land, reflecting that increases in land evapotranspiration and moisture import from the ocean are not expected to keep up with increasing temperature under global warming (Byrne & O'Gorman, 2018). Empirical estimates of GPP sensitivity to temperature that implicitly include VPD effects (or vice versa) are based on a present climate and may not hold in a warmer climate. Furthermore, increasing atmospheric CO_2 concentrations may partially offset VPD-driven stomatal responses (Lloyd & Farquhar, 2008; Dusenge et al., 2019), but are not expected to mitigate the effects of temperature-driven biochemical responses.

The challenge of disentangling temperature and VPD effects has led to substantial discussion of the extent to which VPD vs. direct temperature effects are driving the observed photosynthetic declines with increasing temperature in tropical forests, with some evidence for both effects. Many recent observational studies support the hypothesis that, in the present climate, VPD effects are stronger than direct temperature effects, based on leaf gas exchange measurements (Vargas-G & Cordero, 2013; Slot & Winter, 2016; Slot et al., 2016; dos Santos et al., 2018), analysis of ecosystem-level observations (Wu et al., 2017; dos Santos et al., 2018; Fu et al., 2018), and experimental decoupling of temperature and VPD (M. N. Smith et al., 2020). However, some analysis of leaf-level observations suggest that direct temperature effects may be substantial for some tropical tree species (Slot and Winter 2017a,b; Doughty et al. 2023).

Terrestrial biosphere models differ in the strength of temperature and VPD effects under present day and future conditions. Rowland et al. (2015) compared five land system models under present day conditions, and found that modeled VPD effects are stronger than direct temperature effects

in all models, but that the magnitude of overall (temperature + VPD effects) varies substantially across models. Galbraith et al. (2010) found that in a high-emissions scenario, Amazonian total vegetation carbon decreased, but that the extent to which this was due to temperature vs. VPD effects varied across three models - in two models, direct temperature effects dominated, and in one model temperature and VPD effects contributed approximately equally to vegetation carbon declines. It is challenging to determine exactly what drives differences in the strength of temperature and VPD effects on GPP between models, because in modern land models temperature and VPD effects on GPP are emergent properties that result from multiple leaf-, plant-, and ecosystem-level processes. Temperature and VPD effects can vary between models due to different assumptions about the temperature responses of photosynthetic rates (Galbraith et al., 2010; Rowland et al., 2015), stomatal conductance, plant hydraulics, plant functional traits, and other plant and soil processes which indirectly control photosynthesis and stomatal conductance.

In this study, we systematically quantify how different model assumptions control the strength of temperature and VPD effects (as measured via the GPP responses of tropical forests), and present a framework for comparing different hypotheses encoded in models with ecosystem-level observational constraints. We focus on the impacts of plant hydraulics and photosynthetic temperature acclimation because previous work has shown that they influence plants' responses to temperature and VPD (Lombardozzi et al., 2015; Kennedy et al., 2019), but most land surface models used to assess global carbon cycle feedbacks do not include either process (Table A.1). In our analysis, we distinguish between structural assumptions (what equations are used to represent plant processes; e.g. the equations that govern water transport along the soil-plant-atmosphere continuum) and parameter assumptions (how those equations are parameterized; e.g. the value for maximum xylem conductivity). We ask the following questions: (1) How do photosynthetic temperature acclimation and plant hydraulics influence the modeled strength of temperature vs. VPD effects on GPP? (2) How do plant functional traits control apparent GPP responses to temperature? (3) Which structural and parameter assumptions are consistent with observed variations in the apparent GPP sensitivity to temperature across three different tropical forest sites? and (4) How do different assumptions about the relative strength of temperature vs. VPD effects influence projected GPP responses to warming?

2.2 Methods

2.2.1 Site descriptions

We analyze three tropical forest sites which span distinct temperature-VPD regimes (Figure A.1): the Biosphere 2 experimental tropical forest (B2), the kilometer 67 Amazonian evergreen forest eddy covariance site (K67), and the Tesopaco Mexican tropical deciduous forest eddy covariance site (MX-Tes). All sites regularly exceed 30°C, but the typical VPD at 30°C differs between the sites: 0.75 kPa (B2), 1.49 kPa (K67), and 2.75 kPa (MX-Tes).

K67 is a tropical evergreen forest located in the Tapajós National Forest near Santarém, Pará, Brazil; the site is described in more detail in Hutyra et al. (2007) and Restrepo-Coupe et al. (2013). Eddy covariance data for this site was collected by the Large-scale Biosphere-Atmosphere Experiment in Amazonia (LBA). K67 experiences an annual mean temperature of 26°C, annual mean relative humidity of 84.6%, and 1,993 mm mean annual rainfall. Temperatures can reach up to 33°C on hourly timescales.

MX-Tes is a tropical dry deciduous forest in Sonora, Mexico (Perez-Ruiz et al., 2010). The mean annual temperature at MX-Tes is 24°C, mean relative humidity is 48%, and hourly temperatures can reach up to 42°C. The site receives 712 mm mean annual rainfall, which primarily falls during the July-September wet season, and most trees lose their leaves during the dry season. We only analyze data from Tesopaco during the growing season, which we define as July to September based on leaf area index observations (M. N. Smith et al., 2020).

B2 is an experimental evergreen tropical forest biome within the Biosphere 2 Earth science facility in Arizona, USA. The mean annual temperature at B2 is 27.2°C, and hourly temperatures can reach up to 49°C. The annual mean rainfall is 1,300 mm and mean relative humidity is 82%. B2 differs from natural tropical forests in several ways. Firstly, B2 maintains high humidity levels even at temperatures greater than 30°C, which means the VPD associated with a given temperature is typically lower than it would be in a natural tropical temperature-VPD regime (M. N. Smith et al., 2020, Figure A.1). Additionally, the seasonality of temperature and VPD is stronger in B2, and there is no rainfall seasonality. B2 also experiences lower solar radiation and higher CO_2 concentrations than natural forest sites. Differences between B2 and natural tropical forests are discussed in more depth in M. N. Smith et al. (2020), Rosolem et al. (2010), and Arain et al. (2000).

2.2.2 Model descriptions

We run simulations using two different terrestrial biosphere models: the Functionally Assembled Terrestrial Ecosystem Simulator (FATES; Koven et al., 2020) and the Community Land Model version 5 (CLM5; Lawrence et al., 2019). We run single-site simulations of K67, B2, and MX-Tes from 2002-2011, 1998-2003, and 2004-2009, respectively, with simulations forced with gap-filled historical meteorological data. For each model, we run four different model configurations where we turn on and off photosynthetic temperature acclimation and plant hydraulics.

FATES model

FATES is a size- and age-structured vegetation demographic model. We use the static stand structure configuration of the model, a reduced complexity mode in which a site's stand structure and leaf area are held constant over time and taken from forest inventory data. This configuration allows us to look at the direct response of ecosystem function to parameter and structural perturbation in the absence of internal feedbacks due to the effects of growth and mortality on ecosystem function. The default FATES model configuration represents stomatal conductance using the Ball-Berry model (Ball et al., 1987).

The default FATES configuration ($\text{FATES}_{\text{NoAcclimNoHydro}}$) does not include either photosynthetic temperature acclimation or plant hydraulics. In a modified version of FATES, $\text{FATES}_{\text{HydroOnly}}$, we turn on the plant hydraulics module (Christoffersen et al., 2016; C. Xu et al., 2023), which dynamically calculates water transport along the soil-plant-atmosphere continuum and determines vegetation water stress as a function of leaf water potential. In $\text{FATES}_{\text{AcclimOnly}}$, we implement the photosynthetic temperature acclimation scheme developed by Kumarathunge et al. (2019), which allows plants to change the shape of their photosynthesis temperature response curves in response to changing temperature. Finally, in $\text{FATES}_{\text{AcclimAndHydro}}$ we turn on both plant hydraulics and photosynthetic temperature acclimation.

In the default FATES configuration ($\text{FATES}_{\text{NoAcclimNoHydro}}$), the maximum potential rate of electron transport (J_{max}) and the maximum rate of carboxylation (V_{cmax}) change with leaf temperature (T_v):

$$J_{max} = f(T_v)J_{max25} \tag{2.1}$$

	Variable	ΔH_a (J/mol)	ΔH_d (J/mol)	ΔS (J/mol/K)
Default FATES	J_{max}	43,540	152,040	495
	V_{cmax}	65,330	149,250	485
Modified Kumarathunge Scheme	J_{max}	40,710	200,000	658.77 - $0.84T_{growth}$
	V_{cmax}	42.6 + $1{,}140T_{growth}$	200,000	645.13 - $0.38T_{growth}$

Table 2.1: Temperature dependence parameters for photosynthesis.

$$V_{cmax} = f(T_v)V_{cmax25} \tag{2.2}$$

where J_{max25} and V_{cmax25} are J_{max} and V_{cmax}, respectively, at 25°C. $f(T_v)$ is the peaked Arrhenius function (Equation 2.3):

$$f(T_v) = \left[exp\left(\frac{\Delta H_a}{298.15R}\left(1 - \frac{298.15}{T_v}\right)\right)\right]\left(\frac{1 + exp(\frac{298.15\Delta S - \Delta H_d}{298.15R})}{1 + exp(\frac{T_v\Delta S - \Delta H_d}{T_v R})}\right) \tag{2.3}$$

where R is the universal gas constant, ΔH_a is the activation energy term (J/mol), ΔH_d is the deactivation energy term (J/mol), and ΔS is the entropy term (J/K/mol). In default FATES, the temperature dependence parameters for C3 photosynthesis (ΔH_a, ΔH_d, and ΔS) are constant for all C3 plants (Table 2.1). Photosynthetic rates therefore respond to temperature, but the shape of that temperature response is fixed. In the observationally derived Kumarathunge et al. (2019) temperature acclimation scheme, temperature dependence parameters ΔH_a and ΔS can acclimate to plants' growth temperature (T_{growth}) and home temperature (T_{home}), where T_{growth} is defined as the average temperature over the previous 30 days (limited to the range 3-37°C), and T_{home} is defined as the long-term mean maximum temperature of the warmest month of the year (Table 2.1).

The Kumarathunge temperature acclimation scheme also allows the ratio of J_{max} to V_{cmax} to change based on T_{growth} and T_{home} (Equation 2.4)

$$JV_r = \frac{J_{max}}{V_{cmax}} = 2.56 - 0.0375T_{home} - 0.0202(T_{growth} - T_{home}). \tag{2.4}$$

This ratio determines the transition between photosynthesis being limited by carboxylation vs. light, and can thereby also influence the optimum temperature of photosynthesis. Our temperature

acclimation scheme deviates slightly from the original Kumarthunge scheme, because we include only temperature acclimation, and not temperature adaptation effects (which allows plants to adjust their J_{max} temperature dependence curve based on the temperature at the species' seed source, T_{home}). We choose to ignore temperature adaptation effects because in an Earth system modeling context it is challenging to determine a plant functional type's climate of origin in a way that is scalable to the whole globe in both past, present, and future climates, and because Kumarathunge et al. (2019) found that acclimation was a stronger driver of variation in plants' photosynthetic thermal optima than adaptation was. Our modified Kumarathunge scheme (Table 2.1) is identical to the full Kumarathunge et al. (2019) scheme under the condition where $T_{home} = T_{growth}$.

CLM5 model

We use the satellite phenology configuration of CLM5, which is a reduced complexity mode of the model that prescribes leaf area and vegetation height. As with the FATES configuration, this CLM5 configuration allows us to isolate direct responses without confounding feedbacks due to changes in leaf area. The default version of CLM5 ($\text{CLM5}_{\text{AcclimAndHydro}}$) includes both plant hydraulics (Kennedy et al., 2019) and the Kattge & Knorr (2007) photosynthetic temperature acclimation scheme (Lombardozzi et al., 2015), and represents stomatal conductance using the Medlyn et al. (2011) model. In addition to the default CLM5 model, we run three additional model configurations where we turn on and off photosynthetic temperature acclimation and plant hydraulics: $\text{CLM5}_{\text{AcclimOnly}}$, in which we turn off the plant hydraulics module; $\text{CLM5}_{\text{HydroOnly}}$, in which we revert to the photosynthetic temperature response functions from an older version of CLM (documented in Lombardozzi et al., 2015); and $\text{CLM5}_{\text{NoAcclimNoHydro}}$, in which we turn off both plant hydraulics and photosynthetic temperature acclimation.

2.2.3 Observational data (environmental driver data, forest structure data, and flux calculations)

We use gap-filled meteorological data to force the models and net ecosystem exchange (NEE) data from the FLUXNET2015 dataset (Pastorello et al., 2020) for K67, from Rafael Rosolem (Rosolem et al., 2010; M. N. Smith et al., 2020) for B2, and from the AmeriFlux FLUXNET data product for

MX-Tes (Yepez & Garatuza, 2021). We calculate GPP by assuming that daily ecosystem respiration rates are equal to night-time NEE following the methodology in M. N. Smith et al. (2020).

For CLM5 simulations, we prescribe leaf area and vegetation height based on observations reported in the literature. At K67 we set leaf area to 6 m^2/m^2 (based on Restrepo-Coupe et al., 2017), at Biosphere 2 we hold leaf area constant at 5 m^2/m^2 (based on Rosolem et al., 2010), and at MX-Tes we prescribe a seasonally varying leaf area index which ranged from 0.3 to 4.1 m^2/m^2 throughout the year, based on the average monthly leaf area index in M. N. Smith et al. (2020). We set vegetation height to 33.2 m for K67 (based on the observationally-derived gridded CLM input dataset at that location), 11.5 m for B2 (from B2 forest inventory data) and 14 m for MX-Tes (Sanchez-Mejia et al., 2021).

For FATES simulations, we prescribe the forest structure (tree diameter distribution) to match forest inventory data, and hold this forest structure constant over time. We use 2012 forest inventory data for K67, 2000 forest inventory for B2, and 2009 forest inventory data for MX-Tes (Sanchez-Mejia et al., 2021). For B2, we modify FATES' default allometric scaling relationships to achieve the observed distribution of tree heights, which was necessary because B2 trees are shorter for a given stem diameter than trees at natural tropical forests (Rascher et al., 2004; M. N. Smith et al., 2020).

Our analysis focuses on GPP under high light conditions, and site-specific light saturation thresholds were estimated from observed relationships between downward shortwave radiation and NEE. We use light saturation thresholds of 600 W/m^2 for K67, 300 W/m^2 for MX-Tes, and 200 W/m^2 for B2. We refer to GPP above these light thresholds as light-saturated GPP.

2.2.4 Synthetic meteorology method for calculating light-saturated GPP responses to temperature and VPD

We calculate light-saturated GPP temperature response curves by binning light-saturated GPP by air temperature in 1°C bins. We refer to the modeled *apparent GPP temperature response* as the binned response curve for actual GPP associated with a given temperature in observations, and we refer to the *direct GPP temperature response* as the binned response curve only due to direct temperature effects, which we quantify using FATES and CLM simulations with synthetic

meteorological forcings.

We quantify the extent to which the apparent modeled light-saturated GPP responses to temperature are due to direct temperature effects or VPD effects by running model simulations with synthetic meteorological forcings. We use an "everything but" approach to quantify the effect of each meteorological driver. For example, the direct effect of temperature on modeled GPP is calculated as the difference between modeled historical GPP (in which the model is forced with the observed historical meteorology) and modeled GPP under a synthetic meteorology where temperature is held constant at 25°C and all other meteorological quantities match the observed historical meteorology. Using this approach, we can disentangle the individual contributions of (1) direct temperature effects, (2) direct VPD effects, (3) synergistic VPD-temperature effects, and (4) all other meteorological effects, including solar radiation and precipitation (Table 2.2). The sum of these four terms equals the net effect, and the net effect is equivalent to the apparent GPP response in model simulations forced with the observed site meteorology (see Section 2.2.5). We additionally quantify the effect of soil moisture by running synthetic meteorology simulations where rainfall is held constant throughout the year at 0.005 mm/s, which constantly saturates the soil and relieves any soil moisture stress.

2.2.5 Decomposition of meteorological drivers

We decompose the modeled light-saturated GPP into four different components: (1) the direct temperature effect, (2) the VPD effect, (3) the synergistic effect, and (4) other meteorological effects. We first decompose the modeled GPP into the temperature and VPD combined effects and into other meteorological effects, such that $\beta_{total} = \beta_{T+VPD} + \beta_{other}$:

$$\beta_{total}(T_a) = \Delta GPP_{historical}(T_a) \tag{2.5}$$

$$\beta_{T+VPD}(T_a) = \Delta GPP_{historical}(T_a) - \Delta GPP_{LowVPDLowTemp}(T_a) \tag{2.6}$$

$$\beta_{other}(T_a) = \Delta GPP_{LowVPDLowTemp}(T_a) \tag{2.7}$$

where T_a is the air temperature and ΔGPP_X is the difference between the light-saturated GPP in model experiment X (as described in Table 2.2) and the historical light-saturated GPP at 25°C.

We then further decompose β_{T+VPD} into the direct temperature effect β_T, the VPD effect β_{VPD}, and the synergistic temperature-VPD effect β_{syn}, such that $\beta_{T+VPD} = \beta_T + \beta_{VPD} + \beta_{syn}$:

$$\beta_T(T_a) = \Delta GPP_{historical}(T_a) - \Delta GPP_{LowTemp}(T_a) \tag{2.8}$$

$$\beta_{VPD}(T_a) = \Delta GPP_{historical}(T_a) - \Delta GPP_{LowVPD}(T_a) \tag{2.9}$$

$$\beta_{syn}(T_a) = \beta_{T+VPD}(T_a) - \beta_T - \beta_{VPD}(T_a) \tag{2.10}$$

It follows from these definitions that $\beta_{total} = \beta_T + \beta_{VPD} + \beta_{syn} + \beta_{other}$.

Experiment Name	Meteorological Forcing (at the lowest atmospheric level)						
	Temperature	Relative Humidity (%)	Incident solar radiation	Precipitation	Incident longwave radiation	Wind	Surface pressure
Historical	Historical	Historical	Historical	Historical	Historical	Historical	Historical
LowVPD	Historical	Modified so that VPD is 0.4 kPa*	Historical	Historical	Historical	Historical	Historical
LowTemp	25°C	Modified so that the VPD matches the historical VPD	Historical	Historical	Historical	Historical	Historical
LowVPDLowTemp	25°C	Modified so that VPD is 0.4 kPa*	Historical	Historical	Historical	Historical	Historical

* Modified so that VPD at the lowest atmosphere level is 0.4 kPa, which is the average VPD at temperatures 24.5-25.5°C in the historical record.

Table 2.2: Description of synthetic meteorological forcings.

2.2.6 Perturbed parameter ensemble

We quantify how plant functional traits relating to photosynthesis, stomatal conductance, and plant hydraulics modify the strength of direct and indirect temperature effects by running a small perturbed parameter ensemble in $\text{FATES}_{\text{AcclimAndHydro}}$, where we perturb plant functional trait parameters one at a time to low-end, median, and high-end values based on the existing literature (Table A.2). We run twelve parameter perturbation simulations for four FATES parameters. We quantify the modeled strength of direct and indirect temperature effects for each ensemble member using the same synthetic meteorology method described above.

2.2.7 Idealized future climate treatments

We quantify how K67 responds to warming in different model configurations by applying five idealized climate treatments: (E1) temperature increase, (E2) temperature and VPD increase (under constant relative humidity), (E3) temperature increase and relative humidity decrease, (E4) VPD increase, and (E5) relative humidity decrease (Figure A.7). We use this factorial idealized climate treatment design in order to disentangle the extent to which GPP changes under warming are due to direct biochemical effects from increasing temperature vs. stomatal effects due to VPD increases, and we assess the impact of constant vs. decreasing relative humidity to represent different expectations about future climate as described further below. In the temperature increase treatment (E1), temperature in the historical meteorological forcing dataset is uniformly increased by 3°C at all points in time, but VPD is held constant at historical levels, and thus relative humidity increases. In the temperature and VPD treatment (E2), both temperature and VPD increase to reflect a 3°C warming and constant relative humidity. In the temperature increase and relative humidity decrease (E3), temperature increases by 3°C and relative humidity decreases by 6%. This idealized relative humidity decrease is consistent with CMIP6 model projections of Amazon climate change - multi-model mean relative humidity decreases by about 4-7% by midcentury and 4-13% by the end of the century, depending on the scenario (Y. Li et al., 2023). In the VPD increase treatment (E4), VPD is increased to reflect the VPD change that would occur under 3°C warming and constant relative humidity, but temperature is held constant at historical levels. In the relative humidity decrease (E5), VPD is increased to reflect the VPD change that would occur under 3°C warming and -6% decrease in relative humidity, but temperature is held constant at historical levels. We additionally run two of these climate treatments (E1 and E3 above) under elevated CO_2 concentrations of 560 ppm. We use this CO_2 concentration because it is two times the preindustrial CO_2 concentrations - in medium to high emission scenarios, this CO_2 concentration is reached between 2049 and 2069 (Meinshausen et al., 2020).

2.3 Results

2.3.1 Structural influences on the strength of temperature and VPD effects

To evaluate how different model structural assumptions influence the apparent GPP response to temperature, we run site-level simulations of K67 where we turn on and off photosynthetic temperature acclimation and plant hydraulics, resulting in a total of eight model configurations (see Methods). In observations at K67, light-saturated GPP declines by about 38% as temperature increases from 25°C to 32°C (Figure 2.1a). In all simulations of K67 under current conditions, light-saturated GPP declines as temperature increases, which is qualitatively consistent with observations (Figure 2.1a). The $CLM5_{AcclimAndHydro}$ and $CLM5_{HydroOnly}$ apparent GPP temperature response curves (green and blue dashed lines, respectively) most closely match this observed apparent GPP temperature response.

We then disentangle the direct and indirect effects of temperature and other meteorological drivers by running model experiments in which only one driver is allowed to vary at a time using synthetic meteorology (see section 2.2.5). Across all model configurations, the apparent GPP response to temperature (defined in section 2.2.4, black horizontal line shows observations and black circles show modeled apparent GPP change) does not reflect the actual GPP response to direct temperature effects as quantified through direct modifications to meteorological forcing (Figure 2.1c). Rather, the apparent GPP response to temperature constitutes the combined effect of direct temperature effects (red bars), VPD effects (blue bars), synergistic VPD-temperature effects (purple bars), and other meteorological quantities that covary with temperature (orange bars).

The relative impact of temperature and VPD on GPP varies depending on model structural assumptions (Figure 2.1b-c). When neither photosynthetic temperature acclimation nor plant hydraulics are turned on, direct temperature effects in both FATES and CLM5 are stronger than VPD effects (gray circle and gray triangle, respectively, Figure 2.1b). Turning on photosynthetic temperature acclimation weakens direct temperature effects (moving from gray to yellow, Figure 2.1b), and adding plant hydraulics strengthens VPD effects (moving from gray to blue, Figure 2.1b). Weakening direct temperature effects and strengthening VPD effects have counteracting influences on the apparent GPP responses to temperature, such that turning on both photosynthetic temperature acclimation and plant hydraulics yields a combined temperature and VPD effect which

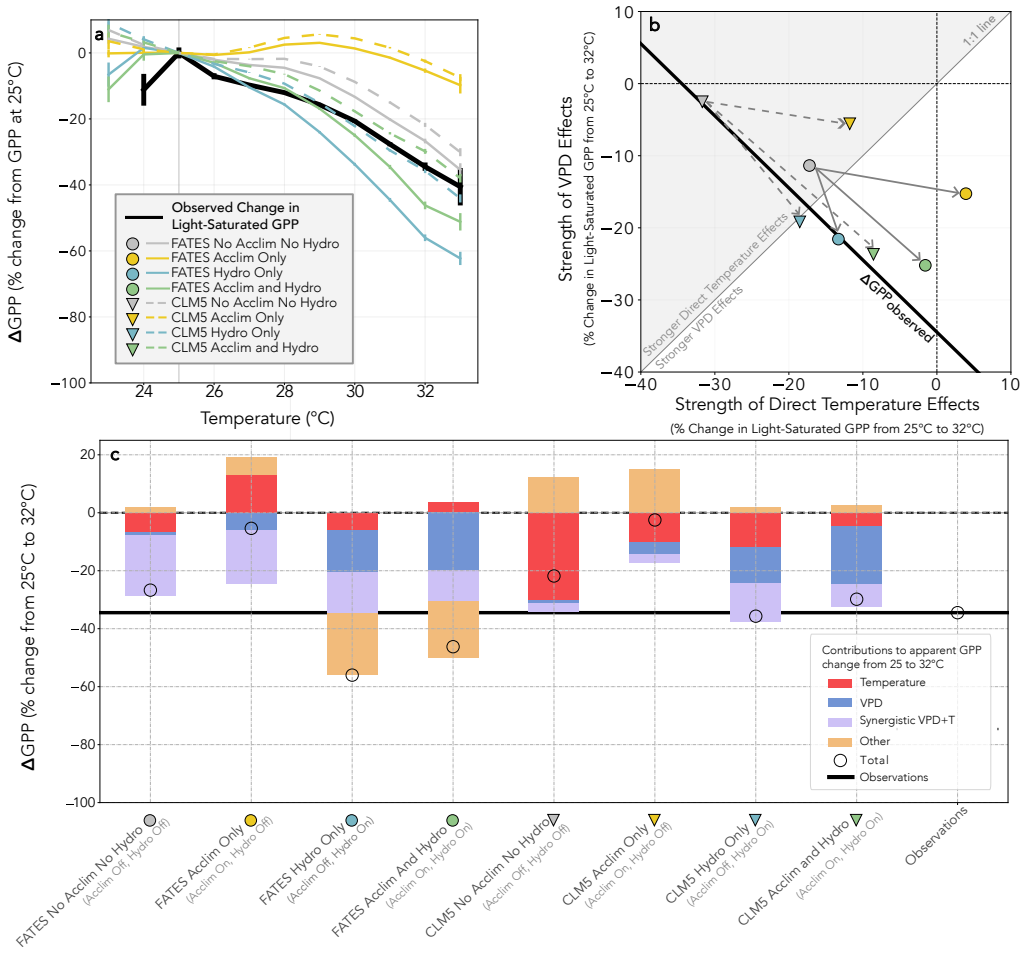

Figure 2.1: Process assumptions modify the strength of direct and indirect temperature effects. (a) The apparent light-saturated GPP response to temperature at the K67 site in observations and in different model configurations of FATES and CLM5. (b) The modeled strength of direct temperature effects and VPD effects, quantified as the percent change in light-saturated GPP from 25°C to 32°C as calculated from synthetic meteorology simulations. More negative values indicate stronger temperature and VPD effects on GPP. Synergistic (nonlinear) temperature-VPD effects are attributed equally to direct temperature and VPD effects, e.g. the temperature effect plotted on the x-axis is equal to the direct temperature effect plus $\frac{1}{2}$ of the temperature-VPD synergistic effects. The gray 1:1 line delineates whether temperature or VPD effects are dominant. Points above the 1:1 line indicate that direct temperature effects are stronger than VPD effects, while points below the 1:1 line indicate that VPD effects are stronger. The black line marks the total apparent GPP response to temperature from 25°C to 32°C, which is an observational constraint if other meteorological effects are assumed to be zero. The observed ΔGPP is represented as a line to reflect ambiguity as to whether temperature or VPD effects are dominant. (c) The modeled strength of meteorological effects which contribute to the apparent GPP relationship with temperature, which is quantified as the percent change in light-saturated GPP from 25°C to 32°C as calculated from synthetic meteorology simulations. The total (circles) refers to the model output when actual site meteorology is used (equivalent to the sum of temperature, VPD, synergistic VPD+temperature, and other effects).

is similar to the combined effect when both processes are turned off (Figure 2.1). Ultimately, however, this similar combined temperature and VPD effect is achieved through different partitioning between direct temperature and VPD effects under different model structural assumptions (moving from gray to green, Figure 2.1b). Model configurations with both processes turned off exist in the stronger direct temperature effects regime (above 1:1 line, Figure 2.1b), while model configurations with both processes turned on exist in the stronger VPD effects regime (below 1:1 line, Figure 2.1b).

From Figures 2.1b and c, we find that model configurations that include plant hydraulics and temperature acclimation have different emergent strengths of VPD vs. temperature effects for the same overall combined VPD and temperature effect as configurations which do not include these processes. However, the synthetic meteorology simulations also demonstrate that temperature and VPD are not the sole drivers of the apparent GPP response to temperature. The apparent GPP response also is influenced by other environmental factors (orange bars, Figure 2.1c). Turning on plant hydraulics also increases overall soil-plant water stress, especially in FATES (Figure A.3), and this hydraulic stress contributes to apparent GPP declines with temperature because soil moisture is negatively correlated with temperature and VPD over seasonal timescales (Figure A.2). In several model configurations ($\text{FATES}_{\text{AcclimOnly}}$, $\text{CLM5}_{\text{NoAcclimNoHydro}}$, $\text{CLM5}_{\text{AcclimOnly}}$) other environmental factors contribute to the apparent GPP response to temperature even when soil moisture, temperature, and VPD are held constant (blue lines in Figure A.3), suggesting an influence of solar zenith angle or solar radiation.

Of the four FATES model configurations, the apparent GPP temperature response in $\text{FATES}_{\text{NoAcclimNoHydro}}$ (default FATES) is closest to the observed response, followed by $\text{FATES}_{\text{AcclimAndHydro}}$. While $\text{FATES}_{\text{NoAcclimNoHydro}}$ and $\text{FATES}_{\text{AcclimAndHydro}}$ have similar combined temperature and VPD effects (sum of red, blue, and purple bars in Figure 2.1c), the apparent temperature response in $\text{FATES}_{\text{AcclimAndHydro}}$ deviates more from observations (Figure 2.1c) due to additional soil moisture stress (Figure A.3). Observations do not directly measure how much different meteorological drivers contribute to this apparent GPP response to temperature, but previous work using analytical methods such as path analysis (Wu et al., 2017; Fu et al., 2018) and binned regression (Wu et al., 2017; M. N. Smith et al., 2020) suggest that at the K67 site VPD effects are stronger than direct temperature effects, indicating that model configurations in the stronger VPD effects regime

are likely more consistent with observations.

2.3.2 Parametric influences on the strength of temperature and VPD effects

We run a small perturbed parameter ensemble in $\text{FATES}_{\text{AcclimAndHydro}}$ at K67 to identify how plant functional traits influence the apparent GPP temperature response, and the relative strength of direct temperature and VPD effects (see section 2.2.6). We find that the apparent GPP response to temperature is highly sensitive to plant functional parameters (Figure 2.2a). Our parameter ensemble yields more variation in the strength of VPD effects (ranging from -27% to -12% from 25°C to 32°C) than variation in the strength of direct temperature effects (ranging from -6% to +1%) (Figure 2.2b). The maximum rate of Rubisco carboxylase activity (V_{cmax}) exerted a particularly strong control on VPD effects. Even though we sample a broad parameter space, the $\text{FATES}_{\text{AcclimAndHydro}}$ model always shows that VPD effects are stronger than direct temperature effects (Figure 2.2b), suggesting that the relative importance of direct temperature or VPD effects in models is relatively robust to parameter choice, and depends more on model structural assumptions (i.e. Figure 2.1b).

The large variation in the apparent GPP response to temperature across our ensemble is primarily due to other meteorological effects (orange bars, Figure 2.2c) such as soil moisture and the uncertainty in the value of selected parameters. Maximum hydraulic conductivity (kmax) exerted a particularly strong control over the apparent GPP response to temperature.

2.3.3 Apparent temperature responses across humidity gradients

In observations, B2 has a weaker apparent GPP response to temperature than natural tropical forest sites (M. N. Smith et al., 2020, Figure 2.3). We run model simulations to test which assumptions are consistent with this cross-site variation in apparent GPP responses to temperature. When photosynthetic temperature acclimation and plant hydraulics are active in CLM5 ($\text{CLM5}_{\text{AcclimAndHydro}}$), modeled apparent GPP temperature response curves match observations relatively well at K67, MXTes, and B2, though GPP declines associated with increasing temperatures are slightly too weak at K67 and B2. As in observations, the modeled K67 and B2 apparent temperature response curves diverge from each other around 28°C. CLM5 is unable to capture this divergence in apparent temperature response curves without including temperature acclimation and plant hydraulics

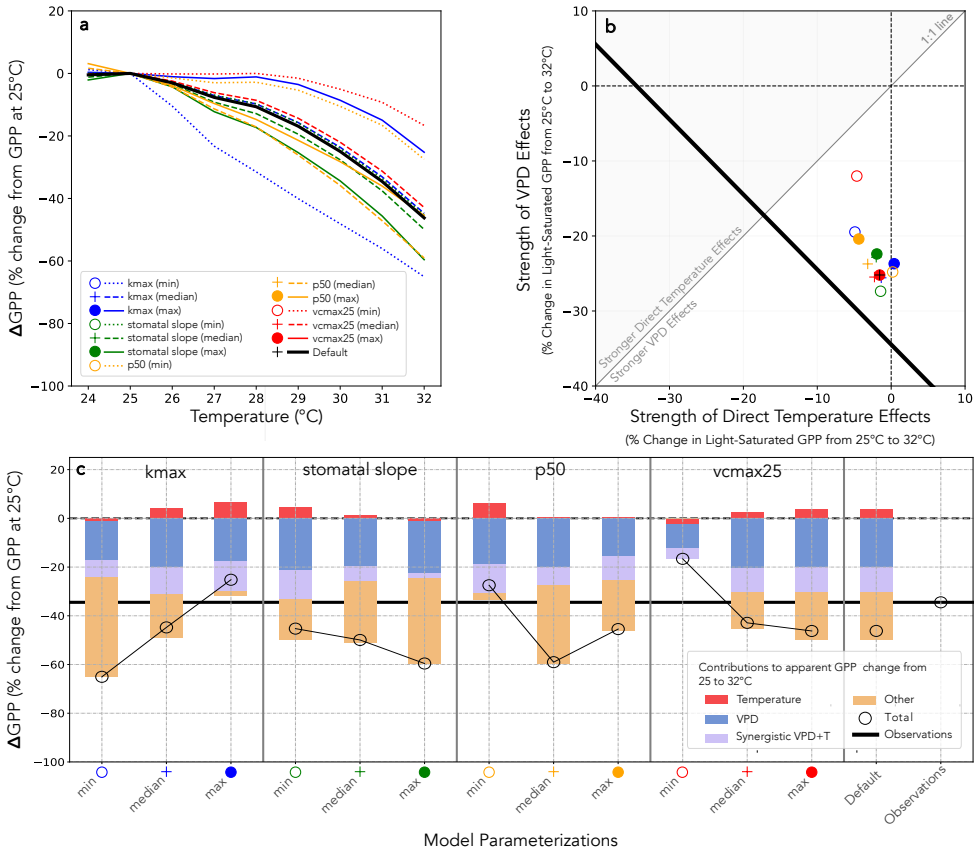

Figure 2.2: Plant functional traits modify the strength of direct and indirect temperature effects at K67. The relative strength of direct temperature effects and VPD effects as in Figure 2.1, but for a perturbed parameter ensemble of $\text{FATES}_{\text{AcclimAndHydro}}$, varying kmax, stomatal slope, p50, and vcmax25.

(compare Figures 2.3a and 2.3b). When these processes are turned off in $CLM5_{NoHydroNoAcclim}$, increasing temperatures are associated with modeled GPP declines that are too weak at K67 and too strong at B2.

In contrast, apparent GPP temperature response curves in $FATES_{AcclimAndHydro}$ do not perform well compared to B2 observations when photosynthetic temperature acclimation and plant hydraulics are active (Figure 2.3d). The $FATES_{AcclimAndHydro}$ apparent GPP temperature response fits observations reasonably well at K67, but B2 and MX-Tes GPP declines too much with increasing temperature in $FATES_{AcclimAndHydro}$. The strong apparent GPP temperature response in $FATES_{AcclimAndHydro}$ at B2 is driven by soil moisture stress, as diagnosed by synthetic meteorology simulations with fully saturated soils (Figure A.4). Changing B2 plant hydraulic traits so that B2 trees have higher maximum xylem hydraulic conductivity (16.04 kg/MPa/m/s compared to 3 kg/MPa/m/s) flattens the $FATES_{AcclimAndHydro}$ B2 apparent GPP temperature response by alleviating this water stress at B2 (dashed red line in Figure 2.3d). Turning off photosynthetic temperature acclimation and plant hydraulics also improves the apparent GPP temperature response curves in FATES (Figure 2.1c). In $FATES_{NoAcclimNoHydro}$, modeled apparent GPP temperature response curves match observed response curves reasonably well, though GPP declines are slightly underestimated at K67 and overestimated at B2. B2 and K67 apparent temperature response curves diverge from each other at about 30°C in $FATES_{NoAcclimNoHydro}$.

2.3.4 Different structural assumptions yield diverging projections

In the historical period, a model that features strong direct temperature effects and weak VPD effects (the NoAcclimNoHydro models) can yield a similar apparent GPP response to temperature as a model that features weak direct temperature effects and strong VPD effects (the AcclimAndHydro models; see gray vs. green, Figure 2.1a). The same models project very different responses to anthropogenic forcing however. We illustrate this by showing two idealized forcing experiments for one site (K67): one with an increase of 3°C and the other with an increase of 3°C and a reduction in relative humidity by 6%; both are compared to the historical period. In models without photosynthetic temperature acclimation or plant hydraulics, light-saturated GPP decreases under an idealized increased temperature treatment (Figure 2.4a and c). In $FATES_{NoAcclimNoHydro}$ and

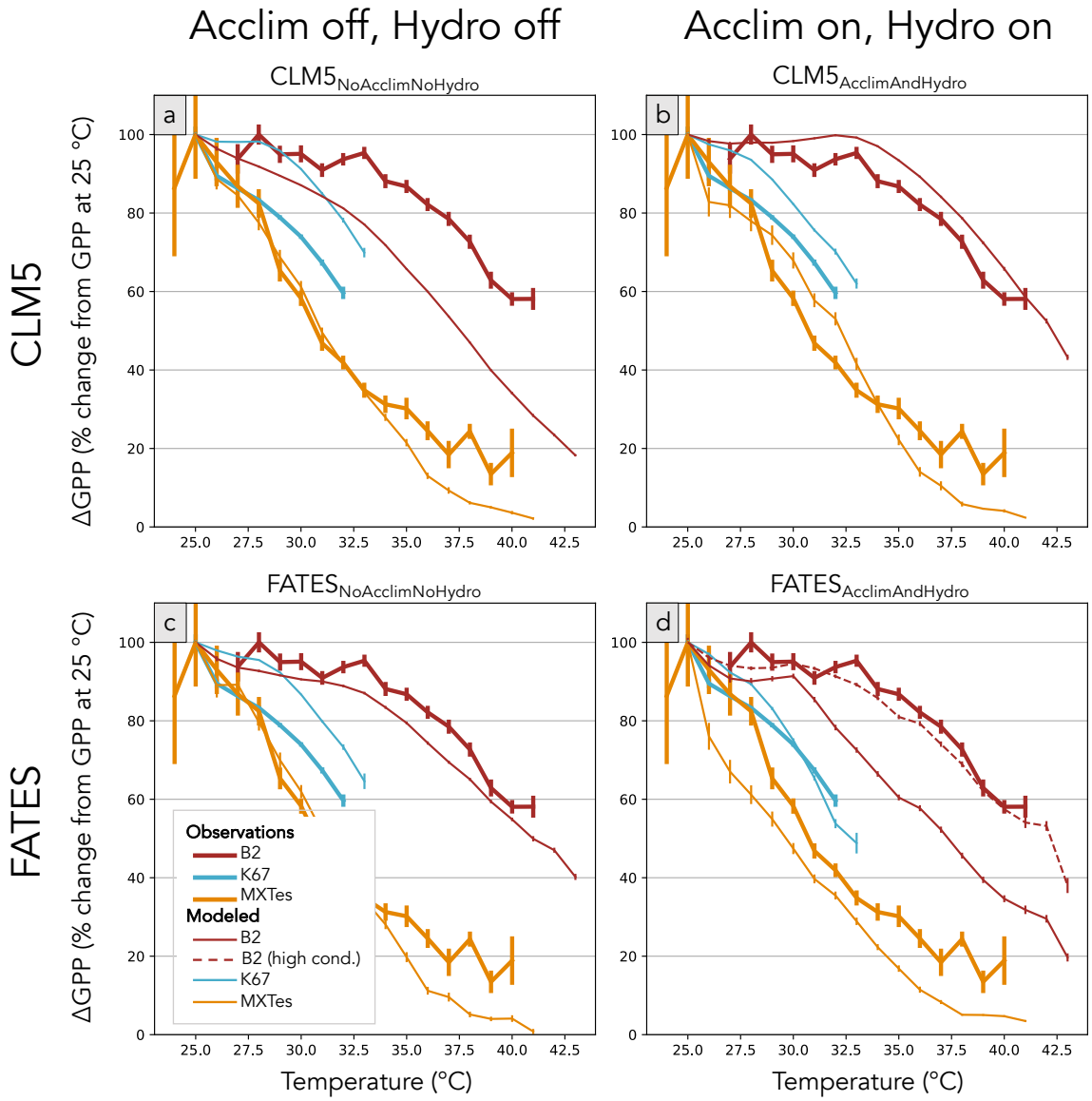

Figure 2.3: Observed and modeled apparent GPP responses to temperature at three tropical forest sites. Each panel compares observed and modeled apparent GPP responses to temperature for a different model configuration. In (a) and (c) photosynthetic temperature acclimation and plant hydraulics are turned off, and in (b) and (d), photosynthetic temperature acclimation and plant hydraulics are turned on. CLM5 is shown in (a) and (b), and FATES is shown in (c) and (d).

$CLM5_{NoAcclimNoHydro}$, increasing temperature by 3°C decreases mean light-saturated GPP by 14% and 11%, respectively. These models are not sensitive to VPD changes, and are therefore not sensitive to different assumptions about relative humidity changes under warming (Figure 2.4a, Figure 2.4c, and Figure A.5). In contrast, temperature increases drive minimal GPP changes in models with photosynthetic temperature acclimation and plant hydraulics turned on (Figure 2.4b and d). In $FATES_{AcclimAndHydro}$ and $CLM5_{AcclimAndHydro}$, the 3°C increase in temperature changes GPP by less than 3% as long as VPD is held constant at historical levels. These models are more sensitive to relative humidity changes under warming (Figure 2.4b, Figure 2.4d, and Figure A.5). If the 3°C temperature increase is accompanied by 6% decrease in relative humidity, GPP decreases by 7 and 9%, respectively. If the 3°C warming treatment is accompanied by an increase in CO_2 concentration, GPP increases in all model configurations due to FATES and CLM's strong CO_2 fertilization effects. However, GPP increases more in $FATES_{AcclimAndHydro}$ and $CLM5_{AcclimAndHydro}$ than in $FATES_{NoAcclimNoHydro}$ and $CLM5_{NoAcclimNoHydro}$ (Figure A.5).

The combined impact of a 3°C warming and a 6% reduction in relative humidity on the light-saturated GPP also differs between models. In $FATES_{NoAcclimNoHydro}$, $CLM5_{NoAcclimNoHydro}$, and $CLM5_{AcclimAndHydro}$, climate treatments shift the mean GPP but lead to minimal changes in the distribution of GPP around the mean. In $FATES_{AcclimAndHydro}$, climate treatments both shift the mean GPP and drive changes in the GPP distribution around the mean. Compared to observed light-saturated GPP, the mean light-saturated GPP for $CLM5_{NoAcclimNoHydro}$ and $FATES_{AcclimAndHydro}$ most closely match observations. There are biases in the GPP distributions in all models (Figure 2.4).

2.4 Discussion

2.4.1 Photosynthetic temperature acclimation and plant hydraulics

We find that both photosynthetic temperature acclimation and plant hydraulics govern the strength of direct temperature effects and VPD effects on photosynthesis (Figure 2.1), underscoring the importance of improving our scientific understanding and model representations of these processes. Models can achieve the same overall present day GPP response to temperature and VPD by excluding both of these processes (which yields stronger direct temperature effects) or by including both

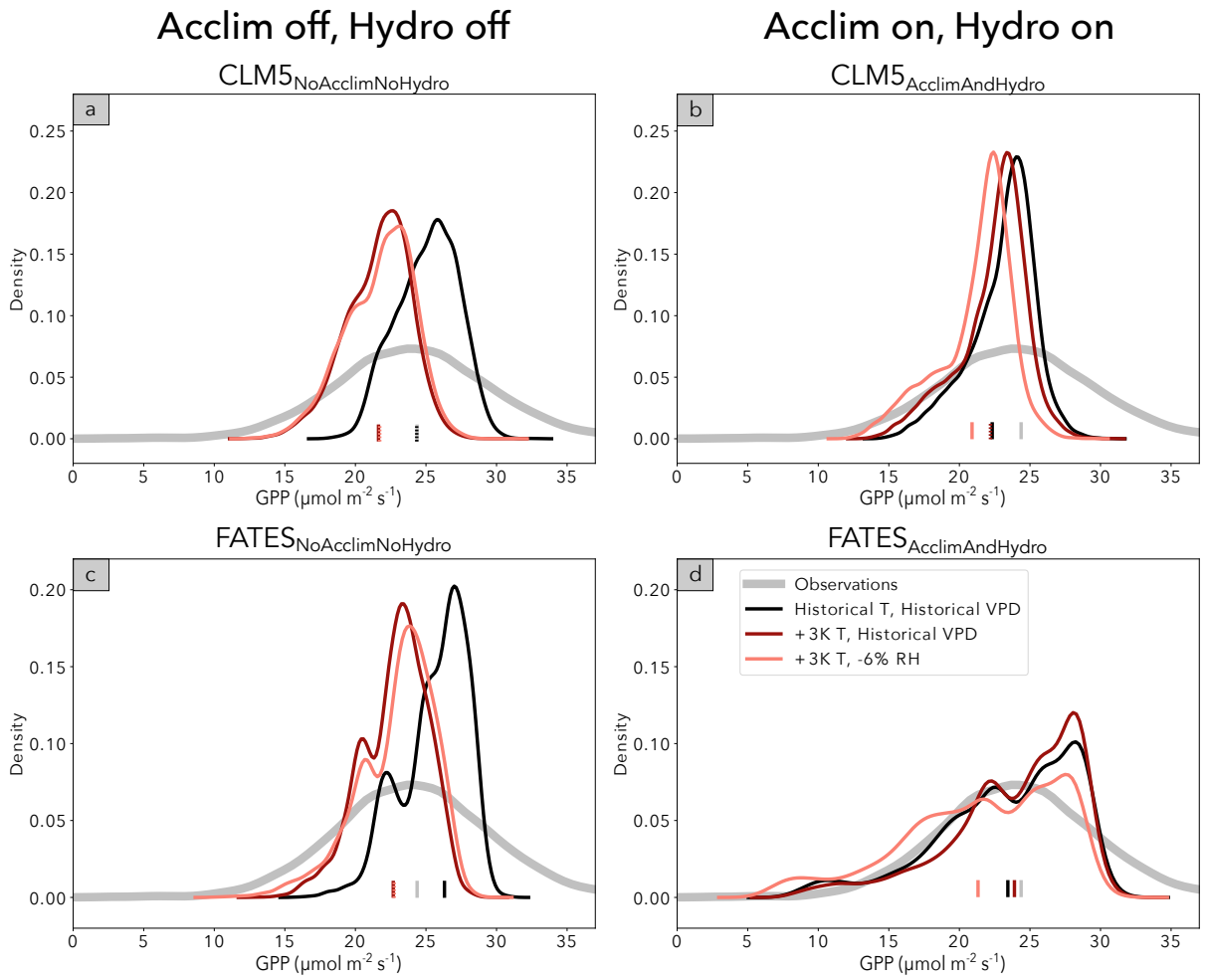

Figure 2.4: Shifts in the distribution of light-saturated photosynthesis at K67 under idealized climate treatments. Distributions of light-saturated GPP at K67 under different climate treatments for CLM5 (a-b) and FATES (c-d). In (a) and (c), photosynthetic temperature acclimation and plant hydraulics are turned off. In (b) and (d), photosynthetic temperature acclimation and plant hydraulics are turned on.

of these processes (which yields stronger VPD effects). However, these two sets of assumptions yield diverging predictions of ecosystem resilience to warming (Figure 2.4). Assumptions consistent with stronger direct temperature effects resulted in larger GPP declines under warming, while assumptions consistent with stronger VPD effects resulted in more resilient GPP under warming. This suggests that the relative strength of direct temperature vs. VPD effects on GPP in the present day may be a useful diagnostic for GPP responses to future warming. It has long been recognized that land surface models tend to fit historical data relatively well, but then diverge from each other under future conditions (Friedlingstein et al., 2006, 2013; Lovenduski & Bonan, 2017; Booth et al., 2017), in part due to the challenge of equifinality (J. Tang & Zhuang, 2008; Fisher & Koven, 2020). This study identifies that the tradeoff between weak VPD effects and strong temperature effects vs. strong VPD effects and weak temperature effects is an important axis along which compensating errors may occur in models.

Photosynthetic temperature acclimation and plant hydraulics are well established processes with important effects on ecosystem functioning, so broadly we expect that model configurations that include these processes should be more realistic than model configurations that exclude them. Previous observationally-based studies indicate that VPD effects are stronger than direct temperature effects at K67 in particular (Wu et al., 2017; Fu et al., 2018; M. N. Smith et al., 2020), and at tropical forests in general (M. N. Smith et al., 2020). This suggests that structural assumptions that put models in the stronger VPD effect regime are more realistic, and that models without photosynthetic temperature acclimation or plant hydraulics may match observations by assuming unrealistically strong direct temperature effects. Most land models used to quantify carbon cycle responses to warming as part of the Coupled Model Intercomparison Project Phase 6 (CMIP6) do not include photosynthetic temperature acclimation or plant hydraulics (Table A.1), so we hypothesize that such land models may overestimate the strength of direct temperature effects and underestimate VPD effects. Given that the present-day partitioning between temperature and VPD effects may be a useful diagnostic for model GPP sensitivity to warming, we call for more modeling centers to use synthetic meteorology methods to explicitly quantify how much modeled apparent GPP responses to temperature in the present day are driven by direct temperature effects, VPD effects, and other meteorological drivers.

In this study we focus on how photosynthetic temperature acclimation and plant hydraulics

influence GPP responses to warming, but we also note that photosynthetic temperature acclimation and plant hydraulics can influence tropical carbon pool responses to concurrent changes in atmospheric CO_2 concentration, precipitation, and other environmental conditions. For example, Lombardozzi et al. (2015) found that turning on photosynthetic and respiratory temperature acclimation yielded a smaller tropical carbon pool increase from 1850 to 2100, compared to simulations when these processes were turned off. This was attributed to the fact that 1850 tropical carbon pools were larger in simulations that included temperature acclimation, but the rate of ecosystem-level carbon accumulation slowed by the end of the 21st century due to limitation of another environmental quantity (e.g. nutrient or water limitation).

2.4.2 Plant functional traits

We find that plant functional traits control the strength of VPD and temperature effects (Figure 2.2), which means that the strength of these effects can differ across time and space due to variation in tropical forest functional composition. This poses a challenge for modeling tropical forest responses at a regional to pan-tropical scale, because doing so will require representing the diversity of plant functional traits which can vary widely both within an ecosystem and geographically. This, paired with the fact that hydraulic trait data for tropical forests is limited, motivates further data collection of tropical tree hydraulic trait data through field campaigns (Tavares et al., 2023; Christoffersen et al., 2016) and satellite-based methods (e.g. Liu et al., 2021). For example, our perturbed parameter ensemble demonstrated that the apparent GPP response to temperature at K67 is highly sensitive to stem maximum hydraulic capacity. However, a previous meta-analysis identified less than 300 observations of this trait for tropical trees (Christoffersen, 2021). Collecting more hydraulic trait data, and developing methods for estimating hydraulic traits based on correlations with environmental conditions or more easily collected plant traits, will enable better model representation of ecosystem photosynthetic responses to temperature, VPD, and soil moisture. Our results also suggest that GPP sensitivities to environmental changes are influenced by variation in plant traits within an ecosystem, due to both variation across trees (e.g. X. Xu et al., 2016) and vertical variation in plant traits and forest microclimates (Vinod et al., 2023).

Previous studies have documented differing strengths of VPD and temperature effects on GPP

across tropical forest sites (Fu et al., 2018), and we demonstrate here that this variation could be partially due to inter-site variation in plant functional traits. Additionally, tropical forest functional composition can change in response to changing climate, thereby driving shifts in tropical forest GPP sensitivities to VPD, temperature, and soil moisture. This nonstationarity in time points to the importance of accounting for dynamic ecosystem functional assembly (Fisher et al., 2015) when predicting tropical forest photosynthesis under novel climates on longer timescales.

2.4.3 Multiple hypotheses consistent with apparent GPP responses to temperature at Biosphere 2

From observations alone, it is challenging to identify the unique features of Biosphere 2 (see section 2.2.1) that enable the site to maintain high photosynthetic rates even at high temperatures. Broadly, we expect that models should be able to represent all sites using the same physiological rules, and that B2's shallower apparent GPP temperature response curve could be due to (1) environmental and/or (2) biological differences between B2 and natural forest sites. If environmental differences are the primary driver of the different apparent GPP temperature responses across sites, we would expect that models could represent cross-site variation in GPP temperature response curves using one common set of plant traits for all sites. If biological differences are the primary driver of the different apparent GPP temperature responses across sites, it would be necessary to vary plant traits across sites.

Our results indicate that we cannot currently distinguish between these two perspectives (Figure 2.3). Simulations using CLM suggest that the different apparent GPP temperature responses between the Biosphere 2 forest and the natural tropical forest sites can be explained by environmental differences, but only if both plant hydraulics and photosynthetic temperature acclimation processes are turned on. Considering only CLM simulations would therefore support the idea that $\text{CLM5}_{\text{AcclimAndHydro}}$ includes more realistic set of physiological rules than $\text{CLM5}_{\text{NoAcclimNoHydro}}$, because only $\text{CLM5}_{\text{AcclimAndHydro}}$ is able to capture the variation in GPP temperature responses across humidity gradients.

FATES simulations, however, support the alternative hypothesis that biological differences contribute to the different apparent GPP temperature responses across sites. In $\text{FATES}_{\text{AcclimAndHydro}}$,

environmental differences alone cannot explain the differences in apparent GPP temperature responses across sites because $\text{FATES}_{\text{AcclimAndHydro}}$ cannot capture the shallower temperature response curve at B2. However, $\text{FATES}_{\text{AcclimAndHydro}}$ can capture the variation in GPP temperature responses across sites if B2 trees have higher maximum hydraulic conductivity. This change reduces (but does not eliminate) large biases in FATES' modeled leaf water potential compared to observations (Figure A.6) and aligns with the fact that trees at B2 have lower wood density than most tropical trees, which is associated with higher maximum xylem conductivity (Christoffersen et al., 2016). Prior studies also suggest that the functional composition of B2 may differ from natural tropical forests. For example, over the last twenty years the percentage of trees at B2 that emit isoprene has increased (Taylor et al., 2018), which suggests a shift towards higher community-weighted photosynthetic rates at high temperatures (Taylor et al., 2019).

The different GPP responses between $\text{FATES}_{\text{AcclimAndHydro}}$ and $\text{CLM5}_{\text{AcclimAndHydro}}$ at B2 demonstrate that photosynthetic responses to temperature and VPD are not simply determined by whether or not models include plant hydraulics. The implementation of plant hydraulic processes (which differs between FATES and CLM) matters, as do the specific values of plant hydraulic traits. We also note that soil hydrology is important for capturing the temporal variation in plant leaf water potential, and can therefore also influence photosynthetic responses to VPD. The water transport through plants depends on soil water potential, so soil hydrology biases can lead to inaccurate leaf water potential and water fluxes (Ivanov et al., 2012; Restrepo-Coupe et al., 2017) even if models were to perfectly represent plant hydraulics.

2.4.4 Drivers of GPP variation on different timescales

Predicting tropical forest GPP responses to a warming climate will require understanding biotic and abiotic controls on photosynthesis across a range of timescales, from hours to centuries, and accurately representing these processes in models. This paper focuses on variation in hourly light-saturated GPP, which is the timescale at which land surface models are perhaps most likely to match observations because for several decades or more land surface models have represented instantaneous leaf-level responses to environmental conditions (Fisher and Koven 2020). The fact that structural assumptions not included in many land models can influence photosynthesis at

this timescale underscores the importance of doing this kind of test. Our model simulations did not represent temporal variation in leaf area, leaf age, or plant functional composition, which is a reasonable simplification for this study because on hourly timescales GPP is primarily driven by environmental rather than biotic variability (Wu et al., 2017). However, while the data is hourly, trends may in part be related to factors varying at seasonal timescales. For example, if GPP decreases with increasing temperature and the true driver of this relationship were soil moisture, that would be because higher temperatures are occurring during the dry season when soil moisture is lower, creating a spurious correlation that occurs over seasonal timescales.

Ultimately, however, it is necessary to compare models and observations at all timescales, and biotic variation is increasingly important when considering GPP variability beyond hourly timescales (Wu et al., 2017). Mechanistically representing the processes affecting canopy light-use efficiency, such as plant carbon allocation and leaf turnover, will be essential for capturing monthly and interannual GPP responses to temperature and VPD. Previous work has found that forest photosynthetic capacity increases in the dry season (Wu et al., 2017; Albert et al., 2018; Lopes et al., 2016; A. C. I. Tang et al., 2019), and that on monthly timescales VPD increases may increase photosynthesis by stimulating flushing of new leaves (Restrepo-Coupe et al., 2013). Additionally, representing how environmental change alters forest functional composition is an important process on decadal to centennial timescales.

A limitation of our modeling approach is that we represent each site using a single plant functional type, and therefore did not represent within-site functional diversity. Previous work has demonstrated that diversity in plant traits is an important control on ecosystem responses to water stress (Werner et al., 2021) and seasonal to interannual variation in ecosystem functioning (X. Xu et al., 2016). Our simulations also did not represent vertical variations in plant traits and forest microclimates, which previous work suggests is important for forest responses (M. N. Smith et al., 2019), but is often insufficiently represented in models (Vinod et al., 2023). We encourage future work to expand on this study by quantifying how functional diversity and seasonal to interannual biotic variations influence GPP responses to temperature and VPD effects at multiple timescales.

2.5 Conclusions

We demonstrate in this chapter that plant functional parameters and structural assumptions about photosynthetic temperature acclimation and plant hydraulics control the strength of temperature and VPD effects on tropical forest photosynthesis. This led us to identify a novel axis along which compensating errors can occur in models – models can match observed apparent ecosystem-level photosynthesis responses to temperature by excluding both processes (which yields stronger direct temperature effects) or by including both processes (which yields stronger VPD effects). However, these two sets of assumptions yield diverging predictions of ecosystem resilience to warming, underscoring the importance of improving our scientific understanding and model representations of these processes. This study also demonstrates the challenges of disentangling temperature vs. VPD effects from observational data alone. Developing further observational constraints on the partitioning between temperature vs. VPD influences in the historical period should be a future research priority, as should using those observational constraints to evaluate model performance.

Author Contributions

This chapter has been submitted for publication with co-authors Abigail L. S. Swann, Charles Koven, Marielle N. Smith, and Tyeen C. Taylor. CMZ, CDK, and ALSS conceptualized the research project, developed the methodology, and administered the project. ALSS and CDK supervised the project and provided computing resources. CMZ acquired the primary funding, ran model experiments, performed analysis, prepared visualizations, and wrote the original draft. ALSS, CDK, MNS, and TCT reviewed and edited writing. MNS and TCT collected observational data. CMZ and CDK developed code used in this research. CMZ, CDK, MNS, and TCT curated data.

Acknowledgements

CMZ was supported by the U.S. Department of Energy (DOE) Computational Science Graduate Fellowship (DE-SC0020347). ALSS and CMZ were supported by the DOE Regional and Global Model Analysis Program (DE-SC0021209) and the National Science Foundation (NSF) grant AGS-1553715 to the University of Washington. CDK was supported by the Next Generation Ecosystem Experiments-Tropics project, funded by the DOE, Office of Science, Office of Biological and En-

vironmental Research. MNS was supported by NSF DEB grant 1950080 to Michigan State University (MSU). TCT was supported by NSF grant 2111028 to the University of Michigan. We thank FLUXNET, Ameriflux, and Rafael Rosolem for providing publicly accessible net ecosystem exchange data and gap-filled meteorological data. We also thank all scientists, software engineers, and administrators who contributed to the development of FATES and CLM5.

Open Research

The original data for this study are all publicly available. The observational gap-filled meteorological data and net ecosystem exchange (NEE) data are available for K67 at `https://ameriflux.lbl.gov/sites/siteinfo/BR-Sa1`, and for B2 and MXTes at `https://github.com/m-n-smith/B2-temp-paper-datasets`. The output of all model simulations used in this paper is available in the Dryad Digital Repository at `https://doi.org/10.5061/dryad.wdbrv15w2`.

Chapter 3

LAND PROCESSES CAN SUBSTANTIALLY IMPACT THE MEAN CLIMATE STATE

Abstract

Terrestrial processes influence the atmosphere by controlling land-to-atmosphere fluxes of energy, water, and carbon. Prior research has demonstrated that parameter uncertainty drives uncertainty in land surface fluxes. However, the influence of land process uncertainty on the climate system remains underexplored. Here, we quantify how uncertainty in modeling land processes impact climate using a perturbed parameter ensemble for 18 land parameters in the Community Earth System Model (CESM2) under preindustrial conditions. We find that an observationally-informed range of land parameters generate biogeophysical feedbacks that significantly influence the mean climate state, largely by modifying evapotranspiration. The spread in global mean land surface temperature associated with the spread in land parameters is 2.2°C across our ensemble ($\sigma = 0.5$°C) and precipitation uncertainty is significant and spatially variable. Our analysis demonstrates that the impacts of land parameter uncertainty on surface fluxes propagates to the entire Earth system, and provides insights into where and how land process uncertainty influences climate.

Plain Language Summary

Land processes affect climate by controlling the transfer of energy and water from the land to the atmosphere. Previous research has shown that uncertainty in the representation of land processes (e.g. photosynthesis and the movement of water through soils) can drive uncertainty in land-to-atmosphere fluxes. However, it remains unclear how much that land uncertainty impacts climate. Here, we quantify the sensitivity in the mean climate to assumptions about land processes by varying 18 land model parameters to create an ensemble of 36 possible worlds in a global climate model. Global mean land temperature differs by up to 2.2°C across this ensemble, mostly due

to changes in how much water is evaporated from the land surface. Changing land parameters also drives regionally variable changes in mean precipitation. This study highlights a large and underappreciated impact of land processes on the mean climate state, and provides insights into how climate is influenced by land process uncertainty.

Key Points

- Assumptions about land processes substantially impact the climatological mean state terrestrial temperature and precipitation.
- Land parameters influence climate predominantly through changing evapotranspiration.
- Warming driven by land processes activates different atmospheric feedbacks than radiatively-driven warming.

3.1 Introduction

Land models were initially developed to support weather and climate prediction by providing atmospheric models with lower boundary conditions of energy, water, and momentum fluxes. Given this limited scope, early land models were simple biogeophysical models, in which land-to-atmosphere fluxes were determined by prescribed land surface albedo, evaporative resistance, and roughness (Manabe, 1969). Since then, land models have substantially expanded in scope and complexity. Modern land models now represent biogeochemical cycling, hydrology, ecology, land use, and land management, and are used to predict how processes across these domains interact and respond to global change (Fisher & Koven, 2020). This evolution has been accompanied by an increase in the number of model parameters, many of which can influence land-to-atmosphere fluxes by altering the emergent land surface albedo, turbulent fluxes of water and heat, and roughness.

The increasingly complex land model parameter space has driven a large body of research exploring the implications of land parameter uncertainty for land model calibration (Dagon et al., 2020), carbon and water flux uncertainty quantification (Hou et al., 2012; McNeall et al., 2023), and process understanding (Boulton et al., 2017). Earth system parametric uncertainty is often quantified through perturbed parameter ensembles (PPEs), in which multiple poorly constrained parameters are systematically varied within a single model structure. Land PPEs have demon-

strated that parameter uncertainty is a major driver of uncertainty in land-to-atmosphere surface heat and moisture fluxes, at local (Ricciuto et al., 2018; Fisher et al., 2019), regional (Bauerle et al., 2014; Huo et al., 2019), and global scales (Dagon et al., 2020; Zaehle et al., 2005).

Most existing land parameter uncertainty studies have quantified parameters' impact in a land-only framework (Zaehle et al., 2005; Dagon et al., 2020; Ricciuto et al., 2018; Bauerle et al., 2014; Fisher et al., 2019; Dietze et al., 2014; Bauerle et al., 2014), where the atmospheric forcing is an external boundary condition and land surface fluxes do not influence the atmosphere. Only a handful of previous studies have assessed the biogeophysical (Liu et al., 2005; Fischer et al., 2011; Williams et al., 2016) or carbon cycle (Booth et al., 2012, 2017; L. R. Hawkins et al., 2019; McNeall et al., 2023) implications of land parameter uncertainty in a coupled context, or included land parameters in PPEs perturbing parameters across the Earth system (Sexton et al., 2021; Yamazaki et al., 2021). This is in part due to computing constraints. For example, in the Community Earth System Model version 2 (CESM2), a simulation with a dynamic atmosphere requires about ten times more computing time per modeled year than a land-only simulation, and coupled configurations often require more simulated years to establish a signal due to internal variability of the coupled system. Additionally, the prevalence of land-only analyses reflects the land modeling community's focus on how land parameter uncertainty influences terrestrial processes, rather than atmospheric processes. The biogeophysical impact of land parameter uncertainty on atmospheric processes and land-atmosphere interactions remains underexplored. Of the few studies which have assessed land parameter uncertainty in a coupled context, only one has quantified the biogeophysical impact of land parameters on climate globally (Fischer et al., 2011).

This is a problematic gap in the literature because the documented impact of land parameter uncertainty on surface energy fluxes suggests that land parameters influence the mean climate state. It has been established for decades that changes in land surface albedo (Charney et al., 1975; Charney, 1975; Charney et al., 1977), roughness (Sud et al., 1988; White et al., 2021), and capacity to evaporate water (Shukla & Mintz, 1982) can alter temperature and precipitation on global scales. More recently, Laguë et al. (2019) used a modern Earth system model to show that atmospheric feedbacks are critical in determining how land temperatures respond to idealized land surface changes. Extensive previous work has demonstrated that changes in land cover can drive local, regional, and remote climate impacts (e.g. Pongratz et al., 2010; Swann et al., 2012; Boysen

et al., 2020). Additionally, changing land model representations of terrestrial processes such as stomatal conductance and soil hydrology can influence the mean climate state (Lawrence et al., 2007) and frequency of extremes (Kala et al., 2016).

In this study, we aim to close this gap in the literature by using a coupled PPE to address the following questions: (1) to what extent can land parameters impact the mean climate state? and (2) through what mechanisms do land parameters influence climate?

3.2 Methods

3.2.1 Model configuration

We ran PPEs under preindustrial conditions using two configurations of CESM2 (Bitz et al., 2012; Danabasoglu et al., 2020): a coupled configuration ("coupled") and an uncoupled, land only configuration ("land-only"). In both the coupled and land-only PPE, the land model (the Community Land Model version 5, CLM5; Lawrence et al., 2019) was run with prognostic leaf area. In the coupled ensemble, we ran preindustrial simulations with constant greenhouse gas concentrations using an active atmosphere (CAM6; Bogenschutz et al., 2018) and a slab ocean (Danabasoglu & Gent, 2009). Because these simulations have fixed concentrations of greenhouse gasses including CO_2, they capture the biogeophysical impacts of land parameters which is the focus of this paper, but they do not capture biogeochemical feedbacks. The land-only simulations used a custom atmospheric forcing, which was generated by CAM6 in the reference coupled simulation that used default parameters.

Simulations were run using the `branch_tags/PPE.n11_ctsm5.1.dev030` tag for the Community Land Model version 5 (CLM5; Lawrence et al., 2019) and the `cesm2.2.0` tag for all other model components. The land was initialized with the spun-up land state from the default model parameterization which includes the carbon content of soil and vegetation pools. The coupled simulations use the Community Atmosphere Model 6 (CAM6; Bogenschutz et al., 2018), and a slab ocean (Danabasoglu & Gent, 2009) which is based on q-fluxes from preindustrial simulations of the full dynamic ocean model; we did not apply flux corrections. We note that the top of atmosphere energy imbalance is relatively small and changes minimally across the PPE (average=-0.157 W/m^2, σ=0.010 W/m^2; Figure B.1).

Each parameter perturbation simulation, which we refer to as an ensemble member, was run for 140 years under constant preindustrial greenhouse gas concentrations and land use conditions. The first 40 years were discarded as spin up, which is long enough for fast atmospheric processes, leaf area, soil moisture and temperature, and the surface ocean to largely equilibrate (Figure B.2).

3.2.2 Perturbed parameter ensemble design

Our PPEs sampled 18 land parameters (Table B.1), and our parameter selection was informed by the CLM5 PPE project (data and methods description are available via `https://github.com/djk2120/clm5ppe`). The CLM5 PPE differs from ours in that the simulations were run in a land-only configuration forced with observationally-derived atmospheric data for present-day. Nonetheless, the one-at-a-time parameter perturbations provide insight into which parameters might be meaningful for our coupled PPE. We used two parameter selection criteria: (1) that parameters would likely have a large impact on the atmosphere, based on results from the CLM5 PPE, and (2) that parameters spanned different functional areas of the model.

For our first criterion, we ranked all parameters based on multiple metrics of land-to-atmosphere fluxes (Table B.2, Table B.3), globally and for individual biomes, focusing on the quantities that the land model passes to the atmosphere model in CESM2 (Table B.4). We quantified parameters impact on individual biomes by classifying the land surface into the nine Whittaker biomes (Whittaker, 1975) and ice sheets based on each grid cell's mean precipitation and temperature (Table B.5). Out of 205 total parameters, we identified 40 parameters that appeared in the top five for more than five rankings. For our second criterion, we then grouped those top 40 parameters into functional categories, and we selected 18 parameters such that we did not sample more than four parameters from any given functional category. The 18 parameters we selected are described in detail in Table B.1 and span nine functional categories: soil hydrology, stomatal conductance and plant water use, snow, photosynthesis, boundary layer / roughness, radiation, canopy evaporation, biomass heat storage, and temperature acclimation.

For each parameter, we ran two simulations, where the parameter was perturbed to a minimum and maximum value (ensemble n = 36). We used the parameter ranges from the CLM5 PPE, which were determined by domain-area experts based on literature review and expert judgement. Because

some parameters have larger ranges than others, our analysis includes both the sensitivity of the climate system to a change in a parameter combined with the uncertainty in that parameter's range. We note that this one-at-a-time sampling procedure does not account for parameter interactions, though we expect that parameter interactions may be of second-order importance based on Fischer et al. (2011) who finds that nonlinear interactions between parameters were minimal in a stationary climate.

3.3 Results and Discussion

3.3.1 Mean temperature changes

Our ensemble demonstrates that land parameters can substantially impact the mean climate state. Global annual mean land surface temperatures range by 2.2°C across our coupled PPE ($\sigma = 0.5$°C), and by over 3°C at some latitudes ($\sigma > 0.65$°C above 67°N; Figure 3.1a). Seven out of 18 parameters generated a greater than 1°C temperature range (Figure 3.1b), and more than 70% of the land surface experienced statistically significant changes from the control climate in annual mean temperature in 20 out of the 36 ensemble members (Figure B.3). Global mean surface temperatures (including ocean) ranged by 1.1°C ($\sigma = 0.5$°C; Figure B.4-B.5), which is over 40% of the preindustrial absolute temperature range in CMIP6 (2.4°C, σ=0.58°C; Tett et al., 2022) and CMIP5 (E. Hawkins & Sutton, 2016). Three soil hydrology parameters - `frac_sat_soil_dsl_init`, `d_max`, and `fff` - had the largest impact on global mean temperature. Land surface temperature changes in the land-only PPE were generally much smaller than those in the coupled PPE (Figure 3.1), consistent with the fact that atmospheric feedbacks substantially amplify the land surface temperature response to changing land surface properties (Laguë et al., 2019).

Parameters generally impacted surface temperature with a similar spatial pattern globally. The leading pattern of temperature change, as quantified by the first empirical orthogonal function (EOF; Lorenz, 1956) of annual mean surface temperature changes, explains 78% of the variance across our coupled ensemble (Figure 3.2a, Figure B.6) and is highly correlated with the global average mean land temperature change (Figure B.7). As expected, the leading EOF in the land-only ensemble explains less of the temperature variance and has a different spatial pattern (Figure 3.2b), indicating that regional to global-scale atmospheric responses contribute to the consistent

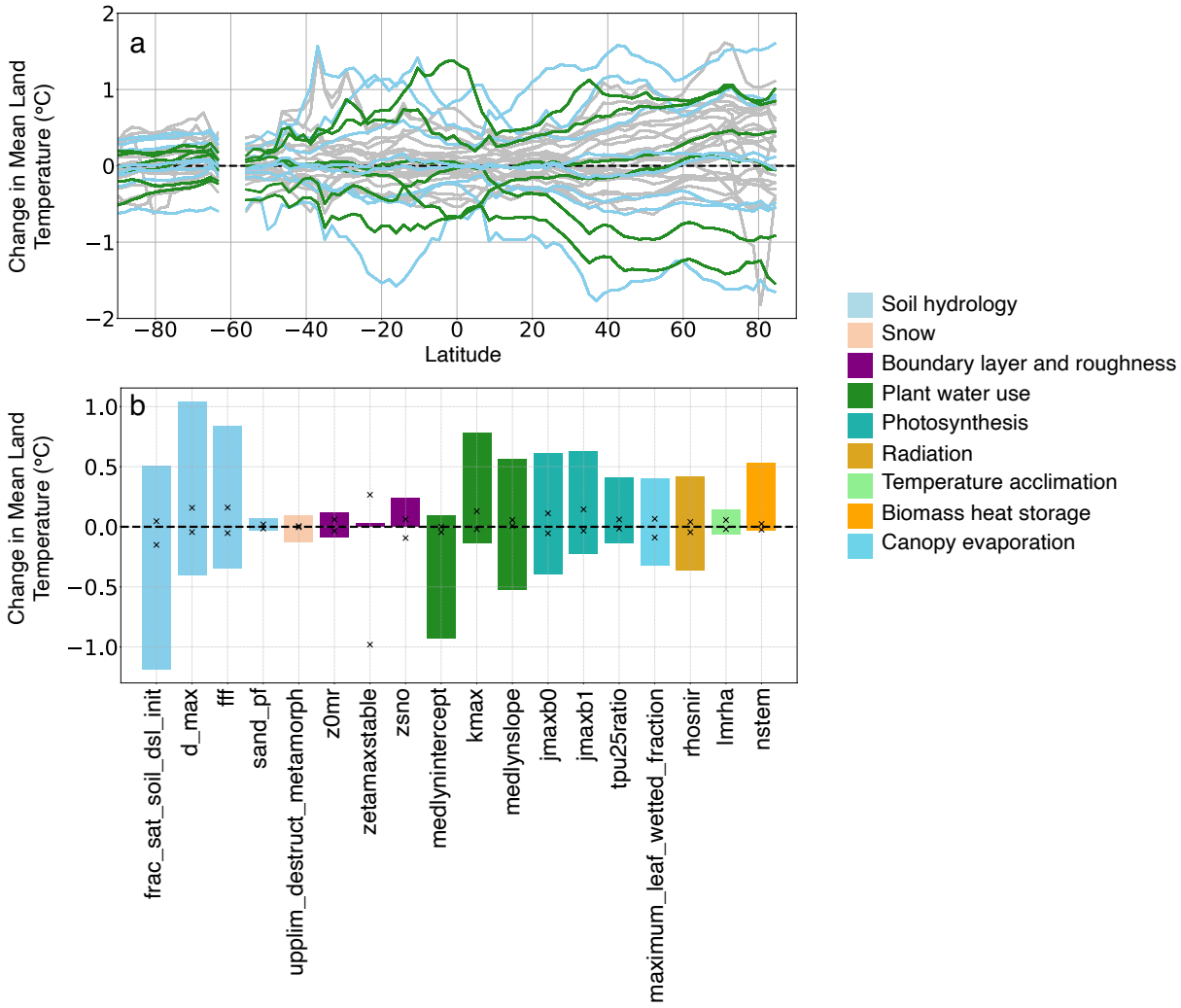

Figure 3.1: Zonal mean (a) and global mean (b) changes in annual land temperature across the coupled PPE, relative to the default simulation. Color indicates parameter category, and only ensemble members perturbing soil hydrology and plant water use parameters are colored in (a). In (b), bars indicate the range of coupled global mean land surface temperature changes associated with each parameter, and Xs mark the range of land-only global mean land surface temperature changes.

coupled PPE pattern of temperature change because the atmospheric motions act to diffuse regional anomalies (in effect, averaging the disparate regional responses). Notably, the leading coupled PPE EOF differs from the typical pattern of radiatively driven warming (e.g. CO_2-driven warming, Figure 3.2c and Appendix B.1), a pattern which is generally consistent across climate models (Proistosescu et al. 2020). This indicates that the dominant coupled spatial pattern is not only due to parameter-driven temperature changes kicking off radiative feedbacks (e.g. ice albedo feedback, water vapor feedback) which have consistent spatial fingerprints. Rather, this suggests that land parameter uncertainty drives a consistent temperature response pattern, despite the fact that parameters influence different terrestrial processes.

The dominant coupled PPE temperature pattern is characterized by temperature sensitivity hotspots in the grassland ecosystems of both North America and eastern Europe / central Asia, and larger temperature changes in the Northern Hemisphere than the Southern Hemisphere. Across the tropics, the temperature response is larger in South America than in tropical Africa or Asia. This pattern resembles the summer temperature response to soil moisture forcing in the Global Land-Atmosphere Climate Experiment (GLACE) experiments (Koster et al., 2006; Seneviratne et al., 2013) which we discuss further in section 3.3. The hemispheric asymmetry of the land parameter temperature pattern reflects the higher land fraction in the Northern Hemisphere, and land perturbations have a larger impact on climate in zonal bands with higher land fraction (Laguë et al., 2021), noting that these are for land-only zonal means and thus already take into account zonal variation in land fraction. Fischer et al. (2011)'s land PPE also generated larger land temperature changes in the Northern Hemisphere than in the Southern Hemisphere, but in Fischer et al. high latitude temperature changes were driven mainly by model sensitivity to snow albedo, while in our PPE most parameters drive high latitude temperature changes. Our PPE generated a larger temperature range than Fischer et al., perhaps in part due to the fact that Fischer et al. used a different slab ocean configuration in their simulations.

3.3.2 Mean precipitation changes

We found that terrestrial precipitation is highly sensitive to land parameter choice. Global annual land mean precipitation ranged by about 5% (σ= 1%) across our ensemble, and in several regions our

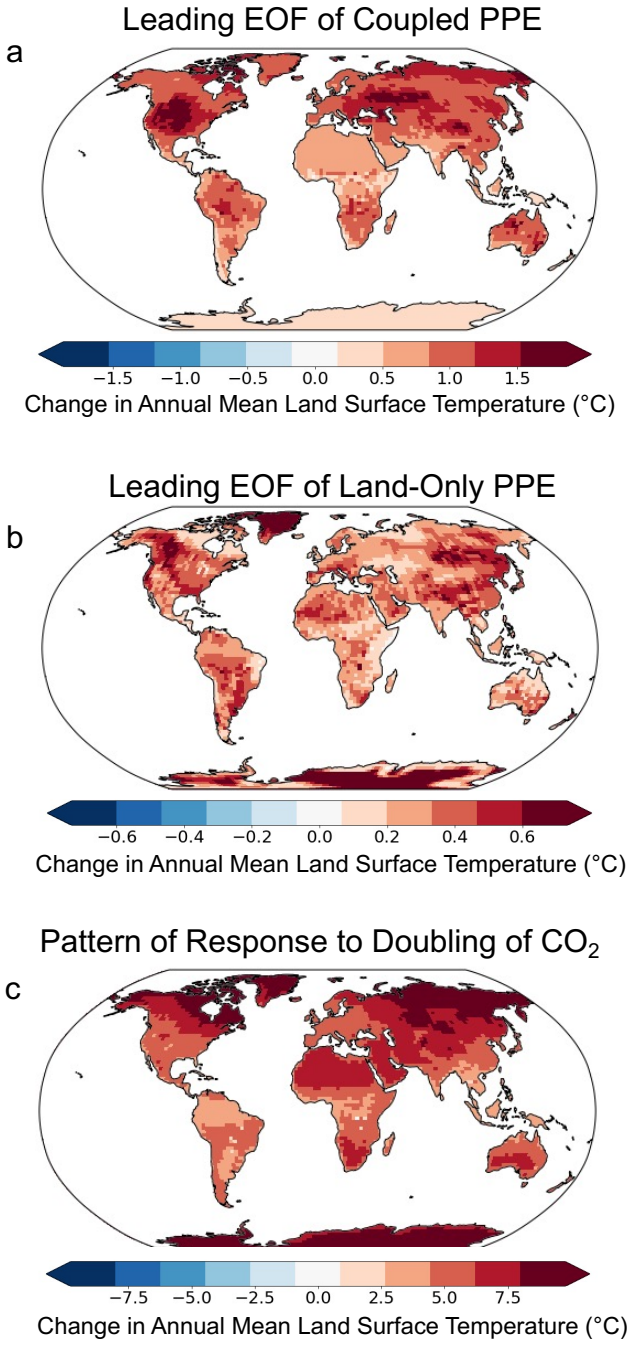

Figure 3.2: Spatial patterns of annual mean temperature change. The leading EOF of annual mean temperature change across (a) the coupled PPE and (b) the land-only PPE explain 78% and 65% of the variance across the coupled and land-only PPEs, respectively. The EOFs are scaled to depict two standard deviations of the variation across the ensemble along that mode of variability. The bottom panel (c) shows the CESM slab ocean model pattern of warming due to a doubling of CO_2 (B.1).

PPE drove annual mean precipitation changes of greater than 30% (Figure 3.3a). The same three soil hydrology parameters which most changed global mean temperature—`frac_sat_soil_dsl_init`, `d_max`, and `fff`—also had the largest impact on precipitation. These three hydrology parameters also generated the most extensive spatial coverage of statistically significant annual mean precipitation changes (Figure B.8). Across the PPE, less of the land surface experienced statistically significant changes in annual mean precipitation compared to statistically significant changes in mean temperature (Figures B.9, B.10).

Changing parameters drove spatially variable signs of precipitation change, in contrast to mostly consistent signs of temperature change globally (Figure B.11). Similarly, while there was a single dominant temperature response pattern across our PPE, the patterns of annual mean precipitation changes were less consistent across ensemble members. The leading EOF of precipitation change explained 48% of the variance across the PPE (Figure 3.3, B.12) compared to the 78% temperature variance explained. This aligns with the fact that precipitation is generally more variable over time than temperature, and some of the variance across the ensemble is likely due to internal variability. Nonetheless, our PPE identified several hotspots where precipitation is sensitive to land parameter choice. In particular the North American Great Plains again emerged as a hotspot when considering precipitation changes on both a percentage (Figure 3.3a) and absolute (Figure B.13) basis.

Surprisingly, precipitation in the Great Plains region was not especially sensitive to land parameters in Fischer et al. (2011). However, this region has been identified as a land-atmosphere coupling hotspot due to soil moisture feedbacks in both modeling (Koster et al., 2006; Santanello et al., 2018; Zheng et al., 2015) and observational (Ferguson et al., 2012; Abdolghafoorian & Dirmeyer, 2021) studies. Many land-atmosphere studies use metrics that quantify covariances of surface fluxes and the land and atmospheric state on daily timescales. Here we are quantifying how land assumptions influence annual mean climatological precipitation rather than daily precipitation variability, but this spatial correspondence suggests that changing land parameters may influence long-term climate through mechanisms similar to the soil moisture feedbacks that drive land-atmosphere coupling on daily timescales.

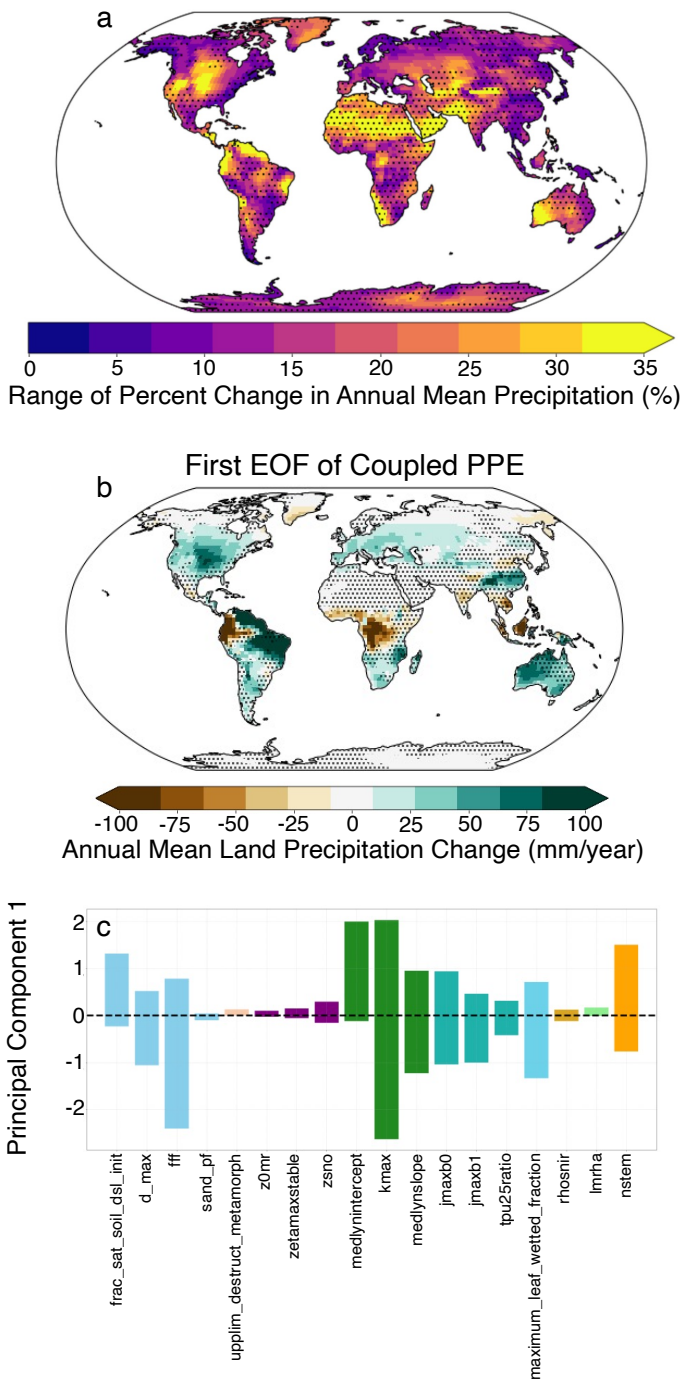

Figure 3.3: Range of annual mean land precipitation change across the coupled PPE. (a) Map of the range of percent changes in annual mean precipitation across the ensemble. Stippling indicates regions where precipitation changes were not statistically significant for 31 out of 36 ensemble members. (b) First EOF of precipitation changes across the coupled PPE. (c) Principal component 1 across parameters. Colors in (c) indicate parameter category as in Figure 3.1.

3.3.3 Mechanisms through which land parameters influence climate

Parameters relating to soil hydrology and plant water use drove the largest temperature and precipitation changes in our ensemble (Figure 3.1b, 3.3c), highlighting that hydrological processes play a critical role in determining land temperature and precipitation. We note that we purposefully chose parameters across a range of model components and that soil hydrology parameters did not dominate the land-only CLM5 PPE rankings of parameters with the largest impact on global temperature (Table B.5), so we did not expect a priori that hydrological processes would dominate the temperature response. We also found that multiple parameters typically evaluated in the context of biogeochemical rather than biogeophysical impacts (e.g., `jmaxb0`, the baseline proportion of nitrogen allocated for electron transport; `jmaxb1` the response of the electron transport rate to light availability) can still generate large climate responses through biogeophysical pathways, consistent with prior work (N. G. Smith et al., 2017). We note that the large climate responses reflect both the climate sensitivity to a change in a parameter and the magnitude of the parameter ranges we tested. Parameters that influence boundary layer processes and roughness length drove the smallest global mean temperature changes, but they generated significant local temperature and precipitation changes, particularly over ice sheets and snow-covered regions (Figure B.3).

It is challenging to fully disentangle the pathways through which parameters influence climate because land parameters alter multiple land surface properties simultaneously. For example, increasing the parameter `kmax`, which sets the maximum plant hydraulic conductance, simultaneously changes the land surface evaporative resistance, albedo, and aerodynamic roughness, all of which influence temperature through different mechanisms. Increasing `kmax` decreases evaporative resistance by increasing the rate at which plants can transpire water, which decreases land temperatures. In regions with abundant soil moisture, increasing `kmax` also decreases plant water stress and increases leaf area, which changes albedo and thereby temperature. Increased photosynthetic rates due to reduced plant water stress also increases vegetation height, which can increase aerodynamic roughness, driving further cooling.

We used multiple linear regression to disentangle the extent to which land precipitation and temperature changes across our coupled PPE are driven by three land surface properties: albedo (α), evaporative fraction (EF), and a measure of aerodynamic coupling (r_a) (Appendix B.2). We

note that we use the term "land surface properties" to refer to these emergent properties of the land surface that directly influence land-to-atmosphere energy and water fluxes, as opposed to "parameters" which are values that are directly encoded in equations representing specific terrestrial processes in the land model. We use albedo, evaporative fraction, and aerodynamic coupling as predictors in our analysis because those are the primary mechanisms through which land surface changes can impact the atmosphere. Our analysis further emphasizes that evapotranspiration changes dominate the spread in land surface temperature and precipitation responses across our PPE. Changes in evaporative fraction explained the most variance across our ensemble, with albedo playing a secondary role (Figure 3.4). Coupled temperature changes due to changes in aerodynamic coupling were minimal. The dominance of the evapotranspiration mechanism in our PPE may in part be due to the subset of parameters we selected from the 40 top parameters identified based on CLM5-PPE output. Nonetheless, our results demonstrate that land parameters' influence on evapotranspiration is an important (and potentially the dominant) mechanism whereby which land parameters influence the mean climate state.

Further, the dominance of the evapotranspiration mechanism across our ensemble may explain why the leading EOF explains such a high percentage of temperature change variance, and why temperature and precipitation changes are correlated with each other (see, e.g., Figures B.6, B.7, and B.12). While we initially designed the PPE to sample multiple processes across CLM's high-dimensional parameter space (including photosynthesis, snow processes, radiation, etc.), parameters mainly impacted surface climate through changes in evapotranspiration, resulting in an ultimately low-dimensional ensemble of climate responses. We hypothesize that the leading EOFs of temperature and precipitation changes capture the atmospheric response to land evapotranspiration changes, which is supported by the strong correlation between land-only changes in evaporative fraction and the leading coupled temperature and precipitation EOFs (Figure B.14). The spatial correspondence of mean climate changes between our PPE and GLACE experiments (Seneviratne et al., 2013) further supports this interpretation, because in GLACE experiments soil moisture forcing is also influencing climate by modifying turbulent fluxes. However, we note that the climate responses in our PPE are not directly driven by soil moisture changes. Rather, land parameter perturbations influence land evaporative resistance, which directly influences land evapotranspiration independently of any soil moisture change. That land evapotranspiration change (and associated

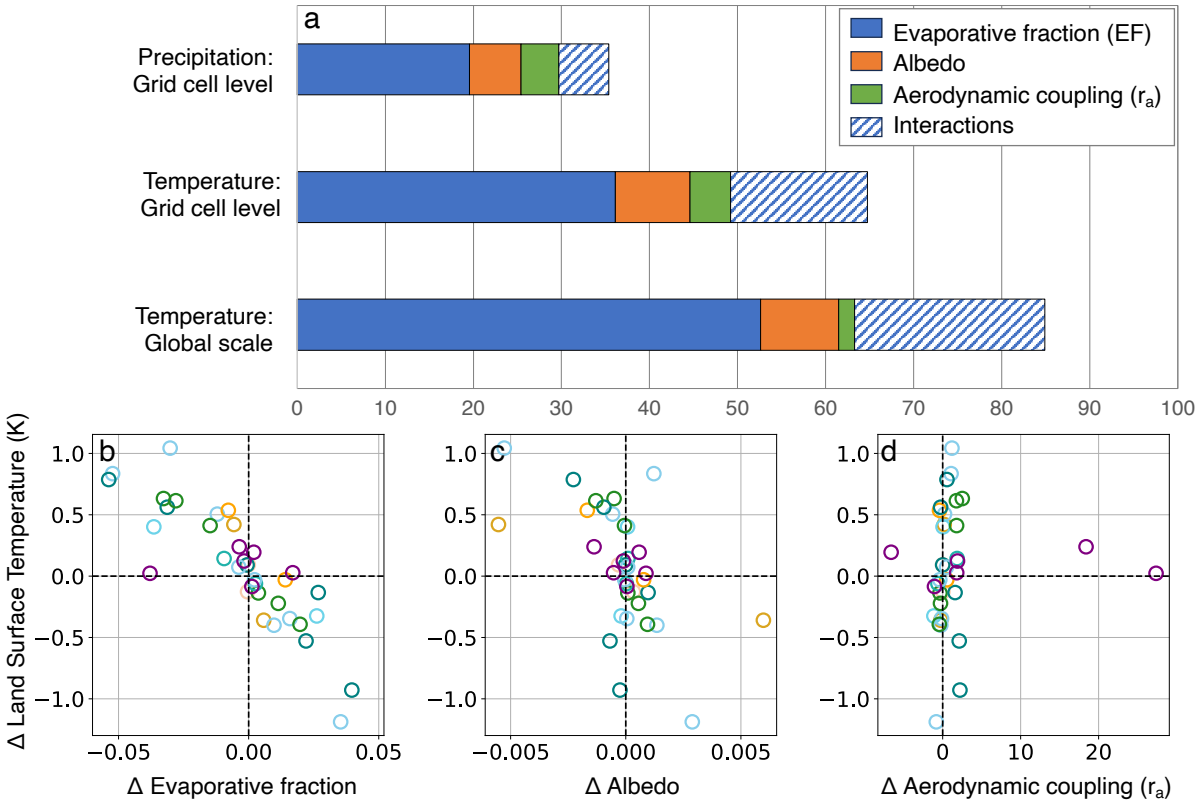

Figure 3.4: Relationship between land-only surface property changes and coupled land surface climate changes. The top panel (a) shows the percent variance of temperature and precipitation changes explained by each land surface property based on multiple linear regression at the grid cell level, and at the global scale for temperature. Solid colors indicate the marginal additional percentage of variance explained by each land surface property when all other predictors are included, and the hatched bar indicates the percentage variance explained by multiple predictors (i.e. the covariance between predictors). The bottom panel shows the relationships between global mean coupled land surface temperature change and land-only change in (b) evaporative fraction, (c) albedo, and (d) aerodynamic resistance across all ensemble members. Colors indicated parameter category, as in Figure 3.1.

climate feedbacks) can in turn influence soil moisture, but in our experimental design soil moisture changes are an effect or feedback, rather than an external forcing.

It has long been recognized that changes in soil moisture and evaporative resistance can impact climate (Shukla & Mintz, 1982; Sellers et al., 1996; Seneviratne et al., 2013; Laguë et al., 2019), but this is the first study to our knowledge that quantifies how parameter uncertainty associated with terrestrial controls on evapotranspiration impacts mean climate, and compares the impact of the evapotranspiration mechanism to other land surface property changes. For example, the only previous study that quantified the global biogeophysical impact of land parameter uncertainty (Fischer et al., 2011) did not evaluate the relative impact of evapotranspiration, albedo, and aerodynamic resistance changes on climate. Leveraging the results of the land-only CLM5-PPE enabled us to take a more systematic approach to parameter selection, yielding new insights which may not have emerged had we chosen parameters based on our own assumptions or prior work. This highlights the value of projects that systematically quantify and report parameter uncertainty in land models (e.g. the CLM5 PPE), which we encourage land modeling groups to incorporate as a standard part of model development and documentation efforts. This study also underscores the importance of developing better observational constraints for land parameters which influence evapotranspiration.

3.4 Conclusions

This study highlights a large and underappreciated impact of land processes in determining the mean climate state. We used a PPE to quantify the biogeophysical impact of land parameters on terrestrial climate. We found that land parameters can substantially impact mean temperature and precipitation, primarily through parameters' influence on evapotranspiration, and that uncertainty associated with soil hydrology and plant water use parameters drive the largest spread in the mean climate state. Uncertainty in land models' representation of land surface fluxes stems from multiple sources: internal variability, model structure, and model parameters. This study focuses on the effect of land parametric uncertainty, but our results demonstrate the importance of land process uncertainty more generally because both model structure and parameters control the land surface properties (e.g., evaporative resistance) that ultimately influence climate.

Biases in land evapotranspiration have been invoked as possible drivers for several persistent

ESM biases (e.g., the central United States warm and dry summer biases, Klein et al., 2006; Cheruy et al., 2014; Williams et al., 2016; Y. Lin et al., 2017; Morcrette et al., 2018; Zhang et al., 2018; Ma et al., 2018; Mueller & Seneviratne, 2014), and this work directly shows how land assumptions can influence the mean climate at regional and global scales, demonstrating the importance of including land perspectives in the assessments of model biases. Additionally, this study underscores that land processes primarily discussed in the context of carbon cycle uncertainty (e.g. photosynthesis) can have large biogeophysical impacts on the physical climate, in addition to their influence on atmospheric CO_2 concentration.

There has been a concerted effort across climate modeling centers to create 'digital twins' of the Earth (e.g., Voosen, 2020; X. Li et al., 2023) by increasing climate model resolution, thereby enabling direct modeling of fine-scale atmospheric processes such as convection that are subgrid-scale parameterizations in coarser scale models (Betancourt, 2022). While increased resolution will likely diminish biases associated with some atmospheric processes, increased resolution does less to improve land process representation because many land processes occur at molecular to hillslope scales and therefore will continue to require subgrid parameterizations (Fisher & Koven, 2020; Reichstein et al., 2019; Balaji et al., 2022). Further, finite computational resources imply tradeoffs between increasing resolution and the number of ensembles to quantify parameter uncertainty and calibrate models. If atmospheric-focused model advancements are not accompanied by efforts to improve land models, land parameter uncertainty may remain a persistent driver of climatological uncertainty and biases, even in the next generation of high-resolution climate models. Recognizing that land process uncertainty influences climate also presents an opportunity for model improvement. The climate modeling community has historically devoted more effort to atmospheric uncertainty than to land uncertainty (Hourdin et al., 2017). We hypothesize that committing comparable resources to land parameter calibration could drive rapid improvements in model representation of present-day climate.

By demonstrating that land parameters influence the mean climate state, we hope that this study will stimulate further research into the climate impacts of land process uncertainty by a broader geophysical research community. In particular, our results suggest there is potential for land parameter uncertainty to influence the sensitivity of land temperature trends to historical and future climate forcing, and we plan to test this in future work. Because the evaporative fraction

influences how much the land surface warms in response to radiative forcing, we hypothesize that changing parameters that influence the baseline evaporative fraction will influence the modeled trajectory of land surface temperatures under increasing greenhouse gas concentrations, even if the evaporative fraction were to remain constant over time. Furthermore, land processes influence how the evaporative fraction changes over time, for example due to plant physiological responses to CO_2 (Lemordant et al., 2018). Quantifying how land parameter uncertainty influences future land temperature trajectories should be a high research priority.

While land modeling has substantially expanded beyond its initial scope of providing lower atmospheric boundary conditions into its own subdiscipline and research community, land models' continued role as atmospheric boundary conditions means that a broader climate science community must engage with land processes (and uncertainty therein) in order to understand and model the physical climate system.

Author Contributions

This chapter is in revision at Geophysical Research Letters with co-authors Daniel Kennedy, Katherine Dagon, David M. Lawrence, Amy Liu, Gordon Bonan, Charles D. Koven, Danica Lombardozzi, and Abigail L. S. Swann. CMZ and ALSS conceptualized the research project and administered the project. CMZ and ALSS developed the methodology, in consultation with DK, KD, and DML. CMZ acquired the primary funding, ran model experiments, performed analysis, curated data, prepared visualizations, and wrote the original draft. ALSS supervised the project and provided computing resources. CMZ, DK, and KD developed analysis code used in this research. DK, KD, DML, AL, GB, CDK, DL, and ALSS reviewed and edited writing.

Acknowledgements

CMZ was supported by the U.S. Department of Energy (DOE) Computational Science Graduate Fellowship (DE-SC0020347). The DOE Office of Biological and Environmental Research Regional and Global Model Analysis Program supported ALSS, AL, and CMZ (DE-SC0021209); KD (DE-SC0022070); and CDK and DML (DE-AC02-05CH11231 through the RUBISCO SFA). The National Science Foundation (NSF) also supported ALSS and CMZ (AGS-1553715) and KD (NSF IA

1947282). The CESM project is supported primarily by the NSF. This material is based upon work supported by the National Center for Atmospheric Research, which is a major facility sponsored by the NSF under Cooperative Agreement No. 1852977. The Computational and Information Systems Laboratory at NCAR provided computing and data storage resources, including the Cheyenne supercomputer (https://doi.org/10.5065/D6RX99HX). We thank all scientists, software engineers, and administrators who contributed to CESM2's development.

Open Research

The model output used in this paper is available via the Dryad Digital Repository (doi:10.5061/dryad.0k6djhb73; private peer review link: https://datadryad.org/stash/share/RGub3FTU5e5U5bLCB9bZTf96oz66ffR5DBgD3h-tGHk). Code used to run simulations and analyze model output are available at https://github.com/czarakas/coupled_PPE.

Chapter 4

ATMOSPHERIC FEEDBACKS MODULATE CHANGES IN LAND WATER AND CARBON FLUXES

Abstract

Terrestrial processes such as photosynthesis and the movement of water through soils can influence climate from local to global scales by controlling land-to-atmosphere fluxes of water, energy, and carbon. Terrestrial processes are also influenced by climate, as demonstrated by the large body of research exploring how the terrestrial water and carbon cycles respond to climate change. Biogeophysical land-atmosphere feedbacks can therefore potentially modulate changes in land surface water and carbon fluxes. However, the influence of land-atmosphere feedbacks on terrestrial processes has been underexplored. We use a novel experimental design of paired perturbed parameter ensembles (PPEs) to isolate the extent to which atmospheric feedbacks modulate land parameters' impact on the global water and carbon cycles. We perturb 18 land parameters spanning a wide range of terrestrial processes in two PPEs: one where the atmosphere can respond to land surface changes, and one where the land is forced with a fixed atmosphere. We found that atmospheric feedbacks' influence on evapotranspiration depends on the climatological moisture regime: atmospheric feedbacks dampen evapotranspiration changes in wet regions but amplify evapotranspiration changes in some dry regions. Land-atmosphere feedbacks do not consistently amplify or dampen photosynthesis changes, but we identified regional hotspots where land-atmosphere feedbacks have a larger impact on photosynthesis. Our analysis provides insights into where and how atmospheric feedbacks modulate terrestrial processes, posing a challenge to the widespread practice of developing and evaluating land models in an uncoupled configuration and then deploying them to understand and predict terrestrial processes in a coupled context.

4.1 Introduction

Terrestrial processes such as photosynthesis and the movement of water through soils influence climate from local to global scales by modifying land-to-atmosphere fluxes of water, energy, and momentum. These processes are also directly influenced by climate, due to their dependence on air temperature, relative humidity, net radiation, and soil moisture. The land and atmosphere are therefore a coupled system, in which biogeophysical land-atmosphere feedbacks can potentially modulate changes in land surface water and carbon fluxes. An extensive body of literature has long established mechanisms through which land processes impact the atmosphere (i.e., the land-to-atmosphere branch of this coupled system), as well as how the atmosphere impacts land water and carbon fluxes (i.e., the atmosphere-to-land branch). However, the impact of coupled feedbacks in modulating changes in land water and carbon fluxes remains underexplored.

In the atmosphere-to-land branch of the coupled system, it has been long established that climate is a primary control on evapotranspiration (ET) and photosynthetic rates. Evapotranspiration is fundamentally limited by terrestrial water availability and the atmospheric demand for water (Budyko, 1974), which are determined by soil moisture (and therefore precipitation), near-surface vapor pressure deficit (which is a function of temperature and relative humidity), and net radiation at the land surface. Similarly, it is long established that on short timescales photosynthetic rates vary with air temperature, vapor pressure deficit, and soil moisture. On longer timescales, climate is the dominant filter on where different plant types grow (Whittaker, 1975). This climate sensitivity of the terrestrial water and carbon cycles has stimulated an entire field of global change research that seeks to understand how the water and carbon cycles respond to modern climate change.

In the land-to-atmosphere branch of this coupled system, it has similarly long been recognized that land surface water and energy fluxes exert a strong control on Earth's physical climate, stemming back to Shukla & Mintz (1982). Since then, multiple studies have demonstrated that changing biogeophysical land surface properties can impact air temperature (Sellers et al., 1996), precipitation (Kooperman et al., 2018; Saint-Lu et al., 2019), relative humidity (Lemordant et al., 2018), and cloud cover (Zarakas et al., 2020; Kim et al., 2020; Teuling et al., 2017). Idealized model experiments have found that decreasing evapotranspiration drives substantial global warming (Laguë et al., 2019; Kong et al., 2023), changes in the spatial distribution of precipitation (Pietschnig et

al., 2021), and changes in shortwave and longwave radiative fluxes due to changes in cloud cover and air temperature (Kong et al., 2023). Model analysis of the biogeophysical impacts of plant physiological responses to CO_2 similarly indicate that physiologically driven evapotranspiration declines lead to warming (Zarakas et al., 2020), decreases in relative humidity (Lemordant et al., 2018), zonally asymmetric changes in tropical precipitation (Kooperman et al., 2018), and decreases in cloud cover (Park et al., 2021). An extensive body of literature on the impacts of changes in vegetation cover provide further evidence of land surface biogeophysical impacts on atmospheric processes, in both modeling (Pongratz et al., 2010; Swann et al., 2012; Boysen et al., 2020) and observational (Teuling et al., 2017) studies, though such studies typically do not disentangle the impact of changing evapotranspiration from changing albedo and land surface roughness.

The fact that so many studies have identified strong land-to-atmosphere and atmosphere-to-land branches of the coupled land-atmosphere system suggest a potential for land-atmosphere feedbacks to further modulate changes in land surface water and carbon fluxes. However, the atmosphere's role in modulating land-driven changes in water and carbon fluxes remains unquantified on a global scale. Most previous studies evaluate the biogeophysical impact of land surface changes either in a land only context (i.e., not accounting for land-atmosphere feedbacks at all) or in a fully coupled context (i.e., quantifying the net change in land fluxes without the ability to attribute how much of the response is from feedbacks). While some coupled studies invoke land-atmosphere feedbacks as important drivers of the net coupled land surface changes (e.g. pointing to moisture recycling in the Amazon as likely amplifying the photosynthesis response to land cover change), it is rare for coupled modeling studies to unambiguously disentangle the extent to which (or mechanisms through which) land-atmosphere feedbacks contribute to the net coupled land response. In isolation, neither coupled nor land-only simulations alone are able to directly disentangle the influence of land-atmosphere feedbacks on the overall coupled change in land water and carbon fluxes.

There have been a handful of studies which have isolated the influence of atmospheric feedbacks on land surface fluxes through complementary coupled and land-only simulations. Laguë et al. (2019) compared coupled and land-only simulations to isolate the impact of atmospheric feedbacks on land surface climate, focusing on atmospheric amplification of land-driven temperature changes. Shum et al. (2023) used an unconventional combination of coupled and land-only simulations to show how forest establishment in North American high latitudes drives regional climate changes

which would encourage further boreal forest expansion. A few studies have also combined coupled simulations with model-derived vegetation climate sensitivities to estimate the extent to which changes in vegetation cover can drive regional climate changes that influence photosynthesis (Y. Li et al., 2022; Staal et al., 2023).

However, prior work has focused on idealized changes to land surface properties and specific regional dynamics. We still lack a global understanding of how coupled land-atmosphere feedbacks modulate changes in the terrestrial water and carbon cycles. In this study, we quantify how biogeophysical land-atmosphere feedbacks modulate changes in land water and carbon fluxes using a unique paired perturbed parameter ensemble experimental design to isolate the atmosphere's role in modulating terrestrial processes. We ask the following questions: (1) how do land-atmosphere feedbacks modulate land-driven changes in mean evapotranspiration and photosynthesis, and (2) what mechanisms determine the sign and spatial pattern of these land-atmosphere feedbacks?

4.2 Methods

4.2.1 Paired perturbed parameter ensembles

We ran paired perturbed parameter ensembles (PPEs) under preindustrial conditions using two configurations of CESM2 (Danabasoglu et al., 2020): a coupled configuration ("coupled") and an uncoupled, land only configuration ("land-only"), which are described in detail in section 3.2. For both PPEs, we ran one-at-a-time parameter perturbation experiments for 18 land parameters, where we perturbed each parameter to a minimum and maximum value (ensemble n = 36) based on plausible parameter ranges determined by the CLM5-PPE. The parameter selection procedure and model configurations are described in more detail in section 3.2.2. The 18 parameters we sampled parameterize diverse terrestrial processes, including soil hydrology, photosynthesis, and stomatal conductance. The land parameters included in our PPE are described in detail in Table B.1, and our parameter selection was informed by the CLM5 PPE project (data and methods description are available via `https://github.com/djk2120/clm5ppe`). We note that the goal of this study is not to quantify parameter uncertainty, but rather to leverage this PPE dataset to gain mechanistic insights into how atmospheric feedbacks modulate changes in terrestrial processes.

In the coupled PPE, the atmosphere responds to changes in land surface parameters (i.e. atmo-

spheric feedbacks are turned on), while in the land-only PPE, the atmospheric state is prescribed at 3-hourly resolution to match the atmosphere simulated by CAM6 in the reference coupled simulation that used default parameters (i.e. atmospheric feedbacks are turned off). We can therefore quantify the impact of atmospheric feedbacks on terrestrial processes by making pairwise comparisons between each coupled and land-only ensemble member. This study focuses on land-atmosphere feedbacks over non-glaciated land, so we exclude all gridcells which contain snow during all months of the average year.

4.2.2 Disentangling the land-to-atmosphere and atmosphere-to-land branches of land-atmosphere feedbacks

We identify the mechanisms through which atmospheric feedbacks modulate changes in land surface processes by decomposing the overall feedback into two branches: the land-to-atmosphere branch and the atmosphere-to-land branch. Atmospheric feedbacks can modulate terrestrial processes only when changing land processes impact atmospheric quantities that are inputs to the land model (Table 4.1). We therefore focus on these quantities, particularly near-surface atmospheric temperature, precipitation, and humidity, and surface radiation.

Isolating how land surface fluxes impact the atmosphere

We use linear regression to quantify the sensitivity of atmospheric state variables to local changes in evapotranspiration. We regress coupled changes in atmospheric state variables on land-only evapotranspiration changes in order to isolate the land-to-atmosphere branch of the land-atmosphere feedback. In the coupled PPE, changes in evapotranspiration are due to both land parameter changes and atmospheric changes (e.g., evapotranspiration changes driven by changes in precipitation), but in the land-only PPE, evapotranspiration changes are only due to initial land surface parameter perturbation. We define the sensitivity of atmospheric state variables to changes in evapotranspiration as the slope of the regression. For example, we calculate the precipitation sensitivity to evapotranspiration ($\frac{\partial P_{coupled}}{\partial ET_{land-only}}$) by regressing coupled changes in precipitation against land-only changes in evapotranspiration for each grid cell across the 36 PPE ensemble members.

Category	Field
Temperature	Temperature at lowest atmospheric level
	Potential temperature at lowest atmospheric level
Precipitation	Liquid precipitation
	Solid precipitation
Humidity	Specific humidity
Surface radiation	Incident direct beam visible solar radiation
	Incident direct beam near-infrared solar radiation
	Incident diffuse visible solar radiation
	Incident diffuse near-infrared solar radiation
	Incident longwave radiation
Wind	Zonal wind at atmospheric reference height
	Meridional wind at atmospheric reference height
Height and pressure	Atmospheric reference height
	Atmosphere model's surface height
	Pressure
Biogeochemistry	Carbon dioxide (CO_2) concentration*
	Nitrogen deposition rate*
	Lightning frequency*
	Aerosol deposition rate

Table 4.1: Atmospheric inputs to the land model in CESM. Adapted from Table 2.4 in the CLM5 Technical Note

$*$ These quantities cannot change in our model configuration

Simulation	Variable	Variable description	Perturbation
Increase temp	a2x3h_Sa_tbot	Temperature at the lowest model level	+1 K
Decrease temp	a2x3h_Sa_tbot	Temperature at the lowest model level	-1 K
Increase precip	a2x3h_Faxa_rainl	Large-scale precipitation rate	+10%
	a2x3h_Faxa_rainc	Convective precipitation rate	+10%
	a2x3h_Faxa_snowl	Large scale snow rate	+10%
	a2x3h_Faxa_snowc	Convective snow rate	+10%
Decrease precip	a2x3h_Faxa_rainl	Large-scale precipitation rate	-10%
	a2x3h_Faxa_rainc	Convective precipitation rate	-10%
	a2x3h_Faxa_snowl	Large scale snow rate	-10%
	a2x3h_Faxa_snowc	Convective snow rate	-10%
Increase SW_{down}	a2x1hi_Faxa_swndr	Direct near-infrared incident solar radiation	+10%
	a2x1hi_Faxa_swvdr	Direct visible incident solar radiation	+10%
	a2x1hi_Faxa_swndf	Diffuse near-infrared incident solar radiation	+10%
	a2x1hi_Faxa_swvdf	Diffuse visible incident solar radiation	+10%
Increase LW_{down}	a2x3h_Faxa_lwdn	Downward longwave heat flux	+10%
Increase humidity	a2x3h_Sa_shum	Specific humidity at the lowest model level	+10%

Table 4.2: Idealized land-only simulations.

Isolating how atmospheric changes impact land surface fluxes

We identify how changes in atmospheric quantities influence land surface fluxes by running additional idealized land-only simulations. We ran idealized land-only simulations where we modified the atmospheric quantities that impact the atmosphere (Table 4.2). This method allows us to quantify the terrestrial response to mean state climate changes, but does not assess the terrestrial response to shorter timescale atmospheric variability, which land parameter perturbations can also impact. From these simulations, we calculate the land sensitivity to that meteorological driver (e.g. the sensitivity of evapotranspiration to precipitation change is $\frac{\partial ET}{\partial P}$).

Decomposing the influence of atmospheric feedbacks upon evapotranspiration and photosynthesis

We then quantify the extent to which different atmospheric quantities contribute to the overall fractional change in evapotranspiration due to atmospheric feedbacks ($\Delta ET_{feedback}$) using Equation 4.1:

$$\Delta ET_{feedback} = \sum_X \left(\frac{\partial X_{coupled}}{\partial ET_{land-only}} \frac{\partial ET}{\partial X} \right) \tag{4.1}$$

where $\frac{\partial X_{coupled}}{\partial ET_{land-only}}$ is the sensitivity of atmospheric quantity X to changes in evapotranspiration (as diagnosed through regression), and $\frac{\partial ET}{\partial X}$ is the sensitivity of evapotranspiration to changes in atmospheric quantity X (as diagnosed through idealized synthetic meteorology simulations using the land-only model configuration). We sum over the major atmospheric inputs to the land model: temperature at the lowest atmospheric level, total precipitation, specific humidity at the lowest atmospheric level, incident solar radiation, and incident longwave radiation.

We use a similar equation for gross primary production (GPP), with the key difference being that we do the decomposition using the simulated coupled change in each atmospheric quantity (ΔX) instead of the sensitivity of the atmospheric quantity to changes in GPP, because we found that atmospheric responses to GPP were parameter dependent (as described in Section 4.3):

$$\Delta GPP_{feedback} = \sum_X \left(\Delta X \frac{\partial GPP}{\partial X_{coupled}} \right) \tag{4.2}$$

4.2.3 Potential evapotranspiration

We calculate potential evapotranspiration (ET in units of mm/s or L in units of W/m^2) from monthly data using the Penman-Monteith equation:

$$L = \lambda ET = \frac{sR^*_{net} + \frac{\rho_a c_p}{r_{ah}} D}{(1 + \frac{r_{aw}}{r_{ah}})\gamma + s} \tag{4.3}$$

which represents potential evapotranspiration as a function of the net radiation at surface minus ground heat uptake (R^*_{net} in W/m^2) and the vapor pressure deficit (D in Pa). s is the change in saturation vapor pressure per degree (Pa/K), ρ_a is the density of near-surface air (kg/m^3), and γ is the psychrometric constant. C_p and λ are the specific heat of dry air ($J/(kgK)$) and the latent heat of vaporization (J/kg), respectively. Potential evapotranspiration also depends on two resistances: r_{ah}, the aerodynamic resistance to water vapor transfer from the surface to near-surface air (s/m), and r_{aw}, the aerodynamic resistance to heat transfer from the surface to near-surface air (s/m). We calculate changes in potential evapotranspiration to illustrate changes in atmospheric controls

on evapotranspiration in coupled simulations. We therefore use the default FAO (Allen et al. 1998) definitions of r_{ah} and r_{aw} for a reference crop, for which r_{aw} is 70 s/m and r_{ah} is defined as a function of wind speed:

$$r_{ah} = \frac{ln(\frac{z_m - \frac{2}{3}h}{0.123h})ln(\frac{z_m - \frac{2}{3}h}{0.0123h})}{k^2 u_z} \tag{4.4}$$

where z_m is the height of wind and humidity measurements, $h = 0.12$ is the reference crop height, $k = 0.41$ is von Karman's constant, and u_z is the wind speed at height z_m.

4.3 Results and Discussion

4.3.1 Atmospheric modulation of evapotranspiration changes

We found that atmospheric feedbacks substantially modulate evapotranspiration changes, and that the sign of the impact of atmospheric feedbacks varies spatially (Figure 4.1a). Atmospheric feedbacks generally dampen land-driven changes in evapotranspiration in climatologically wet regions, while in warm and dry regions atmospheric feedbacks either amplify evapotranspiration changes or are not statistically significant (Figure 4.1a-b). In the Budyko framework (Budyko, 1974), this corresponds to dampening atmospheric feedbacks in energy-limited locations where there is more annual precipitation than energy available to evaporate it ($R_{net} < \lambda P$, where P is the precipitation rate) and amplifying feedbacks or no feedbacks in moisture-limited locations where evapotranspiration (ET) is instead controlled by water availability. The magnitude of this atmospheric modulation is significant, particularly in the energy-limited regime, where atmospheric feedbacks can dampen evapotranspiration changes by 20 to 60%.

The Amazon (Figure 4.2f) is a classic energy-limited region, both in our model experiments and in observations. In the Amazon (indicated by a black circle in Figure 4.1a), increasing the maximum hydraulic conductance of plants (`kmax`) leads to a 20.2 W/m^2 increase in evapotranspiration in a land-only framework. If the atmosphere is allowed to respond to that land surface change, the same parameter perturbation leads to a much smaller increase in evapotranspiration of 13.2 W/m^2, indicating that atmospheric feedbacks dampen the initial evapotranspiration change by about 35%. This linear scaling is remarkably consistent at this location across the whole PPE (average dampening is 37%, R^2=0.94). In contrast, a site in Eastern Ukraine (Figure 4.1e) is an

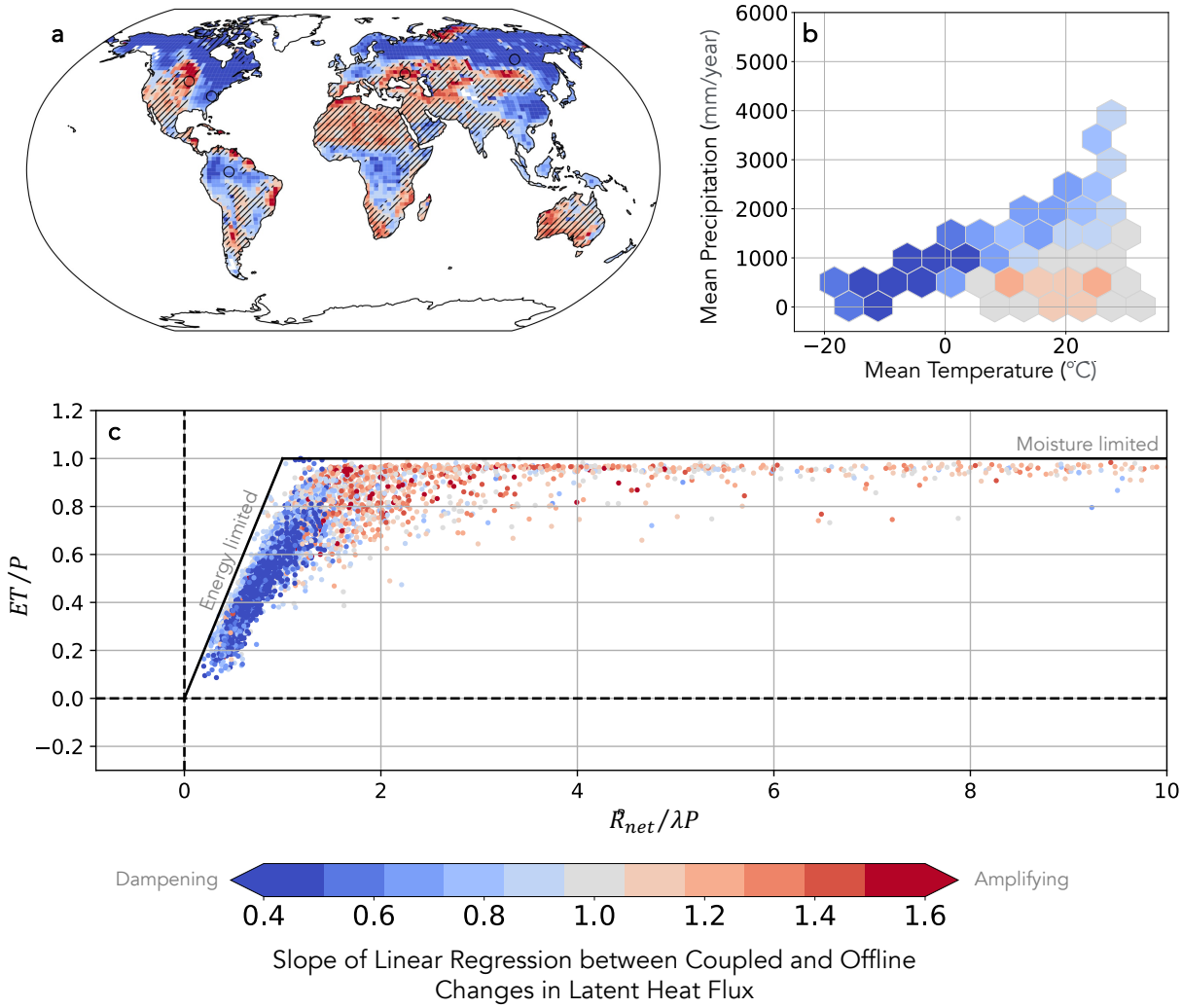

Figure 4.1: Influence of atmospheric feedbacks on land evapotranspiration. Slope of regression between coupled and land-only changes in evapotranspiration (a) spatially, (b) average in each mean climate space (T, P), and (c) in the Budyko energy- and moisture-limited framework (Budyko, 1974). Reds indicate regions where land-atmosphere feedbacks amplify changes in evapotranspiration, and blues indicate regions where land-atmosphere feedbacks dampen changes in evapotranspiration. Stippling indicates regions where the slope is not statistically significantly different from 1. In (b), the average slope in (a) is binned by climate space (annual mean temperature and precipitation). Only climate bins that contain greater than 10 gridcells in (a) are shown. In (c), the grid cell values shown in (a) are plotted in relation to the Budyko framework, where black lines indicate theoretical energy limits ($\lambda ET = R_{net}$) and moisture limits ($ET = P$) on evapotranspiration. Analysis in (a)-(c) excludes land that is covered in snow year round. ET, R_{net}, and P in (c) are from the coupled reference case.

example of a water-limited site in this ensemble. Here, soil hydrology parameters have the largest impact on evapotranspiration, for example decreasing the decay factor for fractional saturated area (`fff`) to the minimum value decreases evapotranspiration by 5.3 W/m^2 in a land-only framework, but by 7.9 W/m^2 in a coupled framework (48% amplification). On average, atmospheric feedbacks amplify evapotranspiration changes by 72% at this location (R^2=0.88).

ET differs between the land-only and coupled PPEs due to the influence of atmospheric responses to global-scale land parameter perturbations. Our goal in this study is to quantify the impact of global-scale atmospheric feedbacks on land surface fluxes, and to identify where, and through what mechanisms, atmospheric feedbacks lead evapotranspiration to respond differently in a coupled context than in a land-only context. We therefore adopt the null hypothesis that atmospheric feedbacks do not modulate changes in land surface fluxes (i.e., in each grid cell that $\Delta ET_{coupled} = \Delta ET_{land-only}$, or in the context of the linear regression, that the slope equals 1). However, we note that in the coupled context, both local and remote land surface changes can impact the atmosphere in a given grid cell.

We do not directly disentangle locally-driven atmospheric changes from remotely-driven atmospheric changes, but use the fraction of variance explained by local regression with land-only evapotranspiration changes as a proxy for the extent to which local to regional evapotranspiration changes are responsible for the observed atmospheric feedbacks (see section 4.3.2). In many tropical and temperate humid to semi-arid regions, local regression explains a large fraction of variance across the coupled PPE, suggesting a dominant role of local to regional land surface changes. However in deserts and the high-latitudes, local evapotranspiration changes explain less than 10% of the variance in the coupled ensemble, suggesting that the coupled evapotranspiration changes in those locations are driven by atmospheric responses to remote land surface changes. For example, in the northern Russia example location (Figure 4.2b), the slope of the line of best fit is statistically significantly different from one, indicating that atmospheric responses significantly alter evapotranspiration changes, and that local land-only evapotranspiration changes are a poor predictor of coupled evapotranspiration responses (and consequently, if one were to try to use a land-only PPE to estimate how global-scale parameter uncertainty impacts high-latitude evapotranspiration fluxes, the land-only PPE would give the wrong answer). However, this linear regression only explains 27% of the variance in evapotranspiration across the coupled PPE at this site, indicating that in the

coupled PPE, evapotranspiration may be primarily responding to remotely-driven climate changes. This would be consistent with prior work which has shown that evapotranspiration changes in mid-to-high latitudes can drive Arctic amplification (Park et al., 2020) and alter atmospheric energy transport (Laguë et al., 2019).

In the global average, atmospheric feedbacks slightly dampen global mean changes in evapotranspiration (by 14% on average, Figure 4.2a) because most of the Earth's evapotranspiration occurs in wet regions, so the wet regime atmospheric feedbacks dominate the global signal. The one amplifying exception is the minimum decay factor for fractional saturated area (`fff`), which has the largest impact on evapotranspiration in desert and semi-arid regions.

Mechanism

The impact of atmospheric feedbacks on evapotranspiration varies depending on the climatological water regime because changing land evapotranspiration impacts multiple atmospheric quantities simultaneously, and the climatological water regime determines which atmospheric changes exert the strongest control on evapotranspiration at that location. We can see this climatological dependence clearly in idealized simulations where we modify temperature and precipitation independently (Figure 4.3). Increasing precipitation increases evapotranspiration, with the largest evapotranspiration increases occurring in moisture-limited locations (Figure 4.3a-c). Increasing temperature also increases evapotranspiration, but has the largest impact in energy-limited locations (Figure 4.3d-f) because increasing temperature while maintaining constant specific humidity increases the atmospheric demand for moisture due to the Clausius-Clapeyron relationship.

Atmospheric feedbacks dampen evapotranspiration changes in energy-limited regions because (1) increasing evapotranspiration decreases the atmospheric demand for moisture and (2) evapotranspiration in these regions is limited by the atmospheric demand for water and energy available to evaporate water (i.e., the potential evapotranspiration, PET), rather than by water availability. Increasing evapotranspiration decreases PET (Figure 4.4a) primarily by decreasing the vapor pressure deficit (Figure 4.4c), which is the atmospheric demand for moisture. This VPD decrease is driven by the fact that increasing evapotranspiration cools (Figure 4.5a) and generally moistens (Figure 4.5b) the near-surface air. This leads to global increases in near-surface relative humidity

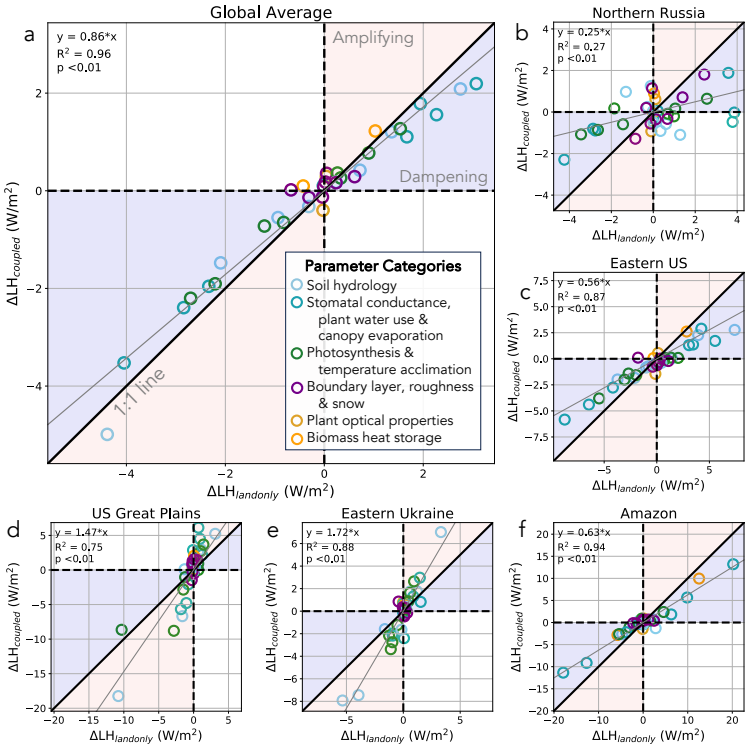

Figure 4.2: Relationship between land only and coupled changes in latent heat flux, globally (a) and for several example locations (b-f), as marked in Figure 4.1. Each point is a different paired ensemble member (n = 36), and color indicates the parameter category. The parameter perturbations and categories are described in Table B.1. Shading indicates whether land-atmosphere feedbacks amplify (red) or dampen (blue) evapotranspiration changes. The thick black line indicates the 1:1 line dividing amplifying and dampening feedbacks, and the thin gray line indicates the line of best fit, calculated via ordinary least squares linear regression with y-intercept=0. p-values indicate whether slopes are statistically significantly different from 1.

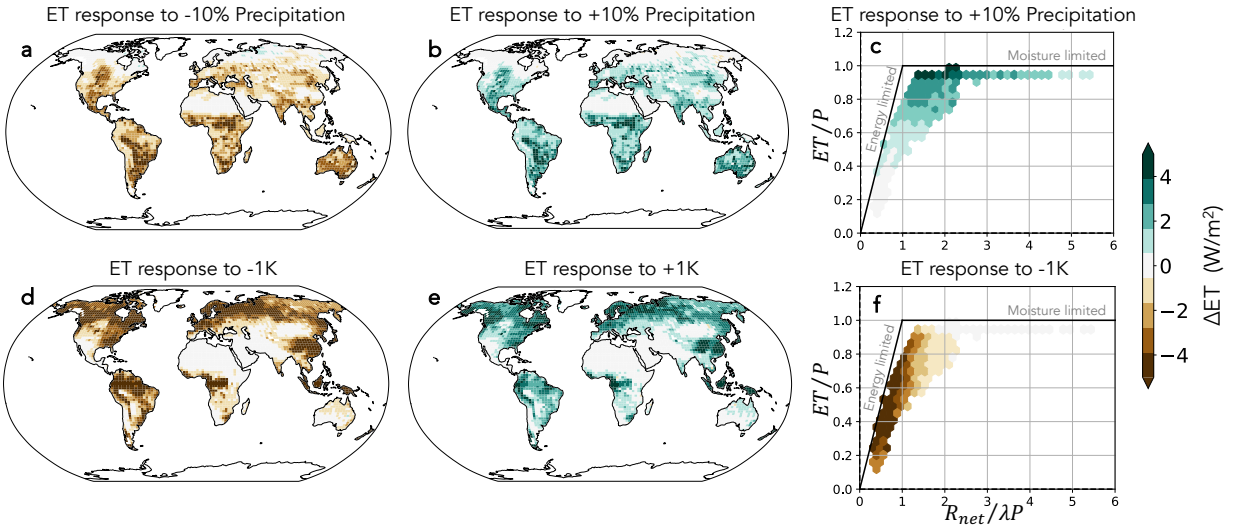

Figure 4.3: How atmospheric changes impact evapotranspiration. Evapotranspiration (W/m^2) response to idealized meteorological treatments of (a) decreasing precipitation, (b) increasing precipitation, (d) decreasing temperature, and (e) increasing temperature. The right column bins the evapotranspiration responses to increasing precipitation (c) and decreasing temperature (f) in the Budyko framework. ET, P, and R_{net} which define the Budyko space in panels (c) and (f) are from the reference simulation. The coupled and land-only reference simulations are identical because the land-only PPE is forced with the meteorology from the coupled reference case.

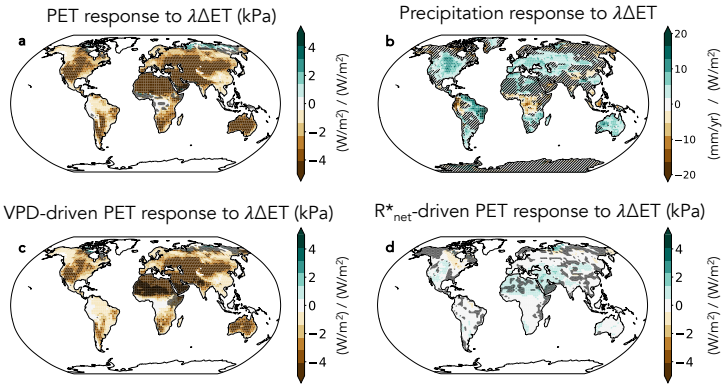

Figure 4.4: ET influences on potential evapotranspiration (PET) and precipitation. Sensitivity of PET and precipitation to ET, quantified by linear regression as described in section 4.2.2. Positive values indicate that increasing evapotranspiration increases the atmospheric variable. Stippling indicates regions where the slope is not statistically significantly different from 0. An increase in ET in drives (a) a decrease in PET and (b) regionally variable changes in precipitation. The PET change in (a) is mostly driven by changes in the VPD component of PET (c), with minimal contributions from the R_{net} component.

(Figure 4.5c) and decreases the vapor pressure deficit (Figure 4.5d). This decrease in the atmospheric demand for moisture dampens the initial evapotranspiration change in regions where evapotranspiration rates are primarily controlled by atmospheric demand. VPD (and consequently, PET) also decreases in water-limited regions, but in those locations this change in atmospheric demand influences evapotranspiration less because evapotranspiration is controlled primarily by precipitation rather than by atmospheric demand for water.

Increasing evapotranspiration also drives radiative changes (Figure 4.6) due to decreases in surface temperature and near-surface air temperature, as well as changes in cloud cover. However, these radiation changes largely cancel each other out, leading to small changes in net absorbed radiation R_{net} and only minor radiation-driven changes in PET (Figure 4.4d).

In contrast, atmospheric responses amplify evapotranspiration changes in some dry regions where (1) increasing evapotranspiration increases precipitation, and (2) evapotranspiration is moisture-limited and therefore more sensitive to precipitation changes. Increasing evapotranspiration increases precipitation in some regions (Figure 4.4b), likely due to a combination of local land-atmosphere coupling (e.g. as is typical in the Great Plains) and larger scale circulation responses

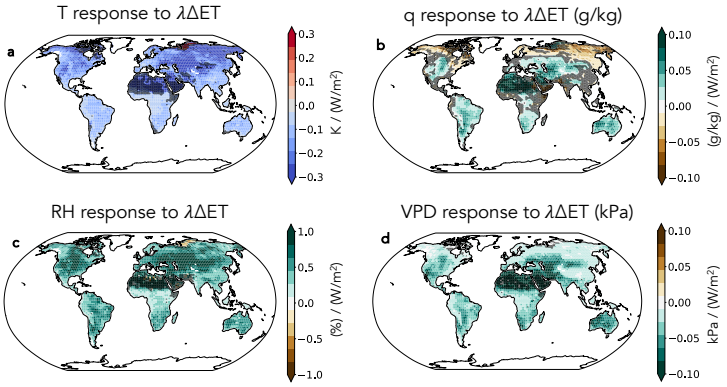

Figure 4.5: Influence of evapotranspiration on vapor pressure deficit. Sensitivity of (a) air temperature, T, (b) specific humidity, q, (c) relative humidity, RH, and (d) vapor pressure deficit, VPD, to changes in ET. Sensitivities are quantified by linear regression as in Figure 4.4. Increasing evapotranspiration decreases T globally (a), and increases q in many regions (b). This leads to a global increase in RH (c) and decrease in VPD (d).

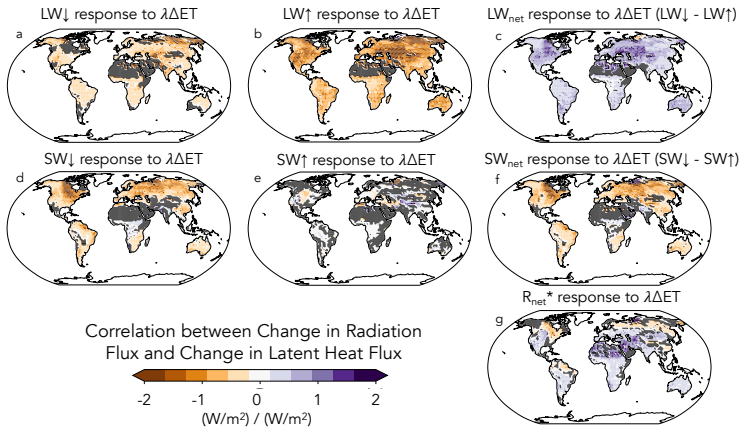

Figure 4.6: Influence of evapotranspiration on net radiation. Sensitivity of surface energy fluxes to changes in evapotranspiration, as in Figure 4.4. Increasing evapotranspiration decreases upwelling longwave, LW↑, (b) and decreases downwelling longwave, LW↓ by a smaller amount (a), leading to an increase in the net longwave flux from the atmosphere to land (c). Increasing evapotranspiration also increases downwelling shortwave, SW↓, (d) and drives small changes in upwelling shortwave, SW↑ (e), leading to a net increase in net shortwave absorbed by the land surface (f). The combined changes in longwave and shortwave radiation result in small, spatially variable changes in net radiation minus storage (R_{net}).

(e.g. asymmetric precipitation responses to evapotranspiration reductions as in Kooperman et al. (2018) or shifts in the inter-tropical convergence zone). Precipitation increases can increase soil moisture, thereby amplifying the initial evapotranspiration increase. Atmospheric feedbacks do not amplify evapotranspiration changes in all dry or transitional locations because increasing evapotranspiration does not increase precipitation in all of these regions. There are also some regions (e.g., the Amazon) where increasing evapotranspiration increases precipitation, but does not lead to an amplifying feedback because evapotranspiration is relatively insensitive to precipitation changes in wet regions.

By linearly combining the land sensitivity to each of these factors, we can decompose the overall land-atmosphere feedback into different components (Figure 4.7). This linear decomposition captures the actual atmospheric modulation reasonably well (compare Figure 4.7a and b), including the emergent dependence on the climatological moisture regime.

Alignment with prior work

While no prior study has quantified the full feedback through which atmospheric responses modulate changes in land evapotranspiration, our results are broadly consistent with prior work. Laguë et al. (2019) discuss the impact of atmospheric feedbacks on latent heat changes in a global mean sense, and note that increasing evaporative resistance drives smaller changes in latent heat flux in land-only simulations than in coupled simulations. They hypothesize that this is due to reduced evapotranspiration driving increased atmospheric demand for water in coupled simulations, which is consistent with the mechanism that we demonstrate here for energy-limited regions.

Additionally, the land-to-atmosphere and atmosphere-to-land branches of our identified feedback mechanism are both supported by first principles. The fact that precipitation would have a bigger impact on ET in moisture-limited regions and that VPD would have a bigger impact on ET in energy-limited regions follows from the long-established Budyko framework. Similarly, on local scales the surface energy budget requires that increasing ET decreases land surface temperatures, which is the dominant driver of VPD declines in our simulations. Multiple studies have demonstrated that this relationship between ET and temperature holds true in a coupled context on regional to to global scales (Shukla & Mintz, 1982) under modern continental configurations

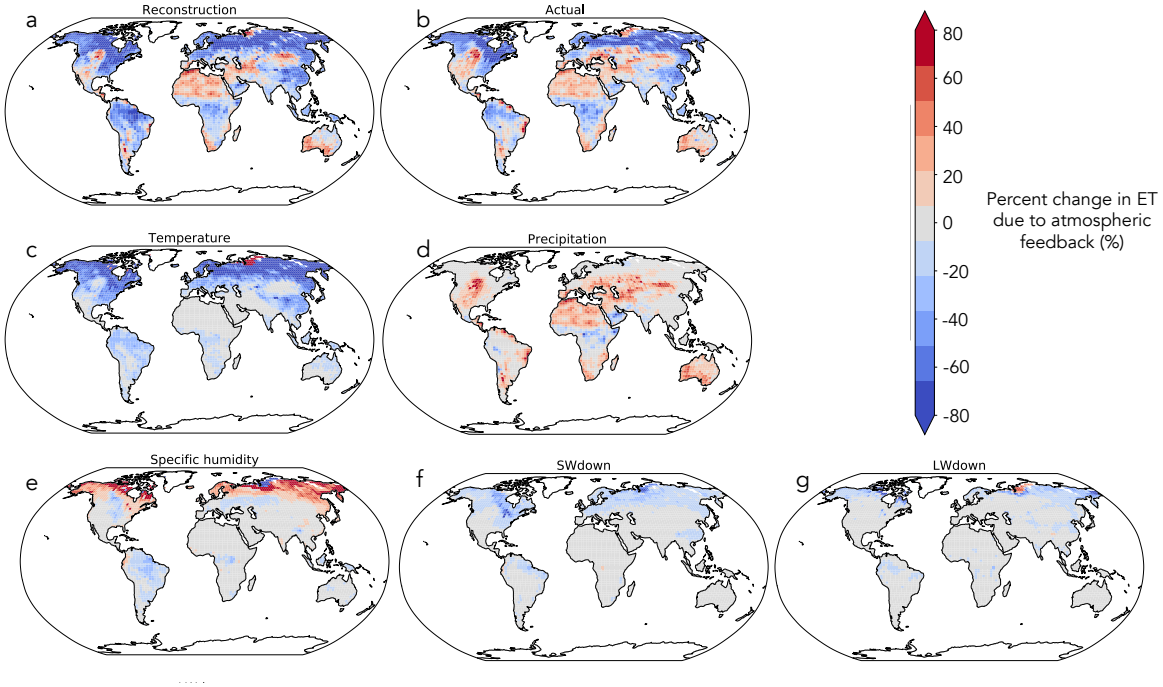

Figure 4.7: Linear decomposition of the atmospheric modulation of evapotranspiration changes. Contribution of temperature (c), precipitation (d), specific humidity (e), downwelling shortwave (f), and downwelling longwave (g) to atmospheric modulation of evapotranspiration changes. Estimated atmospheric modulation of ET changes due to the sum of these terms (a), which can be compared to the actual atmospheric modulation (b) across the PPE. Changes are percent changes relative to the change in ET seen in the ensemble of PPE experiments using the land-only model; positive values indicate a positive (amplifying) atmospheric feedback.

(though see Laguë et al., 2021). In the results presented here we show this directly and explicitly.

The amplifying land-atmosphere feedback mechanism we identified in moisture-limited regions is also consistent with the soil moisture feedbacks literature, though soil moisture forcing studies quantify land-atmosphere feedbacks in an alternative framework. The more traditional land-atmosphere feedback literature adopts a framework where soil moisture is the driver, and the metric of interest is the strength of coupling between soil moisture and precipitation (i.e., $SM_{coupling} = \frac{\partial P}{\partial SM}$) or temperature. This coupling strength can be decomposed into the terrestrial contribution ($\frac{\partial ET}{\partial SM}$) and the atmospheric contribution ($\frac{\partial P}{\partial ET}$), such that $SM_{coupling} = \frac{\partial P}{\partial SM} = \frac{\partial ET}{\partial SM}\frac{\partial P}{\partial ET}$. Analysis of GLACE experiments and observations identify transitional regions to be regions of strong soil moisture-precipitation coupling (Koster et al., 2006; Seneviratne et al., 2013), which align with the regions identified in this study where coupling enhances perturbations in ET compared to land-only perturbations. However, we note that we are quantifying a different kind of atmospheric feedback, in that we consider evapotranspiration to be the driver of the feedback loop, such that soil moisture is a part of the feedback loop rather than an external driver. For example, consider a water-limited location that is unaffected by changes in VPD or net radiation. This study would quantify the atmospheric modulation of long-term ET changes as $\frac{\partial P_{coupled}}{\partial ET_{land-only}}\frac{\partial ET}{\partial P}$, which can be further decomposed into $\frac{\partial P}{\partial ET_{land-only}}\frac{\partial SM}{\partial P}\frac{\partial ET}{\partial SM}$. Our atmospheric modulation metric therefore has the soil moisture coupling strength embedded in it, but is quantifying a different feedback. Our analysis also differs from the traditional land-atmosphere feedback literature in that many (though not all) land-atmosphere feedback papers focus on daily to interannual variability in soil moisture, evapotranspiration, and precipitation, while we are focusing on atmospheric modulation of long-term (climatological) changes in land water fluxes.

Additionally, by adopting a more holistic perspective on land-atmosphere feedbacks beyond just the soil moisture-ET-precipitation feedback, we are able to explore atmospheric feedbacks' influence on ET in regions that are primarily radiation limited and therefore insensitive to soil moisture changes (e.g. the Amazon and temperate mid-latitudes), allowing us to identify the dampening feedback mechanism which is consistent with longstanding theory but underemphasized in the traditional land-atmosphere feedback literature.

4.3.2 Differences between atmospheric modulation of evapotranspiration and photosynthesis

Atmospheric modulation of photosynthesis differs from atmospheric modulation of evapotranspiration in several key ways. First, atmospheric feedbacks have a smaller impact on GPP than on ET (Figure 4.8c-d). Land-only ET changes only explain about 51% of the variance in coupled ET changes while land-only GPP changes explain about 71% of the variance in coupled GPP changes (averaged globally from Figure 4.8d). This means that atmospheric feedbacks change ET more than they change GPP. When considering global mean changes in GPP and ET, land-only GPP changes explain about 98% of the variance in global mean $\Delta GPP_{coupled}$, while land-only ET changes explain about 91% of the variance in global mean $\Delta ET_{coupled}$.

Second, ET and GPP differ in how consistent atmospheric feedbacks are across the PPE. For ET, there is spatial variation in how atmospheric feedbacks modulate ET changes, but for any given location the direction of atmospheric feedbacks are quite consistent (i.e., consistently dampening or consistently amplifying ET changes), regardless of what parameter drove the initial ET change (Figure C.2a-d). Because of this, the line of best fit relating $\Delta ET_{coupled}$ and $\Delta ET_{land-only}$ is statistically different from one across 57% of the land surface. Estimating $\Delta ET_{coupled}$ as a linear function of $\Delta ET_{land-only}$ (i.e., $\Delta ET_{coupled} = m * \Delta ET_{land-only}$) explains additional variance in $\Delta ET_{coupled}$ across the ensemble, particularly in wet regions (Figure 4.8g). In contrast, atmospheric modulation of GPP is more parameter dependent (Figure C.2). Because of this, estimating $\Delta GPP_{coupled}$ as a linear function of $\Delta GPP_{land-only}$ does not meaningfully improve the amount of $\Delta GPP_{coupled}$ variance explained (Figure 4.8h).

Finally, when considering variance in ET and GPP on an absolute basis, atmospheric feedbacks meaningfully impact ET broadly across space globally (Figure 4.8a), while atmospheric modulation of GPP is most important in two regional hotspots: the Amazon and the Great Plains.

4.3.3 Atmospheric feedbacks' modulation of changes in photosynthesis

Due to these differences between atmospheric feedbacks' impact on evapotranspiration vs. photosynthesis, we focus our analysis on the two hotspot regions with the most variance in photosynthesis that is not explained by the land-only simulation: the Amazon and the Northern Great Plains (Fig-

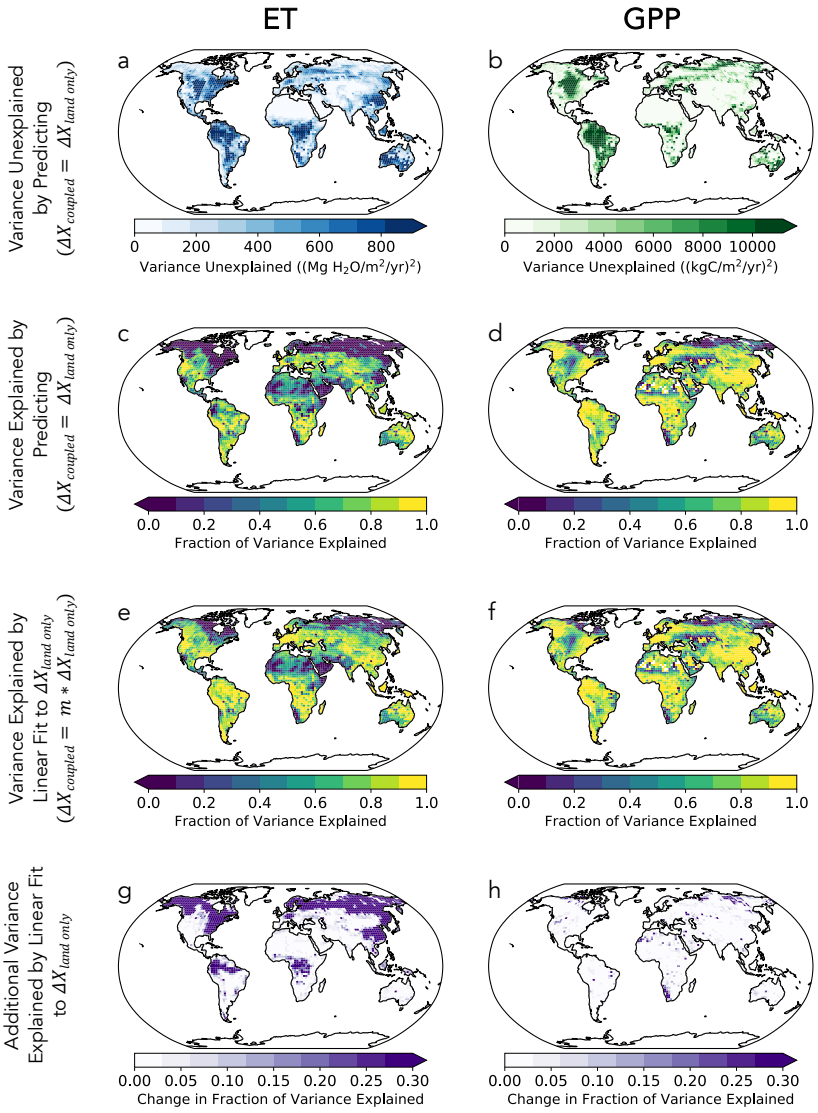

Figure 4.8: Comparison of variance in changes in coupled ET (left) and GPP (right) explained by the land-only PPE. Top row shows the variance unexplained by predicting $\Delta ET_{coupled} = \Delta ET_{land-only}$ (a) and $\Delta GPP_{coupled} = \Delta GPP_{land-only}$ (b). For ET, this is calculated as $\frac{\sum_i (\Delta ET_{coupled} - \Delta ET_{land-only})^2}{n-1}$ for all ensemble members i. Panels (c) and (d) show the *fraction* of variance explained by assuming $\Delta ET_{coupled} = \Delta ET_{land-only}$ (c) and $\Delta GPP_{coupled} = \Delta GPP_{land-only}$ (d). Panels (e) and (f) show the fraction of variance explained by the linear fit of coupled changes to land-only changes. Panels (g) and (h) how much the linear regression increases the fraction of variance explained, compared to assuming the coupled changes will equal the land-only changes.

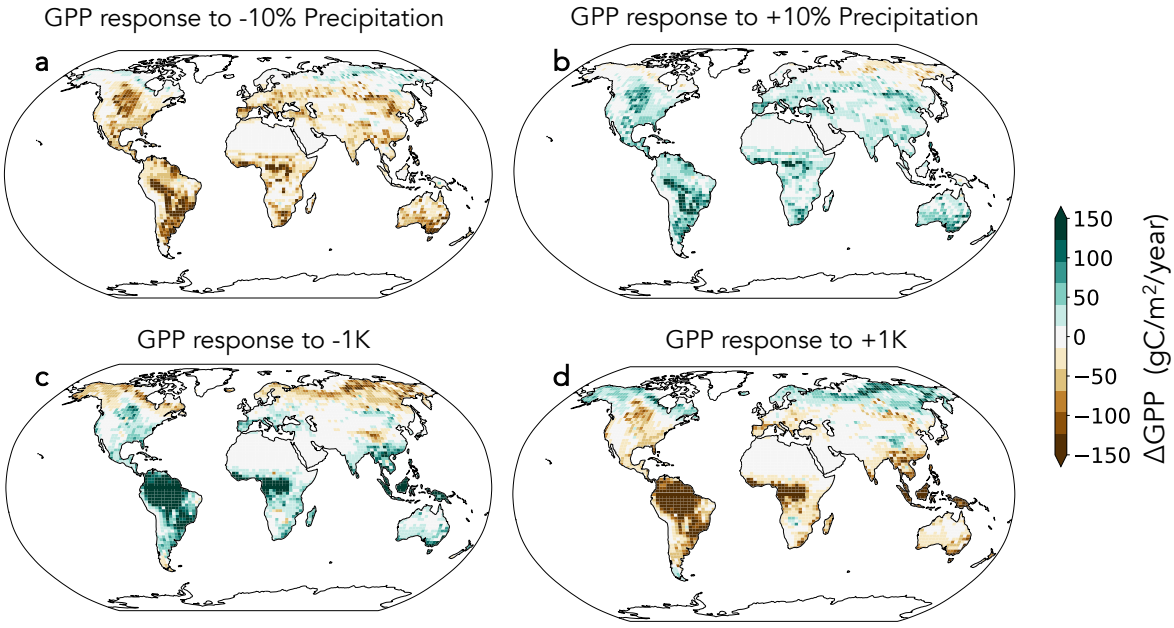

Figure 4.9: How atmospheric changes impact GPP. GPP (W/m^2) response to idealized meteorological treatments of (a) decreasing precipitation, (b) increasing precipitation, (c) decreasing temperature, and (d) increasing temperature.

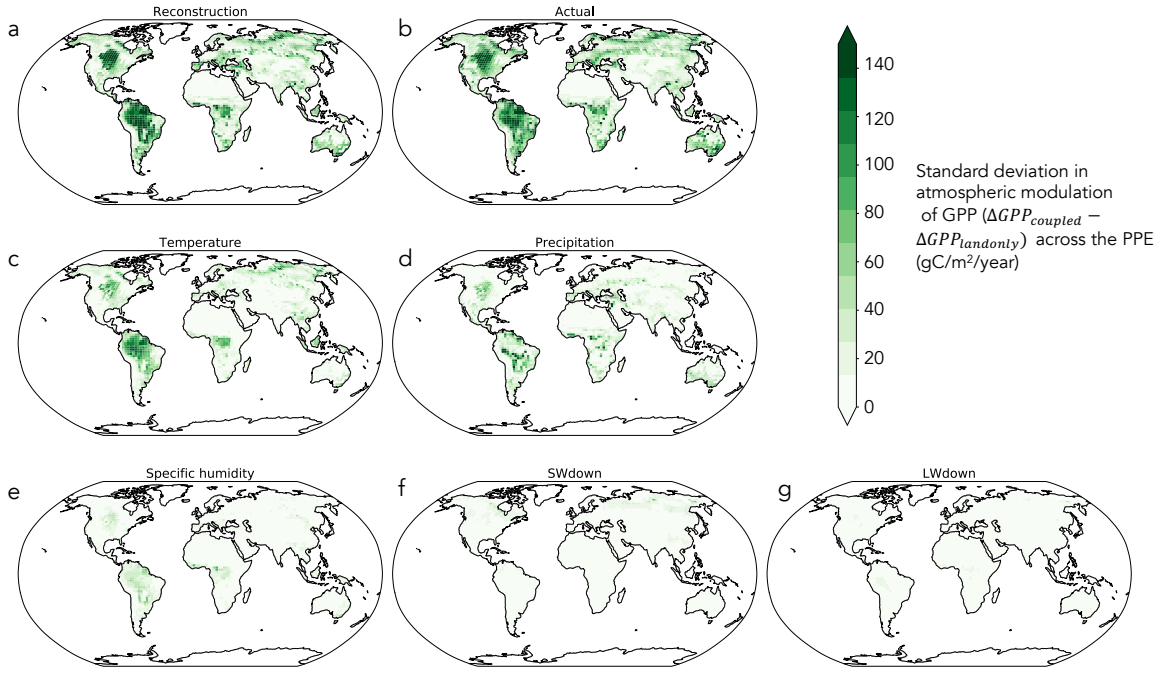

Figure 4.10: Atmospheric drivers of spatial pattern of atmospheric modulation of GPP across PPE. Contribution of temperature (c), precipitation (d), specific humidity (e), downwelling shortwave (f), and downwelling longwave (g) to atmospheric modulation of GPP changes. Estimated atmospheric modulation of GPP changes due to the sum of these terms (a), which can be compared to the actual atmospheric modulation (b) across the PPE. Atmospheric modulation is quantified by the standard deviation in atmospheric feedbacks' impact on GPP ($\Delta\ GPP_{coupled}$ - $\Delta\ GPP_{land-only}$); higher values mean that atmospheric feedbacks have a larger impact on GPP, but this metric does not indicate whether atmospheric feedbacks are amplifying or dampening.

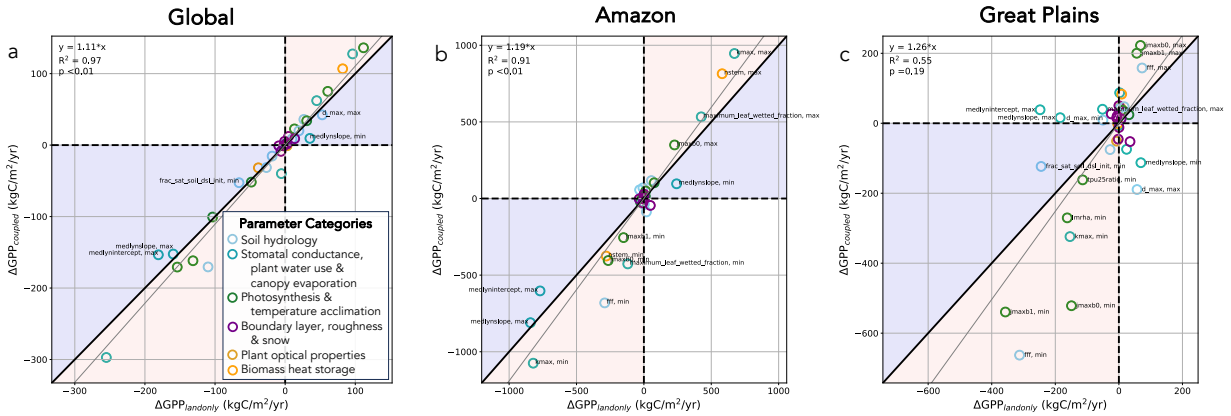

Figure 4.11: Relationship between land-only and coupled changes in gross primary production. As in Figure 4.2, but for gross primary production (GPP), globally (a) and for regional hotspots in the Amazon (b) and Great Plains (c).

ure 4.8b). These regions emerge as hotspots due to the combination of two factors: (1) in these regions changes in land parameters cause large changes in temperature (Figure 3.2) and precipitation (Figure 3.3) across the PPE, and (2) GPP is sensitive to temperature and precipitation in these regions (Figure 4.9). By linearly combining the monthly land sensitivity to temperature and precipitation with the monthly variation in temperature and precipitation across the PPE, we decompose the impact of atmospheric feedbacks on GPP into different components (Figure 4.10). This linear decomposition captures the actual variation in atmospheric modulation reasonably well (compare Figure 4.10a and b), including the emergence of the Amazon and Great Plains as hot spots where atmospheric feedbacks have the greatest influence on GPP. In the Amazon, land-driven air temperature changes have the largest influence on GPP, while atmospheric modulation of GPP in the Great Plains is due to changes in both temperature and precipitation.

Amazon

In the Amazon, atmospheric feedbacks generally amplify the sensitivity of GPP to changes in terrestrial parameters (Figure 4.11b). However, there are two ensemble members for which atmospheric feedbacks dampen ET changes (the minimum `medlynslope` and the maximum `medlynintercept`) and one ensemble member where atmospheric feedbacks are negligible (maximum `medlynslope`).

These parameters influence plant stomatal conductance, controlling the intrinsic water use efficiency (i.e., the leaf-level trade-off between carbon gain and water loss) (Medlyn et al., 2011).

The impact of atmospheric feedbacks on GPP is parameter-dependent because there is no direct feedback between GPP and the atmosphere in our experimental design, due to the fact that our simulations include only biogeophysical feedbacks, rather than biogeochemical feedbacks (i.e., no changes in atmospheric CO_2). Atmospheric feedbacks therefore modulate GPP changes only if a parameter perturbation impacts both GPP and land surface properties, and then those land surface properties impact the atmosphere, which feeds back on GPP. For example, in the Amazon, increasing the maximum hydraulic conductance of plants (`kmax`) both increases evapotranspiration (Section 4.3.1) and increases GPP, because photosynthesis in the default case is limited by leaf water potential, and increased stem hydraulic conductance enables available water in deep soil layers to be transported to the leaves of trees. The atmosphere directly responds to `kmax`'s influence on ET, leading to decreases in regional temperature and vapor pressure deficit. This atmospheric feedback dampens ET changes, but amplifies GPP changes because decreasing temperature increases photosynthetic rates in the tropics (Figure 4.9d). We note that in CESM, this temperature sensitivity is not due to direct temperature effects on photosynthesis, but rather due to the fact that decreasing temperature decreases VPD, and lower VPD increases stomatal conductance which thereby increases photosynthesis (Chapter 2). Atmospheric amplification of `kmax`'s influence on GPP is consistent with prior work that hypothesized that the evolution of angiosperms (which have higher hydraulic conductance) enhance photosynthesis in the Amazon (Lee & Boyce, 2010).

In all simulations, increasing land-only ET consistently leads to cooling of the near-surface air (Figure 4.12a), and the GPP sensitivity to air temperature is also relatively consistent across our PPE (Figure 4.12d). The fact that atmospheric feedbacks are parameter dependent can be largely explained by whether parameters change the coupling between GPP and ET. Atmospheric feedbacks generally amplify GPP changes in the Amazon because GPP changes are often correlated with ET changes (i.e., increasing GPP also increases ET). However, for three outlier stomatal conductance parameter perturbations atmospheric feedbacks do not amplify GPP because these parameters change the coupling between GPP and ET (Figure 4.12c) by directly modifying the leaf-level trade-off between carbon gain and water loss. For the two ensemble members that lead to dampening atmospheric feedbacks, those parameter perturbations alter the coupling between GPP

and ET such that GPP and ET changes are of opposite sign.

The Great Plains

In the Great Plains, the impact of atmospheric feedbacks on GPP is even more parameter dependent than in the Amazon. Of the 16 parameter perturbations which drive GPP changes greater than 5% in the land-only simulations (labeled in Figure 4.11c), atmospheric feedbacks amplify GPP changes for 9 ensemble members, drive sign changes for 6 ensemble members, and dampen GPP changes for 1 ensemble member. Atmospheric feedbacks drive sign changes when the land-only GPP changes are driven by stomatal conductance parameters (`medlynintercept`, `medlynslope`), and atmospheric feedbacks either dampen or change the sign of GPP responses to parameters controlling the dry surface soil layer (`d_max`, `frac_sat_dsl_init`), as described further below.

As in the Amazon, the parameter dependent impact of atmospheric feedbacks on GPP can be explained by differences across parameters in the relationship between GPP and ET changes: atmospheric feedbacks amplify GPP changes when a parameter increases (or decreases) both GPP and ET in tandem, and atmospheric feedbacks dampen GPP or drive sign changes when a parameter modifies GPP and ET in opposite directions (Figure 4.13c). As in the Amazon, changing stomatal conductance parameters (`medlynintercept`, `medlynslope`) causes GPP and ET to change in opposite directions because those parameters mechanistically control the coupling between GPP and transpiration (Figure C.1). Parameters impacting the dry surface layer (DSL; Swenson and Lawrence 2014) cause GPP and ET to change in opposite directions because the dry surface layer parameterization controls rates of soil evaporation and the partitioning between different soil fluxes, which impacts the amount of water available for plants. Decreasing the dry surface layer parameter `d_max` or the fraction of saturated soil for moisture value at which dry surface layer initiates (`frac_sat_soil_dsl_init`) enhances soil evaporation, which reduces the amount of water that makes it into plant-available soil levels. This causes plants to be more stressed by soil moisture, which reduces GPP.

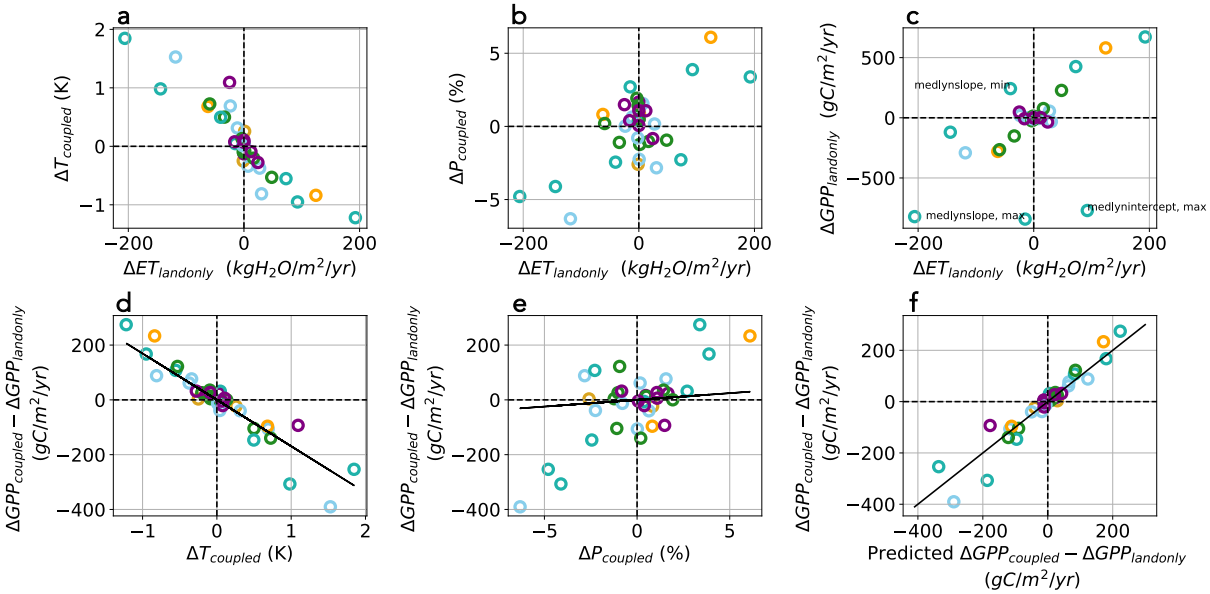

Figure 4.12: Relationships between ET, GPP, temperature, and precipitation in the Amazon. (a) Temperature response to land-only evapotranspiration changes, (b) Precipitation response to land-only evapotranspiration changes, and (c) Relationship between land-only ET and GPP changes. (d) Relationship between coupled temperature changes and atmospheric feedbacks' impact on GPP, where the line indicates the GPP sensitivity to temperature as diagnosed from the idealized climate treatment simulations. (e) Relationship between coupled precipitation changes and atmospheric feedbacks' impact on GPP, where the line indicates the GPP sensitivity to temperature as diagnosed from the idealized climate treatment simulations. (f) Relationship between the predicted impact of atmospheric feedbacks on GPP (as reconstructed from linear decomposition of GPP changes due to individual atmospheric drivers) and actual impact of atmospheric feedbacks on GPP, where the line is the 1:1 line.

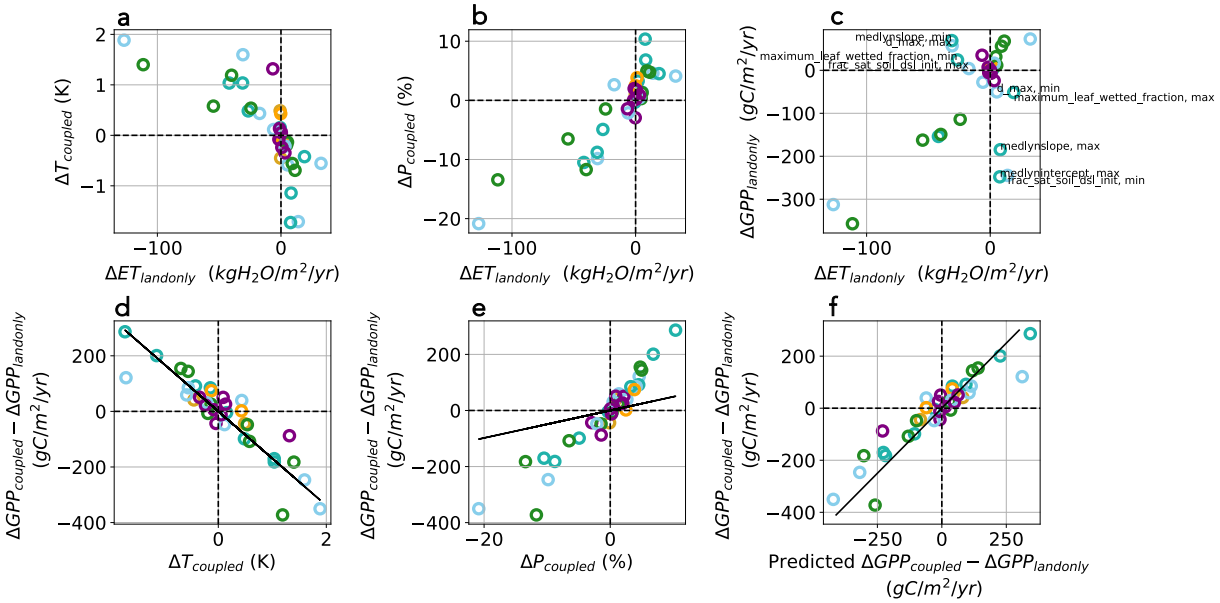

Figure 4.13: Relationships between ET, GPP, temperature, and precipitation in the Great Plains. (a) Temperature response to land-only evapotranspiration changes, (b) Precipitation response to land-only evapotranspiration changes, and (c) Relationship between land-only ET and GPP changes. (d) Relationship between coupled temperature changes and atmospheric feedbacks' impact on GPP, where the line indicates the GPP sensitivity to temperature as diagnosed from the idealized climate treatment simulations. (e) Relationship between coupled precipitation changes and atmospheric feedbacks' impact on GPP, where the line indicates the GPP sensitivity to temperature as diagnosed from the idealized climate treatment simulations. (f) Relationship between the predicted impact of atmospheric feedbacks on GPP (as reconstructed from linear decomposition of GPP changes due to individual atmospheric drivers) and actual impact of atmospheric feedbacks on GPP, where the line is the 1:1 line.

4.4 Conclusions and Implications

We found that atmospheric feedbacks substantially dampen evapotranspiration changes in wet regions, and can amplify evapotranspiration changes in some dry regions. The spatial pattern and magnitude of atmospheric modulation of evapotranspiration is largely consistent across the PPE, regardless of which process drove the initial evapotranspiration change. In contrast, atmospheric modulation of photosynthesis is more parameter dependent, such that atmospheric feedbacks in a given location can dampen or amplify GPP changes depending on the relationship between parameter's influence on GPP and on ET. Atmospheric modulation of photosynthesis is also less important on a global scale, but regionally important in the Amazon and Great Plains. Our finding that atmospheric feedbacks modulate evapotranspiration changes poses a challenge to the widespread practice of developing and evaluating land models in a land only configuration and then deploying them to understand and predict terrestrial processes in a coupled context. Our results indicate that assessing parameters' impact on the water cycle in a land only framework will yield the wrong answer - overestimating parameters' impact by up to 60% in wet regions and underestimating parameters impact in some dry regions.

While this study specifically quantifies how land-atmosphere feedbacks modulate the impact of land parameter uncertainty, it provides more general insights into how land-atmosphere feedbacks modulate any land surface perturbation which alters ET (e.g. due to land cover change or changes in plant functioning). For example, this study suggests that land-only experiments will overestimate the impact of CO_2-driven stomatal closure on ET in wet regions, but underestimate it in dry regions. This study also suggests a possible mechanism for atmospheric responses to amplify long-term feedbacks between hydroclimate and plant functional traits. For example, decreased precipitation and/or increased atmospheric demand for moisture in the Great Plains could drive shifts in plant communities towards more drought tolerant traits (e.g., as in Trugman et al., 2020) that would decrease ET. Our work suggests that such a shift would both decrease precipitation and increase VPD, amplifying water scarcity and potentially driving further shifts towards even more water-conserving plant traits.

Acknowledgements

CMZ was supported by the U.S. Department of Energy (DOE) Computational Science Graduate Fellowship (DE-SC0020347). ALSS and CMZ were also supported by the DOE Office of Biological and Environmental Research Regional and Global Model Analysis Program (DE-SC0021209) and the National Science Foundation AGS-1553715 to the University of Washington. The Computational and Information Systems Laboratory at NCAR provided computing and data storage resources, including the Cheyenne supercomputer (`https://doi.org/10.5065/D6RX99HX`). We thank all scientists, software engineers, and administrators who contributed to CESM2's development.

Chapter 5

CONCLUSIONS AND FUTURE WORK

5.1 Conclusions

This dissertation investigates how vegetation impacts climate and the global water and carbon cycles. In Chapter 2, I demonstrate that plant functional parameters and structural assumptions about photosynthetic temperature acclimation and plant hydraulics control the strength of temperature and VPD effects on tropical forest photosynthesis. I identify a novel axis along which compensating errors can occur in models – models can match observed apparent ecosystem-level photosynthesis responses to temperature by excluding photosynthetic temperature acclimation and plant hydraulics (which yields stronger direct temperature effects) or by including both of these processes (which yields stronger VPD effects). However, these two sets of assumptions yield diverging predictions of tropical photosynthesis responses to warming, with implications for the strength of the carbon-climate feedback. This study underscores that understanding the fate of the tropical forest carbon sink will require improving our scientific understanding and model representations of photosynthetic temperature acclimation and plant hydraulics. This is especially important to recognize because most CMIP6 models do not represent either of these processes.

In Chapter 3, I show that land processes play a large and underappreciated role in determining the mean climate state through biogeophysical feedbacks. This work demonstrates the importance of including terrestrial perspectives when evaluating the drivers of biases in climate models. While Chapter 3 only directly quantifies the biogeophysical impacts of land parameter uncertainty under preindustrial conditions, my findings also suggest there is potential for land parameter uncertainty to generate biogeophysical feedbacks which influence the sensitivity of land temperature trends to historical and future climates.

Finally, in Chapter 4, I show that atmospheric feedbacks are critical for understanding how terrestrial processes impact the water and carbon cycles. Atmospheric feedbacks substantially dampen land-driven evapotranspiration changes in wet regions by up to 60%, and can amplify

evapotranspiration changes in some dry regions. Atmospheric feedbacks also modulate changes in photosynthesis, particularly in the Amazon and the Great Plains, though the sign of atmospheric feedbacks are parameter dependent. This study highlights the importance of studying vegetation and the atmosphere as a coupled system, by showing that using an isolated land-only framework to quantify the impact of terrestrial processes on the carbon and water cycles would yield the wrong answer.

5.2 Future work

By designing and running the coupled PPE for Chapters 3 and 4, I generated a rich and unique dataset that I expect can be used to answer multiple science questions and to inform parameter estimation and uncertainty quantification efforts. I outline some of my ideas for future work below.

5.2.1 Plant influences on drought intensification

Climate change is leading to shifts in the community composition of ecosystems around the world. A robust body of literature has documented changes in species ranges and in the species composition at specific sites from diverse biomes, and further global warming is expected to continue to alter ecosystems' species composition (IPCC 2021). Ecologists are increasingly documenting these community composition shifts not just in terms of changes in specific species at specific sites, but in terms of continental-scale shifts in functional traits. For example, Trugman et al. (2020) documented widespread shifts in the community composition of United States forests towards more drought-resilient traits.

While some studies have shown that climate-driven changes in plant functional traits related to carbon uptake and allocation can influence the surface energy budget (Kovenock and Swann 2018; Verheijen et al. 2013, 2015), no study has quantified the implications of regional shifts in hydraulic traits on the hydrologic cycle. I plan to use the PPE to estimate the hydrologic impact of observed and projected shifts in plant water use traits across the United States. I am particularly interested in quantifying the extent to which changes in plant water use traits influence drought intensification feedbacks, building on the framework outlined by Anderegg et al. (2019). Anderegg et al. (2019) used observations and an offline vegetation model to demonstrate that plant physiological traits

can affect drought intensification feedbacks in the United States. However, their analysis did not consider the implications of changes in plant traits over time. My results in chapters 3 and 4 suggest that changing plant water use traits can drive substantial atmospheric responses, and that these atmospheric responses amplify hydrologic changes in the Great Plains. I am interested in using my PPE dataset to estimate how how changing plant water use traits would impact drought intensification feedbacks.

5.2.2 Connecting the coupled PPE to complementary parameter estimation projects

Developing a climate model that accurately represents reality requires estimating hundreds of model parameters, which span multiple Earth system components and are often poorly constrained by observations. In practice, groups modeling each Earth system component (e.g. land, ocean, atmosphere) are often isolated from each other, and groups separately tune parameters for their Earth system component in an uncoupled configuration. All components are then coupled at the end of the model development cycle to project Earth system responses to global change. Chapter 4 poses a challenge to this practice, since I show that parameters have a different impact on the carbon and water cycles in a coupled context than they do in a land-only context, because atmospheric feedbacks modulate changes in land surface fluxes. Chapter 3 also highlights issues with this parameter tuning norm, since land parameters can drive biases in the mean climate state.

I see several opportunities for my coupled PPE to inform existing parameter estimation efforts. The Community Land Model working group ran a 500 member Latin hypercube PPE which samples a much broader land parameter space than my coupled PPE, but this ensemble was run in a land-only configuration (which is why it is computationally possible for them to sample a larger parameter space). I plan to more comprehensively estimate how land parameter uncertainty can impact mean climate by applying the relationship I developed in Chapter 3 between land-only changes in evaporative fraction and coupled temperature changes to the evaporative fraction generated by this 500 member land-only ensemble. By connecting that broader PPE to temperature, I can also potentially use mean temperature as a constraint to exclude implausible parameter combinations.

Additionally, because atmospheric feedbacks modulate evapotranspiration changes in such a

consistent way across my coupled PPE, my results in Chapter 3 could be applied to land-only evapotranspiration changes to correct for the anticipated impact of atmospheric feedbacks.

5.2.3 Temperature variability

Chapter 3 focuses on how land parameter uncertainty impacts the mean climate state. I also found that land parameter uncertainty impacts the distribution of daily temperature variability, particularly during the summer months. Future work could explore the mechanisms through which land parameters influence this shorter timescale summertime temperature variability, building off the framework developed by Kong et al. (2023).

REFERENCES

Abdolghafoorian, A., & Dirmeyer, P. A. (2021, June). Validating the land–atmosphere coupling behavior in weather and climate models using observationally based global products. *Journal of Hydrometeorology*, *22*(6), 1507–1523. doi: 10.1175/JHM-D-20-0183.1

Albert, L. P., Wu, J., Prohaska, N., de Camargo, P. B., Huxman, T. E., Tribuzy, E. S., ... Saleska, S. R. (2018). Age-dependent leaf physiology and consequences for crown-scale carbon uptake during the dry season in an Amazon evergreen forest. *New Phytologist*, *219*(3), 870–884. doi: 10.1111/nph.15056

Arain, M. A., James Shuttleworth, W., Farnsworth, B., Adams, J., & Lutfi Sen, O. (2000, February). Comparing micrometeorology of rain forests in Biosphere-2 and Amazon basin. *Agricultural and Forest Meteorology*, *100*(4), 273–289. doi: 10.1016/S0168-1923(99)00153-7

Balaji, V., Couvreux, F., Deshayes, J., Gautrais, J., Hourdin, F., & Rio, C. (2022, November). Are general circulation models obsolete? *Proceedings of the National Academy of Sciences*, *119*(47), e2202075119. doi: 10.1073/pnas.2202075119

Ball, J. T., Woodrow, I. E., & Berry, J. A. (1987). A model predicting stomatal conductance and its contribution to the control of photosynthesis under different environmental conditions. In J. Biggins (Ed.), *Progress in Photosynthesis Research: Volume 4 Proceedings of the VIIth International Congress on Photosynthesis Providence, Rhode Island, USA, August 10–15, 1986* (pp. 221–224). Dordrecht: Springer Netherlands. doi: 10.1007/978-94-017-0519-6_48

Bauerle, W. L., Daniels, A. B., & Barnard, D. M. (2014, May). Carbon and water flux responses to physiology by environment interactions: A sensitivity analysis of variation in climate on photosynthetic and stomatal parameters. *Climate Dynamics*, *42*(9), 2539–2554. doi: 10.1007/s00382-013-1894-6

Betancourt, M. (2022, November). *Are We Entering The Golden Age Of Climate Modeling?* http://eos.org/features/are-we-entering-the-golden-age-of-climate-modeling.

Bitz, C. M., Shell, K. M., Gent, P. R., Bailey, D. A., Danabasoglu, G., Armour, K. C., ... Kiehl, J. T. (2012, May). Climate sensitivity of the Community Climate System Model, version 4. *Journal of Climate*, *25*(9), 3053–3070. doi: 10.1175/JCLI-D-11-00290.1

Bogenschutz, P. A., Gettelman, A., Hannay, C., Larson, V. E., Neale, R. B., Craig, C., & Chen, C.-C. (2018, January). The path to CAM6: Coupled simulations with CAM5.4 and CAM5.5. *Geoscientific Model Development*, *11*(1), 235–255. doi: 10.5194/gmd-11-235-2018

Booth, B. B. B., Harris, G. R., Murphy, J. M., House, J. I., Jones, C. D., Sexton, D., & Sitch, S. (2017, April). Narrowing the range of future climate projections using historical observations of atmospheric CO2. *Journal of Climate*, *30*(8), 3039–3053. doi: 10.1175/JCLI-D-16-0178.1

Booth, B. B. B., Jones, C. D., Collins, M., Totterdell, I. J., Cox, P. M., Sitch, S., ... Lloyd, J. (2012, April). High sensitivity of future global warming to land carbon cycle processes. *Environmental Research Letters*, *7*(2), 024002. doi: 10.1088/1748-9326/7/2/024002

Boulton, C. A., Booth, B. B. B., & Good, P. (2017). Exploring uncertainty of Amazon dieback in a perturbed parameter Earth system ensemble. *Global Change Biology*, *23*(12), 5032–5044. doi: 10.1111/gcb.13733

Boysen, L. R., Brovkin, V., Pongratz, J., Lawrence, D. M., Lawrence, P., Vuichard, N., ... Lo, M.-H. (2020, November). Global climate response to idealized deforestation in CMIP6 models. *Biogeosciences*, *17*(22), 5615–5638. doi: 10.5194/bg-17-5615-2020

Budyko, M. I. (1974). *Climate and Life* (Tech. Rep.). New York: Academic Press.

Byrne, M. P., & O'Gorman, P. A. (2018, May). Trends in continental temperature and humidity directly linked to ocean warming. *Proceedings of the National Academy of Sciences*, *115*(19), 4863–4868. doi: 10.1073/pnas.1722312115

Charney, J. G. (1975). Dynamics of deserts and drought in the Sahel. *Quarterly Journal of the Royal Meteorological Society*, *101*(428), 193–202. doi: 10.1002/qj.49710142802

Charney, J. G., Quirk, W. J., Chow, S.-h., & Kornfield, J. (1977, September). A comparative study of the effects of albedo change on drought in semi–arid regions. *Journal of the Atmospheric Sciences*, *34*(9), 1366–1385. doi: 10.1175/1520-0469(1977)034⟨1366:ACSOTE⟩2.0.CO;2

Charney, J. G., Stone, P. H., & Quirk, W. J. (1975, February). Drought in the Sahara: A biogeophysical deedback mechanism. *Science*, *187*(4175), 434–435. doi: 10.1126/science.187.4175.434

Cheruy, F., Dufresne, J. L., Hourdin, F., & Ducharne, A. (2014). Role of clouds and land-atmosphere coupling in midlatitude continental summer warm biases and climate change amplification in CMIP5 simulations. *Geophysical Research Letters*, *41*(18), 6493–6500. doi: 10.1002/2014GL061145

Christoffersen, B. O. (2021). Pantropical tropical tree xylem hydraulic functional traits, 1991 - 2013. 1.0. NGEE Tropics Data Collection.
doi: http://dx.doi.org/10.15486/ngt/1581482

Christoffersen, B. O., Gloor, M., Fauset, S., Fyllas, N. M., Galbraith, D. R., Baker, T. R., ... Meir, P. (2016, November). Linking hydraulic traits to tropical forest function in a size-structured and trait-driven model (TFS v.1-Hydro). *Geoscientific Model Development*, *9*(11), 4227–4255. doi: 10.5194/gmd-9-4227-2016

Dagon, K., Sanderson, B. M., Fisher, R. A., & Lawrence, D. M. (2020, December). A machine learning approach to emulation and biophysical parameter estimation with the Community Land Model, version 5. *Advances in Statistical Climatology, Meteorology and Oceanography*, *6*(2), 223–244. doi: 10.5194/ascmo-6-223-2020

Danabasoglu, G., & Gent, P. R. (2009, May). Equilibrium climate sensitivity: Is it accurate to use a slab ocean model? *Journal of Climate*, *22*(9), 2494–2499. doi: 10.1175/2008JCLI2596.1

Danabasoglu, G., Lamarque, J.-F., Bacmeister, J., Bailey, D. A., DuVivier, A. K., Edwards, J., ... Strand, W. G. (2020, January). The Community Earth System Model version 2 (CESM2). *Journal of Advances in Modeling Earth Systems*, *n/a*(n/a). doi: 10.1029/2019MS001916

De Kauwe, M. G., Medlyn, B. E., Ukkola, A. M., Mu, M., Sabot, M. E. B., Pitman, A. J., ... Briggs, P. R. (2020). Identifying areas at risk of drought-induced tree mortality across South-Eastern Australia. *Global Change Biology*, *26*(10), 5716–5733. doi: 10.1111/gcb.15215

De Kauwe, M. G., Sabot, M. E. B., Medlyn, B. E., Pitman, A. J., Meir, P., Cernusak, L. A., ... Choat, B. (2022). Towards species-level forecasts of drought-induced tree mortality risk. *New Phytologist*, *235*(1), 94–110. doi: 10.1111/nph.18129

Dietze, M. C., Serbin, S. P., Davidson, C., Desai, A. R., Feng, X., Kelly, R., ... Wang, D. (2014). A quantitative assessment of a terrestrial biosphere model's data needs across North American biomes. *Journal of Geophysical Research: Biogeosciences*, *119*(3), 286–300. doi: 10.1002/2013JG002392

dos Santos, V. A. H. F., Ferreira, M. J., Rodrigues, J. V. F. C., Garcia, M. N., Ceron, J. V. B., Nelson, B. W., & Saleska, S. R. (2018). Causes of reduced leaf-level photosynthesis during strong El Niño drought in a Central Amazon forest. *Global Change Biology*, *24*(9), 4266–4279. doi: 10.1111/gcb.14293

Doughty, C. E., & Goulden, M. L. (2008). Are tropical forests near a high temperature threshold? *Journal of Geophysical Research: Biogeosciences*, *113*(G1). doi: 10.1029/2007JG000632

Doughty, C. E., Keany, J. M., Wiebe, B. C., Rey-Sanchez, C., Carter, K. R., Middleby, K. B., ... Fisher, J. B. (2023, September). Tropical forests are approaching critical temperature thresholds. *Nature*, *621*(7977), 105–111. doi: 10.1038/s41586-023-06391-z

Duffy, K. A., Schwalm, C. R., Arcus, V. L., Koch, G. W., Liang, L. L., & Schipper, L. A. (2021, January). How close are we to the temperature tipping point of the terrestrial biosphere? *Science Advances*, *7*(3), eaay1052. doi: 10.1126/sciadv.aay1052

Dusenge, M. E., Duarte, A. G., & Way, D. A. (2019). Plant carbon metabolism and climate change: Elevated CO2 and temperature impacts on photosynthesis, photorespiration and respiration. *New Phytologist*, *221*(1), 32–49. doi: 10.1111/nph.15283

Eller, C. B., de V. Barros, F., Bittencourt, P. R., Rowland, L., Mencuccini, M., & Oliveira, R. S.

(2018). Xylem hydraulic safety and construction costs determine tropical tree growth. *Plant, Cell & Environment*, *41*(3), 548–562. doi: 10.1111/pce.13106

Eller, C. B., Rowland, L., Mencuccini, M., Rosas, T., Williams, K., Harper, A., ... Cox, P. M. (2020). Stomatal optimization based on xylem hydraulics (SOX) improves land surface model simulation of vegetation responses to climate. *New Phytologist*, *226*(6), 1622–1637. doi: 10.1111/nph.16419

European Centre for Medium-Range Weather Forecasts. (2019). *ERA5 reanalysis (monthly mean 0.25 degree latitude-longitude grid).* Boulder CO: Research Data Archive at the National Center for Atmospheric Research, Computational and Information Systems Laboratory.

Ferguson, C. R., Wood, E. F., & Vinukollu, R. K. (2012, June). A global intercomparison of modeled and observed land–atmosphere coupling. *Journal of Hydrometeorology*, *13*(3), 749–784. doi: 10.1175/JHM-D-11-0119.1

Fischer, E. M., Lawrence, D. M., & Sanderson, B. M. (2011, October). Quantifying uncertainties in projections of extremes—a perturbed land surface parameter experiment. *Climate Dynamics*, *37*(7), 1381–1398. doi: 10.1007/s00382-010-0915-y

Fisher, R. A., & Koven, C. D. (2020). Perspectives on the future of land surface models and the challenges of representing complex terrestrial systems. *Journal of Advances in Modeling Earth Systems*, *12*(4), e2018MS001453. doi: 10.1029/2018MS001453

Fisher, R. A., Muszala, S., Verteinstein, M., Lawrence, P., Xu, C., McDowell, N. G., ... Bonan, G. (2015, November). Taking off the training wheels: The properties of a dynamic vegetation model without climate envelopes, CLM4.5(ED). *Geoscientific Model Development*, *8*(11), 3593–3619. doi: 10.5194/gmd-8-3593-2015

Fisher, R. A., Wieder, W. R., Sanderson, B. M., Koven, C. D., Oleson, K. W., Xu, C., ... Lawrence, D. M. (2019). Parametric controls on vegetation responses to biogeochemical forcing in the CLM5. *Journal of Advances in Modeling Earth Systems*. doi: 10.1029/2019MS001609

Friedlingstein, P., Cox, P., Betts, R., Bopp, L., von Bloh, W., Brovkin, V., ... Zeng, N. (2006,

July). Climate–Carbon cycle feedback analysis: Results from the C4MIP model intercomparison. *Journal of Climate*, *19*(14), 3337–3353. doi: 10.1175/JCLI3800.1

Friedlingstein, P., Meinshausen, M., Arora, V. K., Jones, C. D., Anav, A., Liddicoat, S. K., & Knutti, R. (2013, September). Uncertainties in CMIP5 climate projections due to carbon cycle feedbacks. *Journal of Climate*, *27*(2), 511–526. doi: 10.1175/JCLI-D-12-00579.1

Fu, Z., Gerken, T., Bromley, G., Araújo, A., Bonal, D., Burban, B., ... Stoy, P. C. (2018, December). The surface-atmosphere exchange of carbon dioxide in tropical rainforests: Sensitivity to environmental drivers and flux measurement methodology. *Agricultural and Forest Meteorology*, *263*, 292–307. doi: 10.1016/j.agrformet.2018.09.001

Galbraith, D., Levy, P. E., Sitch, S., Huntingford, C., Cox, P., Williams, M., & Meir, P. (2010). Multiple mechanisms of Amazonian forest biomass losses in three dynamic global vegetation models under climate change. *New Phytologist*, *187*(3), 647–665. doi: 10.1111/j.1469-8137.2010.03350.x

Goll, D. (2013). *The influence of phosphorus cycling and temperature acclimation of photosynthesis on the land carbon cycle* (Doctoral dissertation, Hamburg University Hamburg). doi: 10.17617/2.1669156

Grossiord, C., Buckley, T. N., Cernusak, L. A., Novick, K. A., Poulter, B., Siegwolf, R. T. W., ... McDowell, N. G. (2020). Plant responses to rising vapor pressure deficit. *New Phytologist*, *226*(6), 1550–1566. doi: 10.1111/nph.16485

Hawkins, E., & Sutton, R. (2016, June). Connecting climate model projections of global temperature change with the real world. *Bulletin of the American Meteorological Society*, *97*(6), 963–980. doi: 10.1175/BAMS-D-14-00154.1

Hawkins, L. R., Rupp, D. E., McNeall, D. J., Li, S., Betts, R. A., Mote, P. W., ... Wallom, D. C. H. (2019). Parametric sensitivity of vegetation dynamics in the TRIFFID model and the associated uncertainty in projected climate change impacts on Western U.S. forests. *Journal of Advances in Modeling Earth Systems*, *11*(8), 2787–2813. doi: 10.1029/2018MS001577

Hickler, T., Prentice, I. C., Smith, B., Sykes, M. T., & Zaehle, S. (2006). Implementing plant hydraulic architecture within the LPJ Dynamic Global Vegetation Model. *Global Ecology and Biogeography*, *15*(6), 567–577. doi: 10.1111/j.1466-8238.2006.00254.x

Hou, Z., Huang, M., Leung, L. R., Lin, G., & Ricciuto, D. M. (2012). Sensitivity of surface flux simulations to hydrologic parameters based on an uncertainty quantification framework applied to the Community Land Model. *Journal of Geophysical Research: Atmospheres*, *117*(D15). doi: 10.1029/2012JD017521

Hourdin, F., Mauritsen, T., Gettelman, A., Golaz, J.-C., Balaji, V., Duan, Q., ... Williamson, D. (2017, March). The art and science of climate model tuning. *Bulletin of the American Meteorological Society*, *98*(3), 589–602. doi: 10.1175/BAMS-D-15-00135.1

Huang, M., Piao, S., Ciais, P., Peñuelas, J., Wang, X., Keenan, T. F., ... Janssens, I. A. (2019, May). Air temperature optima of vegetation productivity across global biomes. *Nature Ecology & Evolution*, *3*(5), 772–779. doi: 10.1038/s41559-019-0838-x

Huo, X., Gupta, H., Niu, G.-Y., Gong, W., & Duan, Q. (2019). Parameter sensitivity analysis for computationally intensive spatially distributed dynamical environmental systems models. *Journal of Advances in Modeling Earth Systems*, *11*(9), 2896–2909. doi: 10.1029/2018MS001573

Hutyra, L. R., Munger, J. W., Saleska, S. R., Gottlieb, E., Daube, B. C., Dunn, A. L., ... Wofsy, S. C. (2007). Seasonal controls on the exchange of carbon and water in an Amazonian rain forest. *Journal of Geophysical Research: Biogeosciences*, *112*(G3). doi: 10.1029/2006JG000365

Ivanov, V. Y., Hutyra, L. R., Wofsy, S. C., Munger, J. W., Saleska, S. R., de Oliveira Jr., R. C., & de Camargo, P. B. (2012). Root niche separation can explain avoidance of seasonal drought stress and vulnerability of overstory trees to extended drought in a mature Amazonian forest. *Water Resources Research*, *48*(12). doi: 10.1029/2012WR011972

Jones, C. D., Arora, V., Friedlingstein, P., Bopp, L., Brovkin, V., Dunne, J., ... Zaehle, S. (2016, August). C4MIP - The Coupled Climate–Carbon Cycle Model Intercomparison Project:experimental protocol for CMIP6. *Geoscientific Model Development*, *9*(8), 2853–2880. doi: 10.5194/gmd-9-2853-2016

Kala, J., De Kauwe, M. G., Pitman, A. J., Medlyn, B. E., Wang, Y.-P., Lorenz, R., & Perkins-Kirkpatrick, S. E. (2016, March). Impact of the representation of stomatal conductance on model projections of heatwave intensity. *Scientific Reports*, *6*(1), 23418. doi: 10.1038/srep23418

Kattge, J., & Knorr, W. (2007). Temperature acclimation in a biochemical model of photosynthesis: A reanalysis of data from 36 species. *Plant, Cell & Environment*, *30*(9), 1176–1190. doi: 10.1111/j.1365-3040.2007.01690.x

Kennedy, D., Swenson, S., Oleson, K. W., Lawrence, D. M., Fisher, R., da Costa, A. C. L., & Gentine, P. (2019). Implementing plant hydraulics in the Community Land Model, version 5. *Journal of Advances in Modeling Earth Systems*, *11*(2), 485–513. doi: 10.1029/2018MS001500

Kim, J. E., Laguë, M. M., Pennypacker, S., Dawson, E., & Swann, A. L. S. (2020). Evaporative resistance is of equal importance as surface albedo in high-latitude surface temperatures due to cloud feedbacks. *Geophysical Research Letters*, *47*(4), e2019GL085663. doi: 10.1029/2019GL085663

Klein, S. A., Jiang, X., Boyle, J., Malyshev, S., & Xie, S. (2006). Diagnosis of the summertime warm and dry bias over the U.S. Southern Great Plains in the GFDL climate model using a weather forecasting approach. *Geophysical Research Letters*, *33*(18). doi: 10.1029/2006GL027567

Knauer, J., Cuntz, M., Smith, B., Canadell, J. G., Medlyn, B. E., Bennett, A. C., ... Haverd, V. (2023, November). Higher global gross primary productivity under future climate with more advanced representations of photosynthesis. *Science Advances*, *9*(46), eadh9444. doi: 10.1126/sciadv.adh9444

Kong, W., McKinnon, K. A., Simpson, I. R., & Laguë, M. M. (2023, February). Understanding responses of summer continental daily temperature variance to perturbations in the land surface evaporative resistance. *Journal of Climate*, *36*(6), 1653–1678. doi: 10.1175/JCLI-D-21-1011.1

Kooperman, G. J., Chen, Y., Hoffman, F. M., Koven, C. D., Lindsay, K., Pritchard, M. S., ... Randerson, J. T. (2018, May). Forest response to rising CO2 drives zonally asymmetric rainfall change over tropical land. *Nature Climate Change*, *8*(5), 434–440. doi: 10.1038/s41558-018-0144-7

Köppen, W. (1936). Das Geographische System der Klimate. In *Handbuch der klimatologie.*

Koster, R. D., Sud, Y. C., Guo, Z., Dirmeyer, P. A., Bonan, G., Oleson, K. W., ... Xue, Y. (2006, August). GLACE: The Global Land–Atmosphere Coupling Experiment. Part I: Overview. *Journal of Hydrometeorology*, *7*(4), 590–610. doi: 10.1175/JHM510.1

Koven, C. D., Knox, R. G., Fisher, R. A., Chambers, J. Q., Christoffersen, B. O., Davies, S. J., ... Xu, C. (2020, June). Benchmarking and parameter sensitivity of physiological and vegetation dynamics using the Functionally Assembled Terrestrial Ecosystem Simulator (FATES) at Barro Colorado Island, Panama. *Biogeosciences*, *17*(11), 3017–3044. doi: 10.5194/bg-17-3017-2020

Kumarathunge, D. P., Medlyn, B. E., Drake, J. E., Tjoelker, M. G., Aspinwall, M. J., Battaglia, M., ... Way, D. A. (2019). Acclimation and adaptation components of the temperature dependence of plant photosynthesis at the global scale. *New Phytologist*, *222*(2), 768–784. doi: 10.1111/nph.15668

Laguë, M. M., Bonan, G. B., & Swann, A. L. S. (2019, September). Separating the impact of individual land surface properties on the terrestrial surface energy budget in both the coupled and uncoupled land–atmosphere system. *Journal of Climate*, *32*(18), 5725–5744. doi: 10.1175/JCLI-D-18-0812.1

Laguë, M. M., Pietschnig, M., Ragen, S., Smith, T. A., & Battisti, D. S. (2021, March). Terrestrial evaporation and global climate: Lessons from Northland, a planet with a hemispheric continent. *Journal of Climate*, *34*(6), 2253–2276. doi: 10.1175/JCLI-D-20-0452.1

Lawrence, D. M., Fisher, R. A., Koven, C. D., Oleson, K. W., Swenson, S. C., Bonan, G., ... Zeng, X. (2019). The Community Land Model Version 5: Description of new features, benchmarking, and impact of forcing uncertainty. *Journal of Advances in Modeling Earth Systems*, *11*, 4245–4287. doi: 10.1029/2018MS001583

Lawrence, D. M., Thornton, P. E., Oleson, K. W., & Bonan, G. B. (2007, August). The partitioning of evapotranspiration into transpiration, soil evaporation, and canopy evaporation in a GCM: Impacts on land–atmosphere interaction. *Journal of Hydrometeorology*, *8*(4), 862–880. doi: 10.1175/JHM596.1

Lee, J.-E., & Boyce, K. (2010). Impact of the hydraulic capacity of plants on water and carbon fluxes in tropical South America. *Journal of Geophysical Research: Atmospheres*, *115*(D23). doi: 10.1029/2010JD014568

Lemordant, L., Gentine, P., Swann, A. S., Cook, B. I., & Scheff, J. (2018, April). Critical impact of vegetation physiology on the continental hydrologic cycle in response to increasing CO2. *Proceedings of the National Academy of Sciences*, *115*(16), 4093–4098. doi: 10.1073/pnas.1720712115

Li, X., Feng, M., Ran, Y., Su, Y., Liu, F., Huang, C., ... Guo, H. (2023, May). Big Data in Earth system science and progress towards a digital twin. *Nature Reviews Earth & Environment*, *4*(5), 319–332. doi: 10.1038/s43017-023-00409-w

Li, Y., Baker, J. C. A., Brando, P. M., Hoffman, F. M., Lawrence, D. M., Morton, D. C., ... Randerson, J. T. (2023, September). Future increases in Amazonia water stress from CO2 physiology and deforestation. *Nature Water*, *1*(9), 769–777. doi: 10.1038/s44221-023-00128-y

Li, Y., Brando, P. M., Morton, D. C., Lawrence, D. M., Yang, H., & Randerson, J. T. (2022, April). Deforestation-induced climate change reduces carbon storage in remaining tropical forests. *Nature Communications*, *13*(1), 1964. doi: 10.1038/s41467-022-29601-0

Lian, X., Piao, S., Huntingford, C., Li, Y., Zeng, Z., Wang, X., ... Wang, T. (2018, July). Partitioning global land evapotranspiration using CMIP5 models constrained by observations. *Nature Climate Change*, *8*(7), 640–646. doi: 10.1038/s41558-018-0207-9

Lin, Y., Dong, W., Zhang, M., Xie, Y., Xue, W., Huang, J., & Luo, Y. (2017, October). Causes of model dry and warm bias over central U.S. and impact on climate projections. *Nature Communications*, *8*(1), 881. doi: 10.1038/s41467-017-01040-2

Lin, Y.-S., Medlyn, B. E., Duursma, R. A., Prentice, I. C., Wang, H., Baig, S., ... Wingate, L. (2015, May). Optimal stomatal behaviour around the world. *Nature Climate Change*, *5*(5), 459–464. doi: 10.1038/nclimate2550

Liu, Y., Gupta, H. V., Sorooshian, S., Bastidas, L. A., & Shuttleworth, W. J. (2005, April). Constraining land surface and atmospheric parameters of a locally coupled model using observational data. *Journal of Hydrometeorology*, *6*(2), 156–172. doi: 10.1175/JHM407.1

Liu, Y., Holtzman, N. M., & Konings, A. G. (2021, May). Global ecosystem-scale plant hydraulic traits retrieved using model–data fusion. *Hydrology and Earth System Sciences*, *25*(5), 2399–2417. doi: 10.5194/hess-25-2399-2021

Lloyd, J., & Farquhar, G. D. (2008, May). Effects of rising temperatures and [CO2] on the physiology of tropical forest trees. *Philosophical Transactions of the Royal Society B: Biological Sciences*, *363*(1498), 1811–1817. doi: 10.1098/rstb.2007.0032

Lombardozzi, D. L., Bonan, G. B., Smith, N. G., Dukes, J. S., & Fisher, R. A. (2015). Temperature acclimation of photosynthesis and respiration: A key uncertainty in the carbon cycle-climate feedback. *Geophysical Research Letters*, *42*(20), 8624–8631. doi: 10.1002/2015GL065934

Lopes, A. P., Nelson, B. W., Wu, J., Graça, P. M. L. d. A., Tavares, J. V., Prohaska, N., ... Saleska, S. R. (2016, September). Leaf flush drives dry season green-up of the Central Amazon. *Remote Sensing of Environment*, *182*, 90–98. doi: 10.1016/j.rse.2016.05.009

Lorenz, E. N. (1956, December). *Empirical Orthogonal Functions and Statistical Weather Prediction* (Scientific Report No. 1). Cambridge, MA: Massachusetts Institute of Technology, Department of Meteorology.

Lovenduski, N. S., & Bonan, G. B. (2017, April). Reducing uncertainty in projections of terrestrial carbon uptake. *Environmental Research Letters*, *12*(4), 044020. doi: 10.1088/1748-9326/aa66b8

Ma, H.-Y., Klein, S. A., Xie, S., Zhang, C., Tang, S., Tang, Q., ... Wang, Y.-C. (2018). CAUSES: On the role of surface energy budget errors to the warm surface air temperature error over the central United States. *Journal of Geophysical Research: Atmospheres*, *123*(5), 2888–2909. doi: 10.1002/2017JD027194

Manabe, S. (1969, November). Climate and the ocean circulation: I. The Atmospheric circulation and the hydrology of the Earth's surface. *Monthly Weather Review*, *97*(11), 739–774. doi: 10.1175/1520-0493(1969)097⟨0739:CATOC⟩2.3.CO;2

Mau, A. C., Reed, S. C., Wood, T. E., & Cavaleri, M. A. (2018, January). Temperate and tropical forest canopies are already functioning beyond their thermal thresholds for photosynthesis. *Forests*, *9*(1), 47. doi: 10.3390/f9010047

McNeall, D., Robertson, E., & Wiltshire, A. (2023, February). Constraining the carbon cycle in JULES-ES-1.0. *Geoscientific Model Development Discussions*, 1–38. doi: 10.5194/gmd-2022-280

Medlyn, B. E., Duursma, R. A., Eamus, D., Ellsworth, D. S., Prentice, I. C., Barton, C. V. M., ... Wingate, L. (2011). Reconciling the optimal and empirical approaches to modelling stomatal conductance. *Global Change Biology*, *17*(6), 2134–2144. doi: 10.1111/j.1365-2486.2010.02375.x

Meinshausen, M., Nicholls, Z. R. J., Lewis, J., Gidden, M. J., Vogel, E., Freund, M., ... Wang, R. H. J. (2020, August). The shared socio-economic pathway (SSP) greenhouse gas concentrations and their extensions to 2500. *Geoscientific Model Development*, *13*(8), 3571–3605. doi: 10.5194/gmd-13-3571-2020

Mercado, L. M., Medlyn, B. E., Huntingford, C., Oliver, R. J., Clark, D. B., Sitch, S., ... Cox, P. M. (2018). Large sensitivity in land carbon storage due to geographical and temporal variation in the thermal response of photosynthetic capacity. *New Phytologist*, *218*(4), 1462–1477. doi: 10.1111/nph.15100

Morcrette, C. J., Van Weverberg, K., Ma, H.-Y., Ahlgrimm, M., Bazile, E., Berg, L. K., ... Petch, J. (2018). Introduction to CAUSES: Description of weather and climate models and their near-surface temperature errors in 5 day hindcasts near the Southern Great Plains. *Journal of Geophysical Research: Atmospheres*, *123*(5), 2655–2683. doi: 10.1002/2017JD027199

Mueller, B., & Seneviratne, S. I. (2014). Systematic land climate and evapotranspiration biases in CMIP5 simulations. *Geophysical Research Letters*, *41*(1), 128–134. doi: 10.1002/2013GL058055

Naudts, K., Ryder, J., McGrath, M. J., Otto, J., Chen, Y., Valade, A., ... Luyssaert, S. (2015, July). A vertically discretised canopy description for ORCHIDEE (SVN r2290) and the modifications to the energy, water and carbon fluxes. *Geoscientific Model Development*, *8*(7), 2035–2065. doi: 10.5194/gmd-8-2035-2015

Oliver, R. J., Mercado, L. M., Clark, D. B., Huntingford, C., Taylor, C. M., Vidale, P. L., ... Medlyn, B. E. (2022, July). Improved representation of plant physiology in the JULES-vn5.6 land surface model: Photosynthesis, stomatal conductance and thermal acclimation. *Geoscientific Model Development*, *15*(14), 5567–5592. doi: 10.5194/gmd-15-5567-2022

Park, S.-W., Kim, J.-S., & Kug, J.-S. (2020, April). The intensification of Arctic warming as a result of CO2 physiological forcing. *Nature Communications*, *11*(1), 2098. doi: 10.1038/s41467-020-15924-3

Park, S.-W., Kug, J.-S., Jun, S.-Y., Jeong, S.-J., & Kim, J.-S. (2021, August). Role of cloud feedback in continental warming response to CO2 physiological forcing. *Journal of Climate*, *-1*(aop), 1–49. doi: 10.1175/JCLI-D-21-0025.1

Pastorello, G., Trotta, C., Canfora, E., Chu, H., Christianson, D., Cheah, Y.-W., ... Papale, D. (2020, July). The FLUXNET2015 dataset and the ONEFlux processing pipeline for eddy covariance data. *Scientific Data*, *7*(1), 225. doi: 10.1038/s41597-020-0534-3

Peel, M. C., Finlayson, B. L., & McMahon, T. A. (2007, October). Updated world map of the Köppen-Geiger climate classification. *Hydrology and Earth System Sciences*, *11*(5), 1633–1644. doi: 10.5194/hess-11-1633-2007

Pegoraro, E., Rey, A., Abrell, L., Haren, J. V., & Lin, G. (2006). Drought effect on isoprene production and consumption in Biosphere 2 tropical rainforest. *Global Change Biology*, *12*(3), 456–469. doi: 10.1111/j.1365-2486.2006.01112.x

Perez-Ruiz, E. R., Garatuza-Payan, J., Watts, C. J., Rodriguez, J. C., Yepez, E. A., & Scott, R. L. (2010, May). Carbon dioxide and water vapour exchange in a tropical dry forest as influenced by the North American Monsoon System (NAMS). *Journal of Arid Environments*, *74*(5), 556–563. doi: 10.1016/j.jaridenv.2009.09.029

Pietschnig, M., Swann, A. L. S., Lambert, F. H., & Vallis, G. K. (2021, December). Response of tropical rainfall to reduced evapotranspiration depends on continental extent. *Journal of Climate*, *34*(23), 9221–9234. doi: 10.1175/JCLI-D-21-0195.1

Pongratz, J., Reick, C. H., Raddatz, T., & Claussen, M. (2010). Biogeophysical versus biogeochemical climate response to historical anthropogenic land cover change. *Geophysical Research Letters*, *37*(8). doi: 10.1029/2010GL043010

Rascher, U., Bobich, E. G., Lin, G. H., Walter, A., Morris, T., Naumann, M., ... Berry, J. A. (2004). Functional diversity of photosynthesis during drought in a model tropical rainforest –

the contributions of leaf area, photosynthetic electron transport and stomatal conductance to reduction in net ecosystem carbon exchange. *Plant, Cell & Environment*, *27*(10), 1239–1256. doi: 10.1111/j.1365-3040.2004.01231.x

Reichstein, M., Camps-Valls, G., Stevens, B., Jung, M., Denzler, J., Carvalhais, N., & Prabhat. (2019, February). Deep learning and process understanding for data-driven Earth system science. *Nature*, *566*(7743), 195–204. doi: 10.1038/s41586-019-0912-1

Restrepo-Coupe, N., da Rocha, H. R., Hutyra, L. R., da Araujo, A. C., Borma, L. S., Christoffersen, B., ... Saleska, S. R. (2013, December). What drives the seasonality of photosynthesis across the Amazon basin? A cross-site analysis of eddy flux tower measurements from the Brasil flux network. *Agricultural and Forest Meteorology*, *182–183*, 128–144. doi: 10.1016/j.agrformet.2013.04.031

Restrepo-Coupe, N., Levine, N. M., Christoffersen, B. O., Albert, L. P., Wu, J., Costa, M. H., ... Saleska, S. R. (2017). Do dynamic global vegetation models capture the seasonality of carbon fluxes in the Amazon basin? A data-model intercomparison. *Global Change Biology*, *23*(1), 191–208. doi: 10.1111/gcb.13442

Ricciuto, D., Sargsyan, K., & Thornton, P. (2018). The impact of parametric uncertainties on biogeochemistry in the E3SM land model. *Journal of Advances in Modeling Earth Systems*, *10*(2), 297–319. doi: 10.1002/2017MS000962

Rosolem, R., Shuttleworth, W. J., Zeng, X., Saleska, S. R., & Huxman, T. E. (2010). Land surface modeling inside the Biosphere 2 tropical rain forest biome. *Journal of Geophysical Research: Biogeosciences*, *115*(G4). doi: 10.1029/2010JG001443

Rowland, L., Harper, A., Christoffersen, B. O., Galbraith, D. R., Imbuzeiro, H. M. A., Powell, T. L., ... Williams, M. (2015, April). Modelling climate change responses in tropical forests: Similar productivity estimates across five models, but different mechanisms and responses. *Geoscientific Model Development*, *8*(4), 1097–1110. doi: 10.5194/gmd-8-1097-2015

Saint-Lu, M., Chadwick, R., Lambert, F. H., & Collins, M. (2019). Surface warming and at-

mospheric circulation dominate rainfall changes over tropical rainforests under global warming. *Geophysical Research Letters*, *46*(22). doi: 10.1029/2019GL085295

Sanchez-Mejia, Z. M., Garatuza Payan, J., Yepez, E. A., Perez Ruiz, E. R., Peñuelas Rubio, O., Serrano Grijalva, L., ... Siqueiros, E. (2021, March). *Floristic composition surrounding the footprint of eddy covariance and micrometeorology tower in the tropical dry forest, Tesopaco, Sonora (México).*

Santanello, J. A., Dirmeyer, P. A., Ferguson, C. R., Findell, K. L., Tawfik, A. B., Berg, A., ... Wulfmeyer, V. (2018, June). Land–Atmosphere interactions: The LoCo perspective. *Bulletin of the American Meteorological Society*, *99*(6), 1253–1272. doi: 10.1175/BAMS-D-17-0001.1

Sellers, PJ., Bounoua, L., Collatz, GJ., Randall, DA., Dazlich, DA., Los, SO., ... Jensen, TG. (1996, March). Comparison of radiative and physiological effects of doubled atmospheric CO2 on climate. *Science*, *271*(5254), 1402–1406.

Seneviratne, S. I., Wilhelm, M., Stanelle, T., van den Hurk, B., Hagemann, S., Berg, A., ... Smith, B. (2013). Impact of soil moisture-climate feedbacks on CMIP5 projections: First results from the GLACE-CMIP5 experiment. *Geophysical Research Letters*, *40*(19), 5212–5217. doi: 10.1002/grl.50956

Sexton, D. M. H., McSweeney, C. F., Rostron, J. W., Yamazaki, K., Booth, B. B. B., Murphy, J. M., ... Karmalkar, A. V. (2021, June). A perturbed parameter ensemble of HadGEM3-GC3.05 coupled model projections: Part 1: Selecting the parameter combinations. *Climate Dynamics*, *56*(11), 3395–3436. doi: 10.1007/s00382-021-05709-9

Shukla, J., & Mintz, Y. (1982). Influence of land-surface evapotranspiration on the Earth's climate. *Science*, *215*(4539), 1498–1501.

Shum, G. E. M., Laguë, M. M., Rushley, S. S., & Swann, A. L. S. (2023, September). Beautiful days in the neighborhood: Land–atmosphere interactions as drivers of forest expansion. *Earth Interactions*, *27*(1). doi: 10.1175/EI-D-22-0017.1

Slot, M., Garcia, M. N., & Winter, K. (2016, March). Temperature response of CO2 exchange in three tropical tree species. *Functional Plant Biology*, *43*(5), 468–478. doi: 10.1071/FP15320

Slot, M., & Winter, K. (2016). The effects of rising temperature on the ecophysiology of tropical forest trees. In G. Goldstein & L. S. Santiago (Eds.), *Tropical Tree Physiology: Adaptations and Responses in a Changing Environment* (pp. 385–412). Cham: Springer International Publishing. doi: 10.1007/978-3-319-27422-5_18

Smith, M. N., Stark, S. C., Taylor, T. C., Ferreira, M. L., de Oliveira, E., Restrepo-Coupe, N., ... Saleska, S. R. (2019). Seasonal and drought-related changes in leaf area profiles depend on height and light environment in an Amazon forest. *New Phytologist*, *222*(3), 1284–1297. doi: 10.1111/nph.15726

Smith, M. N., Taylor, T. C., van Haren, J., Rosolem, R., Restrepo-Coupe, N., Adams, J., ... Saleska, S. R. (2020, October). Empirical evidence for resilience of tropical forest photosynthesis in a warmer world. *Nature Plants*, *6*(10), 1225–1230. doi: 10.1038/s41477-020-00780-2

Smith, N. G., Lombardozzi, D., Tawfik, A., Bonan, G., & Dukes, J. S. (2017). Biophysical consequences of photosynthetic temperature acclimation for climate. *Journal of Advances in Modeling Earth Systems*, *9*(1), 536–547. doi: 10.1002/2016MS000732

Smith, N. G., Malyshev, S. L., Shevliakova, E., Kattge, J., & Dukes, J. S. (2016, April). Foliar temperature acclimation reduces simulated carbon sensitivity to climate. *Nature Climate Change*, *6*(4), 407–411. doi: 10.1038/nclimate2878

Staal, A., Koren, G., Tejada, G., & Gatti, L. V. (2023, April). Moisture origins of the Amazon carbon source region. *Environmental Research Letters*, *18*(4), 044027. doi: 10.1088/1748-9326/acc676

Sud, Y. C., Shukla, J., & Mintz, Y. (1988, September). Influence of land surface roughness on atmospheric circulation and precipitation: A sensitivity study with a general circulation model. *Journal of Applied Meteorology and Climatology*, *27*(9), 1036–1054. doi: 10.1175/1520-0450(1988)027⟨1036:IOLSRO⟩2.0.CO;2

Swann, A. L. S., Fung, I. Y., & Chiang, J. C. H. (2012, January). Mid-latitude afforestation shifts general circulation and tropical precipitation. *Proceedings of the National Academy of Sciences*, *109*(3), 712–716. doi: 10.1073/pnas.1116706108

Tan, Z.-H., Zeng, J., Zhang, Y.-J., Slot, M., Gamo, M., Hirano, T., ... Restrepo-Coupe, N. (2017, May). Optimum air temperature for tropical forest photosynthesis: Mechanisms involved and implications for climate warming. *Environmental Research Letters*, *12*(5), 054022. doi: 10.1088/1748-9326/aa6f97

Tang, A. C. I., Stoy, P. C., Hirata, R., Musin, K. K., Aeries, E. B., Wenceslaus, J., ... Melling, L. (2019, September). The exchange of water and energy between a tropical peat forest and the atmosphere: Seasonal trends and comparison against other tropical rainforests. *Science of The Total Environment*, *683*, 166–174. doi: 10.1016/j.scitotenv.2019.05.217

Tang, J., & Zhuang, Q. (2008). Equifinality in parameterization of process-based biogeochemistry models: A significant uncertainty source to the estimation of regional carbon dynamics. *Journal of Geophysical Research: Biogeosciences*, *113*(G4). doi: 10.1029/2008JG000757

Tavares, J. V., Oliveira, R. S., Mencuccini, M., Signori-Müller, C., Pereira, L., Diniz, F. C., ... Galbraith, D. R. (2023, May). Basin-wide variation in tree hydraulic safety margins predicts the carbon balance of Amazon forests. *Nature*, *617*(7959), 111–117. doi: 10.1038/s41586-023-05971-3

Taylor, T. C., McMahon, S. M., Smith, M. N., Boyle, B., Violle, C., van Haren, J., ... Saleska, S. R. (2018). Isoprene emission structures tropical tree biogeography and community assembly responses to climate. *New Phytologist*, *220*(2), 435–446. doi: 10.1111/nph.15304

Taylor, T. C., Smith, M. N., Slot, M., & Feeley, K. J. (2019). The capacity to emit isoprene differentiates the photosynthetic temperature responses of tropical plant species. *Plant, Cell & Environment*, *42*(8), 2448–2457. doi: 10.1111/pce.13564

Tett, S. F. B., Gregory, J. M., Freychet, N., Cartis, C., Mineter, M. J., & Roberts, L. (2022, April). Does model calibration reduce uncertainty in climate projections? *Journal of Climate*, *35*(8), 2585–2602. doi: 10.1175/JCLI-D-21-0434.1

Teuling, A. J., Taylor, C. M., Meirink, J. F., Melsen, L. A., Miralles, D. G., van Heerwaarden, C. C., ... de Arellano, J. V.-G. (2017, January). Observational evidence for cloud

cover enhancement over western European forests. *Nature Communications*, *8*(1), 14065. doi: 10.1038/ncomms14065

Trugman, A. T., Anderegg, L. D. L., Shaw, J. D., & Anderegg, W. R. L. (2020, April). Trait velocities reveal that mortality has driven widespread coordinated shifts in forest hydraulic trait composition. *Proceedings of the National Academy of Sciences*, *117*(15), 8532–8538. doi: 10.1073/pnas.1917521117

Vargas-G, G., & Cordero, R. A. (2013, October). Photosynthetic responses to temperature of two tropical rainforest tree species from Costa Rica. *Trees*, *27*(5), 1261–1270. doi: 10.1007/s00468-013-0874-0

Vinod, N., Slot, M., McGregor, I. R., Ordway, E. M., Smith, M. N., Taylor, T. C., ... Anderson-Teixeira, K. J. (2023). Thermal sensitivity across forest vertical profiles: Patterns, mechanisms, and ecological implications. *New Phytologist*, *237*(1), 22–47. doi: 10.1111/nph.18539

Voosen, P. (2020, October). Europe builds 'digital twin' of Earth to hone climate forecasts. *Science*, *370*(6512), 16–17. doi: 10.1126/science.370.6512.16

Werner, C., Meredith, L. K., Ladd, S. N., Ingrisch, J., Kübert, A., van Haren, J., ... Williams, J. (2021, December). Ecosystem fluxes during drought and recovery in an experimental forest. *Science*. doi: 10.1126/science.abj6789

White, R. H., Wallace, J. M., & Battisti, D. S. (2021, July). Revisiting the role of mountains in the Northern Hemisphere winter atmospheric circulation. *Journal of the Atmospheric Sciences*, *78*(7), 2221–2235. doi: 10.1175/JAS-D-20-0300.1

Whittaker, R. H. (1975). *Communities and Ecosystems* (2nd ed.). New York: MacMillan.

Williams, I. N., Lu, Y., Kueppers, L. M., Riley, W. J., Biraud, S. C., Bagley, J. E., & Torn, M. S. (2016). Land-atmosphere coupling and climate prediction over the U.S. Southern Great Plains. *Journal of Geophysical Research: Atmospheres*, *121*(20), 12,125–12,144. doi: 10.1002/2016JD025223

Wolf, A., Anderegg, W. R. L., & Pacala, S. W. (2016, November). Optimal stomatal behavior with competition for water and risk of hydraulic impairment. *Proceedings of the National Academy of Sciences*, *113*(46), E7222-E7230. doi: 10.1073/pnas.1615144113

Wu, J., Guan, K., Hayek, M., Restrepo-Coupe, N., Wiedemann, K. T., Xu, X., ... Saleska, S. R. (2017). Partitioning controls on Amazon forest photosynthesis between environmental and biotic factors at hourly to interannual timescales. *Global Change Biology*, *23*(3), 1240–1257. doi: 10.1111/gcb.13509

Xu, C., Christoffersen, B., Robbins, Z., Knox, R., Fisher, R. A., Chitra-Tarak, R., ... McDowell, N. (2023, November). Quantification of hydraulic trait control on plant hydrodynamics and risk of hydraulic failure within a demographic structured vegetation model in a tropical forest (FATES–HYDRO V1.0). *Geoscientific Model Development*, *16*(21), 6267–6283. doi: 10.5194/gmd-16-6267-2023

Xu, X., Medvigy, D., Powers, J. S., Becknell, J. M., & Guan, K. (2016). Diversity in plant hydraulic traits explains seasonal and inter-annual variations of vegetation dynamics in seasonally dry tropical forests. *New Phytologist*, *212*(1), 80–95. doi: 10.1111/nph.14009

Yamazaki, K., Sexton, D. M. H., Rostron, J. W., McSweeney, C. F., Murphy, J. M., & Harris, G. R. (2021, June). A perturbed parameter ensemble of HadGEM3-GC3.05 coupled model projections: Part 2: Global performance and future changes. *Climate Dynamics*, *56*(11), 3437–3471. doi: 10.1007/s00382-020-05608-5

Yao, Y., Joetzjer, E., Ciais, P., Viovy, N., Cresto Aleina, F., Chave, J., ... Luyssaert, S. (2022, October). Forest fluxes and mortality response to drought: Model description (ORCHIDEE-CAN-NHA r7236) and evaluation at the Caxiuanã drought experiment. *Geoscientific Model Development*, *15*(20), 7809–7833. doi: 10.5194/gmd-15-7809-2022

Yepez, E. A., & Garatuza, J. (2021, January). *AmeriFlux FLUXNET-1F MX-Tes Tesopaco, secondary tropical dry forest* (Tech. Rep.). Lawrence Berkeley National Lab. (LBNL), Berkeley, CA (United States). AmeriFlux; Instituto Tecnologico de Sonora. doi: 10.17190/AMF/1832156

Zaehle, S., Sitch, S., Smith, B., & Hatterman, F. (2005). Effects of parameter uncertainties on the modeling of terrestrial biosphere dynamics. *Global Biogeochemical Cycles*, *19*(3). doi: 10.1029/2004GB002395

Zarakas, C. M., Swann, A. L. S., Laguë, M. M., Armour, K. C., & Randerson, J. T. (2020, October). Plant physiology increases the magnitude and spread of the transient climate response to CO2 in CMIP6 Earth system models. *Journal of Climate*, *33*(19), 8561–8578. doi: 10.1175/JCLI-D-20-0078.1

Zhang, C., Xie, S., Klein, S. A., Ma, H.-y., Tang, S., Van Weverberg, K., ... Petch, J. (2018). CAUSES: Diagnosis of the summertime warm bias in CMIP5 climate models at the ARM Southern Great Plains site. *Journal of Geophysical Research: Atmospheres*, *123*(6), 2968–2992. doi: 10.1002/2017JD027200

Zheng, Y., Kumar, A., & Niyogi, D. (2015, May). Impacts of land–atmosphere coupling on regional rainfall and convection. *Climate Dynamics*, *44*(9), 2383–2409. doi: 10.1007/s00382-014-2442-8

Appendix A

SUPPLEMENT FOR CHAPTER 2

CMIP6 Earth system model	Land Model	Includes Plant Hydraulics?	Includes Photosynthetic Temperature Acclimation?	Plant Hydraulics Implementation	Photosynthetic Temperature Acclimation Implementation
CESM2	CLM5.0	Yes	Yes	Kennedy et al. (2019)	Lombardozzi et al. (2015)[1]
NorESM2-LM	CLM5.0	Yes	Yes	Kennedy et al. (2019)	Lombardozzi et al. (2015)[1]
GFDL-ESM4	GFDL-LM4.1	Yes	No*	Wolf et al. (2016)	Smith et al. (2016)
IPSL-CM6A-LR	ORCHIDEE (v2.0, Water/Carbon/Energy)	No*	Yes	Naudts et al. (2015), Yao et al. (2022)	Vuichard et al. (2019)[1]
CMCC-ESM2	CLM4.5 (BGC mode)	No	Yes	NA	
BCC-CSM2-MR	BCC_AVIM2	No	Yes	NA	
ACCESS-ESM1-5	CABLE2.4	No*	No*	De Kauwe et al. (2020, 2022)	Knauer et al. (2023)[2]
UKESM1-0-LL	JULES-ES-1.0	No*	No*	Eller et al. (2018, 2020)	Mercado et al. (2018)[1], Oliver et al. (2022)[1]
GISS-E2-1-G	GISS LSM	No*	No		NA
E3SM-1-1	ELM (v1.1)	No*	No		NA
EC-Earth-CC	HTESSEL and LPJ-GUESS v4	No*	No	Hickler et al. (2006)	NA
MPI-ESM1-2-LR	JSBACH3.20	No	No*	NA	Goll (2013)[1]
MIROC-ES2L	MATSIRO6.0+VISIT-e ver.1.0	No	No	NA	NA
CanESM5	CLASS3.6/CTEM1.2	No	No	NA	NA
CNRM-ESM2-1	Surfex 8.0c	No	No	NA	NA
MRI-ESM2-0	HAL 1.0	No	No	NA	NA

* There are versions of the land model that include this process (e.g. for specific scientific projects) or model implementation of this process is currently being developed, but these processes are not active in the land model codebase that was used in CMIP6 coupled Earth system model simulations.
[1] These models implement the Kattge and Knorr (2007) temperature acclimation scheme
[2] These models implement the Kumarathunge et al.(2019) temperature acclimation scheme

Table A.1: Processes included in CMIP6 land models. The table includes all Earth system models participating in the Coupled Climate–Carbon Cycle Model Intercomparison Project (C4MIP; Jones et al., 2016).

FATES parameter	FATES parameter description	Default Value	Low Perturbation	Median Perturbation	High Perturbation	Reference for parameter ranges
fates_hydr_kmax_node	maximum xylem conductivity per unit conducting xylem area [kg/MPa/m/s]	3	0.105	3.43	16.038	Christofferson et al. (2021)
fates_leaf_stomatal_slope_ballberry	stomatal slope parameter for Ball-Berry model [unitless]	8	6.98	10.62	18.07	Lin et al. (2015)
fates_hydr_p50_node*	xylem water potential at 50% loss of conductivity	-2.25	-6.3	-1.79	-0.18	Christofferson et al. (2021)
fates_leaf_vcmax25top	maximum carboxylation rate of Rub. at 25C, canopy top	60	7.78	45	60.1	Albert et al. (2018)

Table A.2: Parameter perturbations included in the small perturbed parameter ensemble. For each parameter (each row), three one-at-a-time parameter perturbation experiments were simulated: one low-end simulation, one median, and one high-end simulation, where the low-end, median, and high-end parameter perturbation values were determined based on literature review.

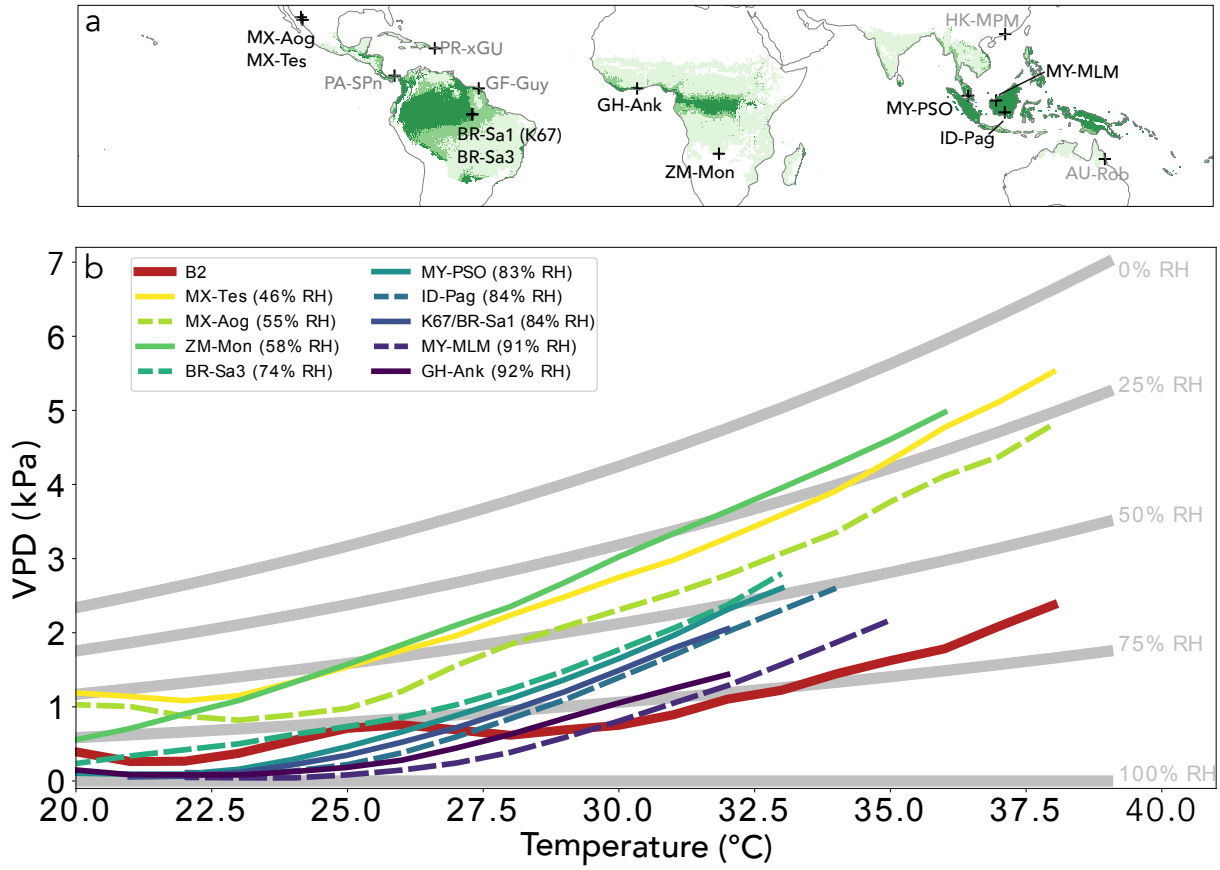

Figure A.1: Temperature-VPD regimes of study sites, compared to other tropical forest sites. (a) Location of tropical forest sites used in this study, along with other tropical forest sites in the FLUXNET and/or Ameriflux networks which have a mean annual temperature > 20°C and are classified as deciduous or evergreen broadleaf tropical forests. Colors indicate the extent of tropical Köppen-Geiger climate classifications (Köppen, 1936; Peel et al., 2007) as calculated from ERA5 Reanalysis (European Centre for Medium-Range Weather Forecasts, 2019). (b) Temperature-VPD relationships for tropical forest sites, based on FLUXNET and/or Ameriflux meteorological data. Curves are calculated by binning VPD by air temperature in 1°C bins, and calculating the mean VPD for each temperature bin. Lines are colored to indicate natural forest sites' average relative humidity. Gray background curves indicate the temperature-VPD relationship for a given relative humidity level.

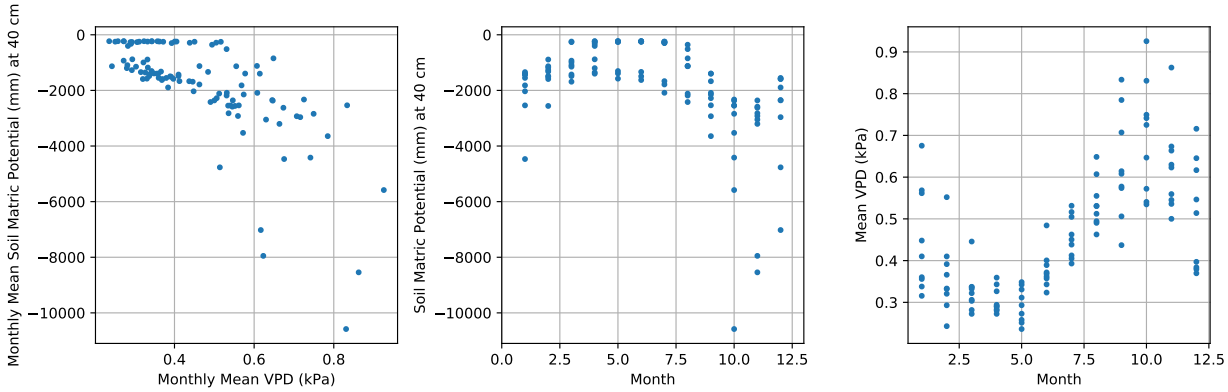

Figure A.2: Variation in VPD and soil moisture on monthly timescales. (a) Relationship between monthly mean VPD at 2m and monthly mean soil matric potential (SMP) at 40 cm depth (note that more negative SMP corresponds to drier soils). Seasonal cycles of (b) SMP and (c) VPD.

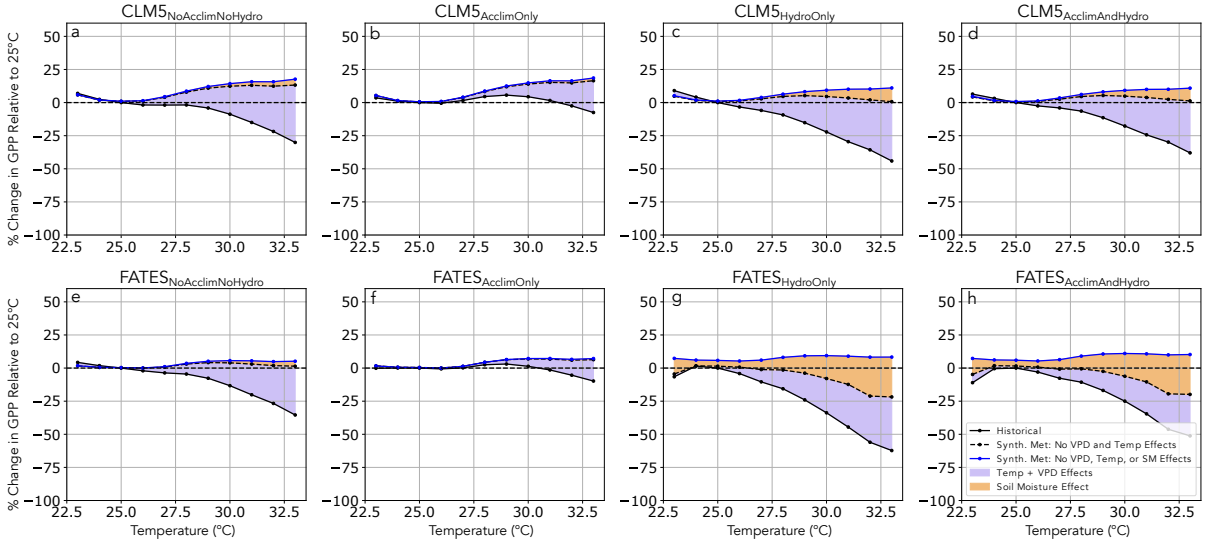

Figure A.3: Soil moisture influences on the apparent GPP response to temperature at K67 for different configurations of CLM5 (a-d) and FATES (e-h). Shaded areas show how much the modeled apparent GPP response to temperature (black line) are due to the combination of temperature and VPD effects (purple shaded area) and soil moisture effects (orange area). These meteorological effects are calculated from synthetic meteorology simulations where temperature and VPD are held constant (dashed black line) and where precipitation is held constant at 0.005 mm/s to fully saturate the soil at all points in time (blue line).

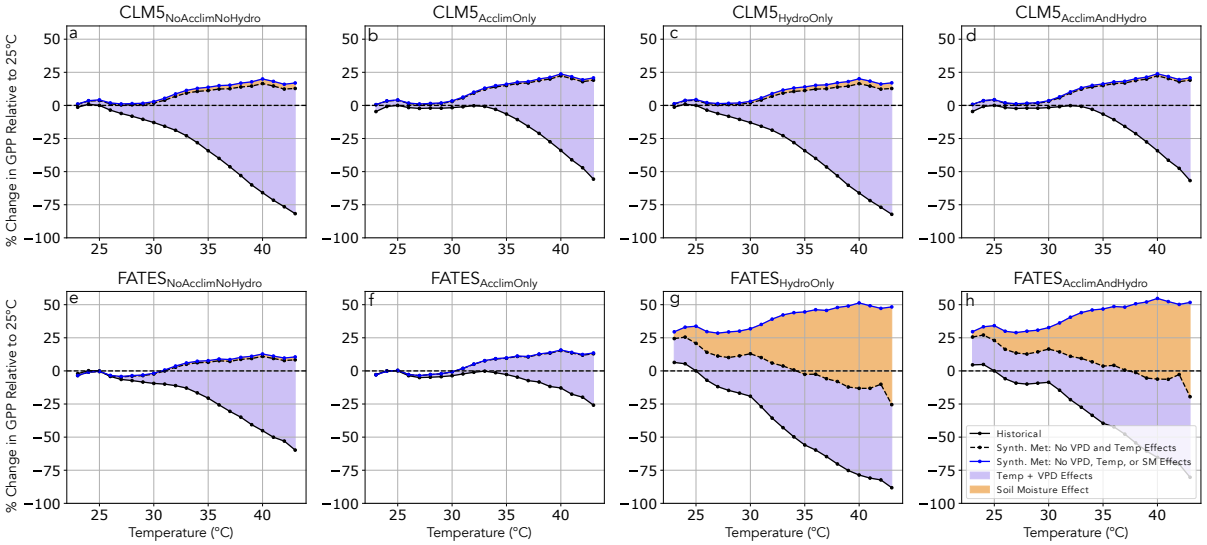

Figure A.4: Soil moisture influences on the apparent GPP response to temperature at Biosphere 2. As in Figure A.3, but at Biosphere 2.

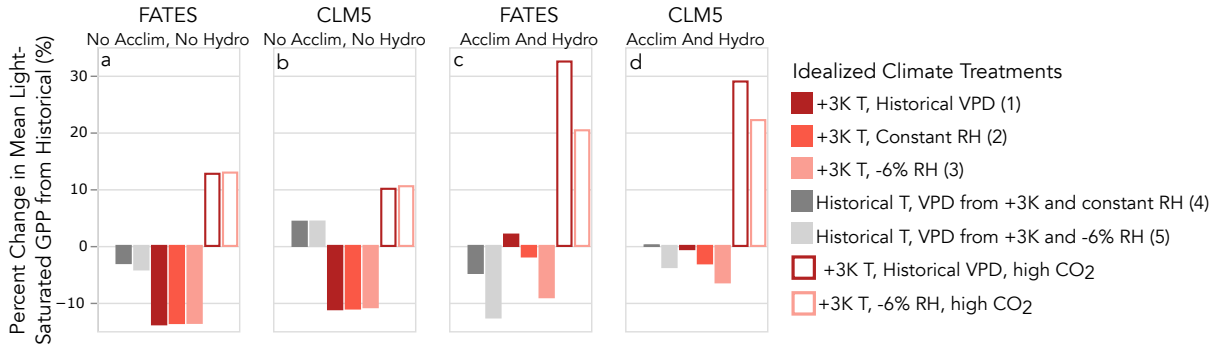

Figure A.5: Mean light-saturated GPP responses at K67 to idealized climate treatments for different model configurations: (a) FATES without temperature acclimation or plant hydraulics, (b) CLM5 without temperature acclimation or plant hydraulics, (c) FATES with active temperature acclimation and plant hydraulics, and (d) CLM5 with active temperature acclimation and plant hydraulics. Solid bars indicate the mean GPP change when the atmospheric CO_2 concentration is held constant at historical levels, and empty bars indicate the change when atmospheric CO_2 concentration is elevated to 560 ppm.

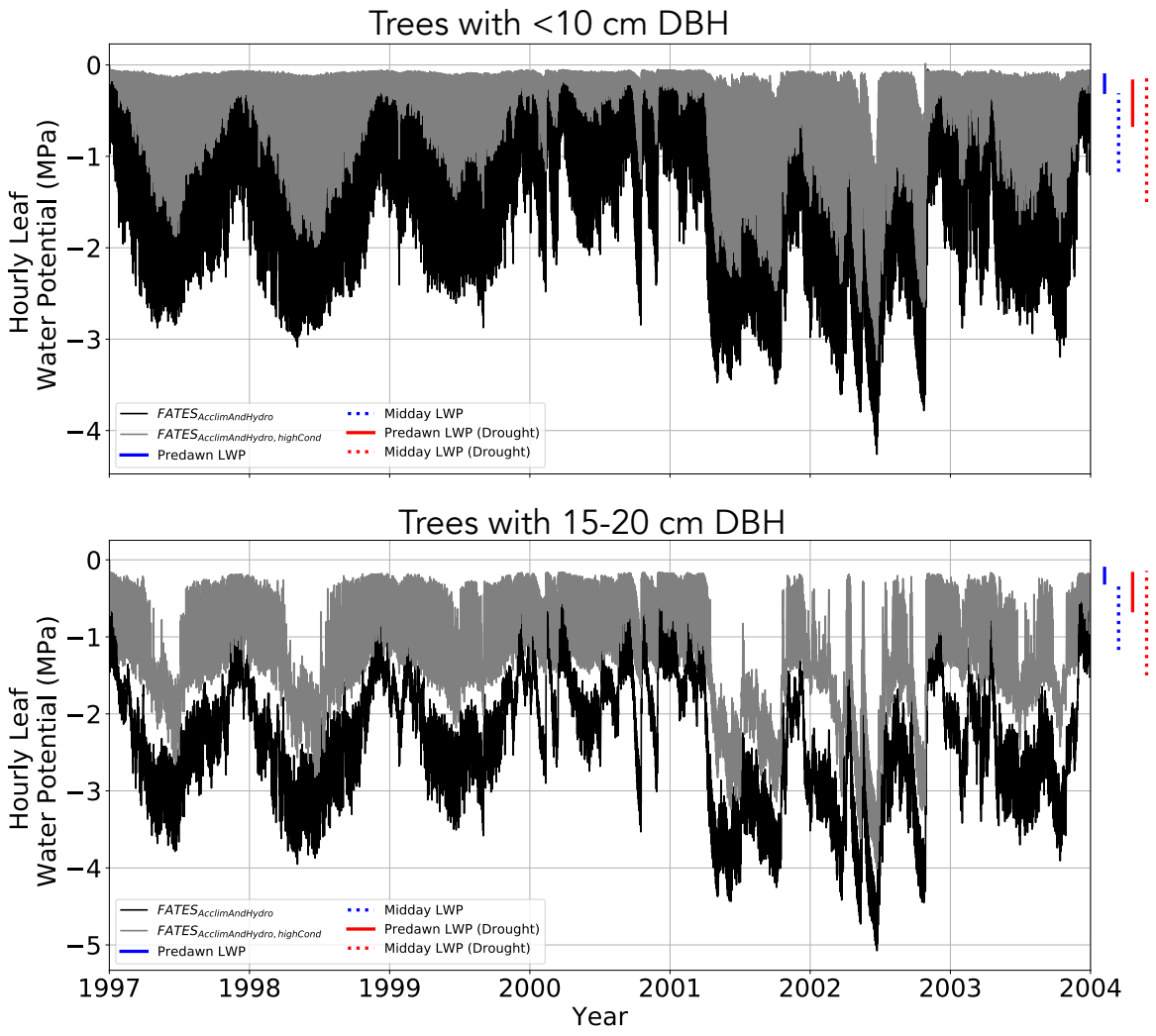

Figure A.6: Modeled leaf water potential for FATES$_{\text{AcclimAndHydro}}$, with default parameters (black) compared to increased maximum hydraulic conductivity (gray). Bars to the right of the plots indicate the range of leaf water potential observations collected in 2002 at Biosphere 2 (Pegoraro et al., 2006) in normal conditions (blue) and during a drought experiment (red).

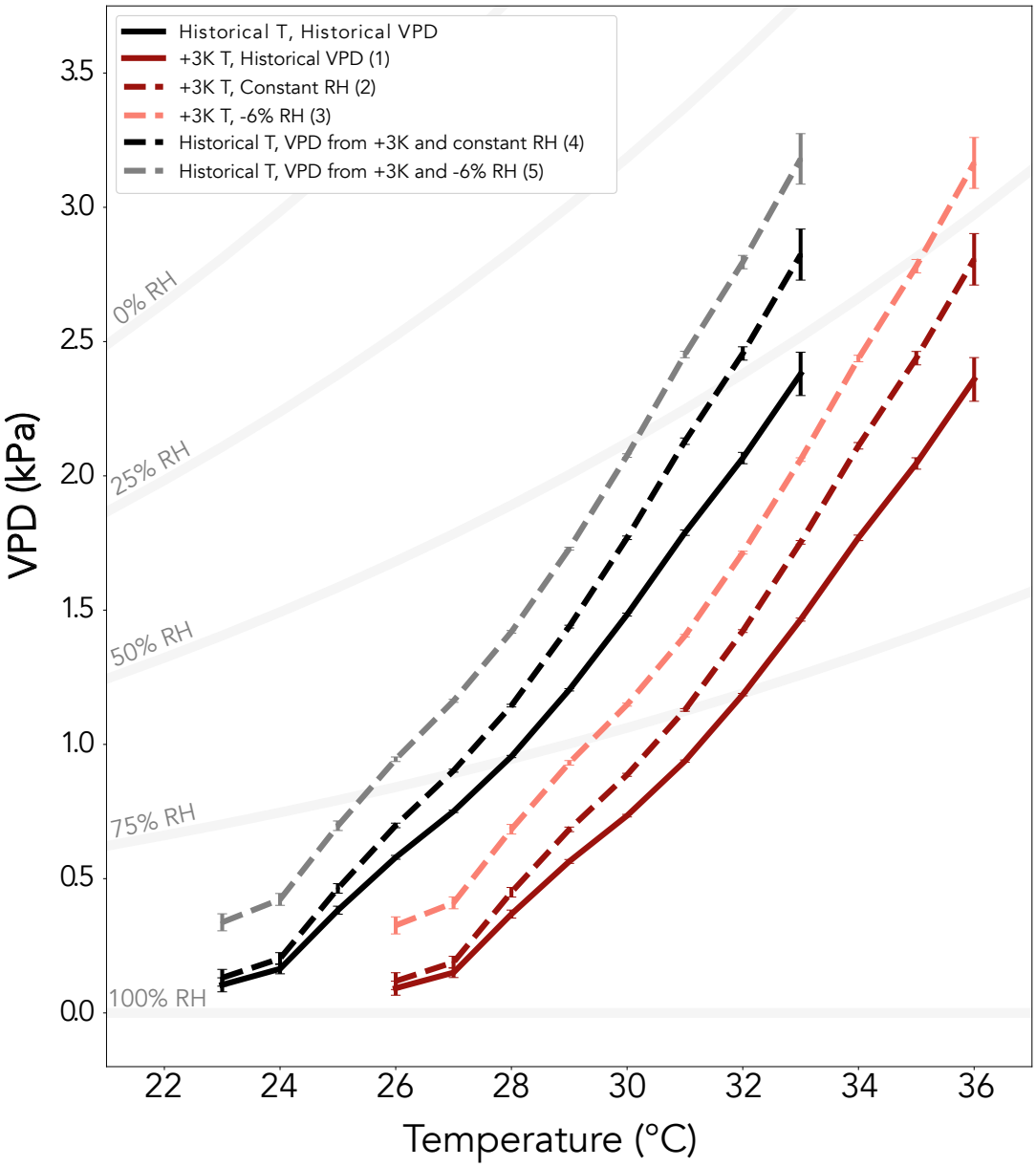

Figure A.7: Idealized climate treatments in temperature-VPD space. Gray background curves indicate the temperature-VPD relationship for a given relative humidity level. Numbers in the legend correspond to the idealized climate treatment numbers in the main text.

Appendix B

SUPPLEMENT FOR CHAPTER 3

B.1 Calculating the pattern of warming due to a doubling of CO_2

We calculated the pattern of warming due to a doubling of CO_2 from two concentration-driven CESM2 simulations: one forced with preindustrial CO_2 concentrations of 284.7 ppm (1xCO_2) and one forced with a doubling of preindustrial CO_2, 569.4 ppm (2xCO_2). We ran simulations with an active land and atmosphere, and a slab ocean. We ran simulations for 120 years, and discarded the first 60 years as spin up. These CESM simulations were run using the `cesm_2_3_beta03` tag and `branch_tags/PPE.n08_ctsm5.1.dev030` tag for CTSM (results are presented in Figure 3.2c). Doubling CO_2 drove a 5.2°C global mean temperature increase (6.5°C global mean land temperature increase), consistent with CESM2's documented high equilibrium climate sensitivity (Gettelman et al. 2019).

B.2 Disentangling drivers of land temperature and precipitation changes

We used multiple linear regression to disentangle the extent to which land precipitation (P) and temperature (T_s) changes across our coupled PPE are driven by three emergent land surface properties: albedo (α), evaporative fraction (EF), and a measure of aerodynamic coupling (r_a). Results are presented in Figure 3.4. First, we diagnosed α, EF, and r_a for each ensemble member of land-only PPE at each grid cell using monthly model output. We calculated r_a by inverting the equation for sensible heat flux. We then use these derived changes in land-only α, EF, r_a as predictors in a multiple linear regression to predict coupled T_s and P change at each point for each month. We used predictors from the land-only rather than the coupled PPE in order to remove the feedback between climate and land surface properties. In the coupled PPE, changes in land surface properties are

due to both land parameter uncertainty and land responses to climate changes (e.g., precipitation changes can influence evaporative fraction), but changes in land surface properties in the land-only PPE isolate the influence of land parameter uncertainty on land surface fluxes. Because this grid cell level analysis does not account for remote or global-scale impacts of parameter perturbations, we also report results from regressions conducted using global averages. We do not perform regressions on global average land precipitation changes because the sign of precipitation changes are more regionally variable.

We calculated the emergent changes in r_s and r_a by inverting the equations for sensible heat flux (S) and latent heat flux (L):

$$S = (\rho C_p(T_s - T_a))/r_a \tag{B.1}$$

$$L = (\rho\lambda(q^*(T_s) - q_a))/(r_a + r_s) \tag{B.2}$$

where ρ is the air density at the lowest atmospheric level, T_a is the air temperature at the lowest atmospheric level, q_a is the specific humidity at the lowest atmospheric level, T_s is land surface skin temperature, and $q^*(T_s)$is the saturated specific humidity at T_s. C_p and λ are the specific heat capacity of dry air and the latent heat of vaporization, respectively. We verified our derived changes in α, r_s, and r_a by demonstrating that they yielded accurate reconstructions of temperature changes in the offline land-only PPE using the two-resistance method (TRM; Rigden and Li 2017). The TRM is ill-suited for attributing quantifying how much the changes in α, r_s, and r_a drive coupled temperature changes to changes in α, r_s, and r_a because it combines all temperature changes from atmospheric feedbacks into one term (due to change in the near-surface air temperature T_a), and cannot distinguish the extent to which T_a changes are driven by changes in α, r_s, and r_a.

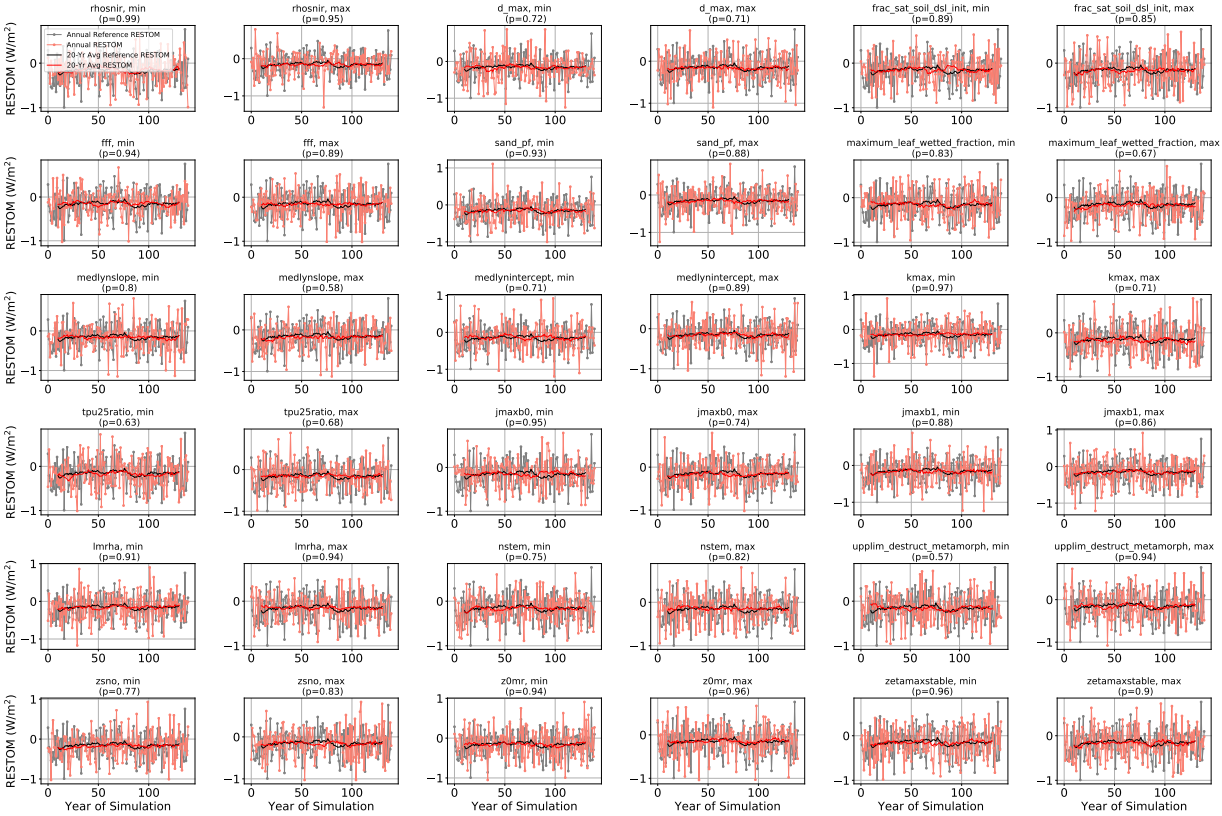

Figure B.1: Time series of the net radiative flux at the top of the model (RESTOM), as calculated from the net solar flux at top of model (FSNT) minus the net longwave flux at top of model (FLNT). The average RESTOM for the last 100 years of the reference case is -0.157 W/m^2. RESTOM varied minimally across the ensemble (σ=0.010 W/m^2), and was not statistically significantly different from the reference case for any ensemble member. We tested whether simulations were different from the reference case using two-tailed Student's t-test on the time series of annual mean RESTOM.

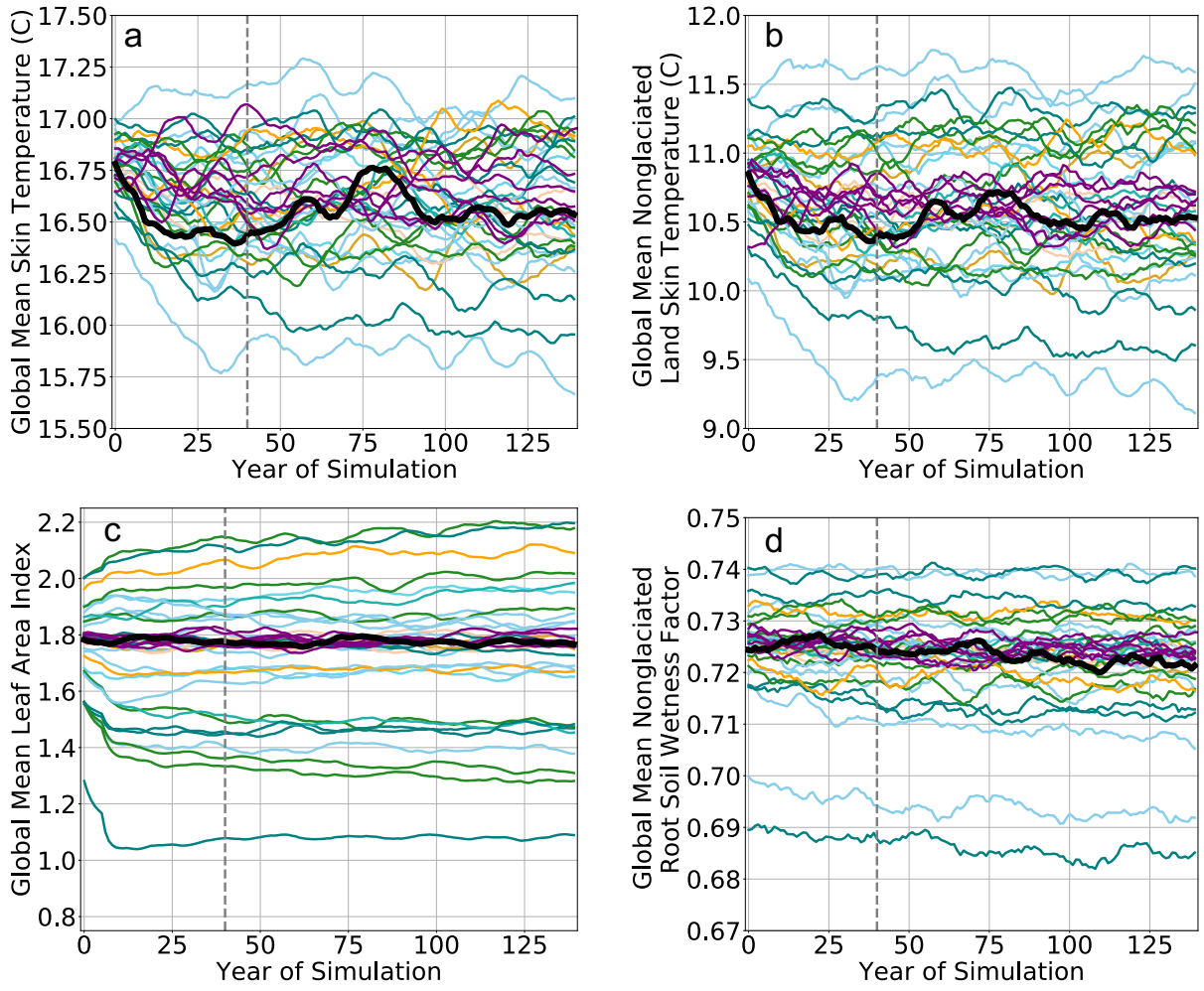

Figure B.2: Time series of annual mean (a) global temperature, (b) global land temperature, (c) global leaf area index, and (d) global root zone soil wetness factor (where 1 indicates no water stress) for each ensemble member of the PPE. The black line indicates the reference simulation, and ensemble members are colored by parameter category as in Figure 3.1. The first 40 years of each simulation (denoted by dashed vertical line) were discarded as spin up. Data in panels (c) and (d) are averaged over non-glaciated land only.

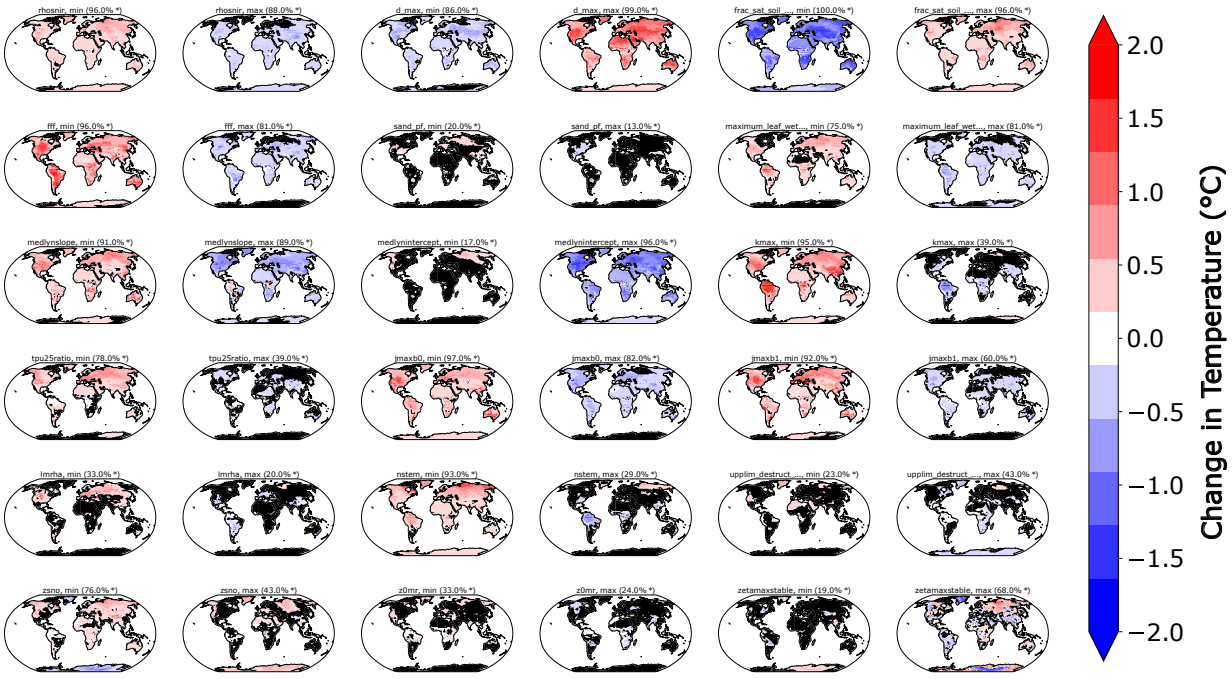

Figure B.3: Maps of annual mean coupled land temperature changes for each ensemble member, compared to the reference case with default parameterizations. For each grid cell, we performed a two-tailed Student's t-test to test whether the ensemble member mean (standard deviation calculated from the distribution from interannual variability in the ensemble member mean) was different from the default mean (standard deviation calculated from the distribution from interannual variability in the default mean). Hatching (black) indicates regions where the temperature change was not significant at the 0.05 significance level. The percentage of land with statistically significant temperature changes is shown in parentheses, and * indicates field significance. We test for field significance using Walker's test.

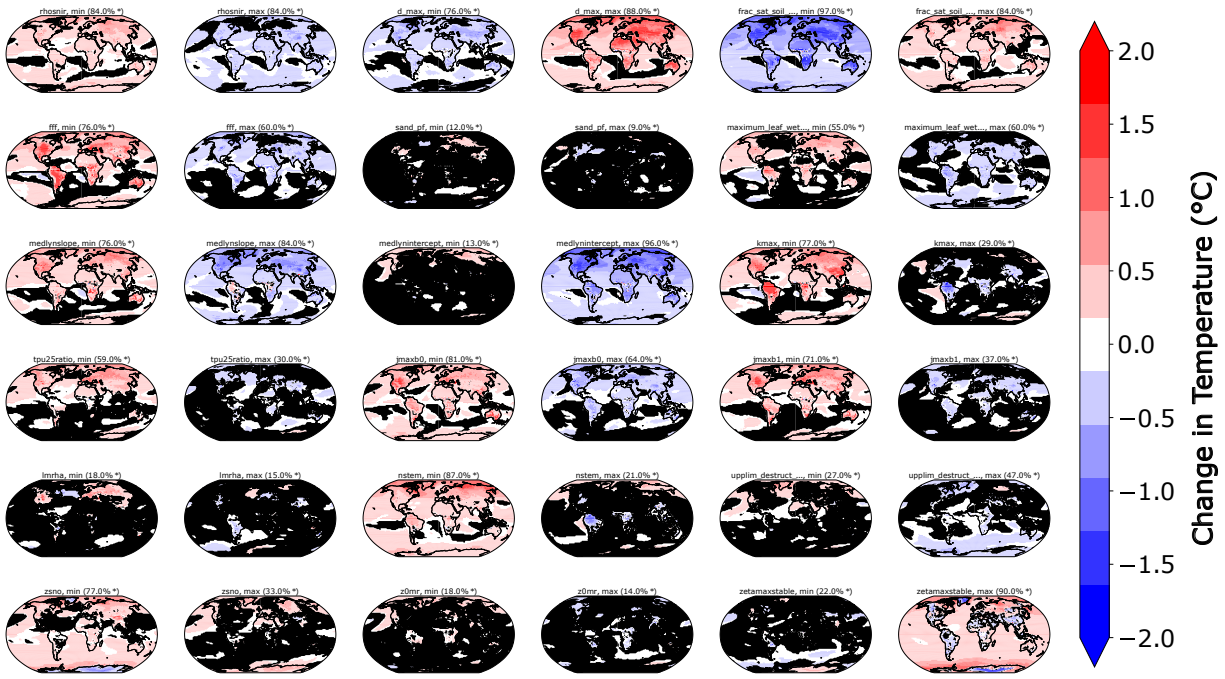

Figure B.4: Maps of annual mean coupled temperature changes for each ensemble member, including both land and ocean. Hatching and significance testing is as in Figure B.3, but the title indicates the total percentage of the Earth surface (including land and ocean) with statistically significant temperature changes.

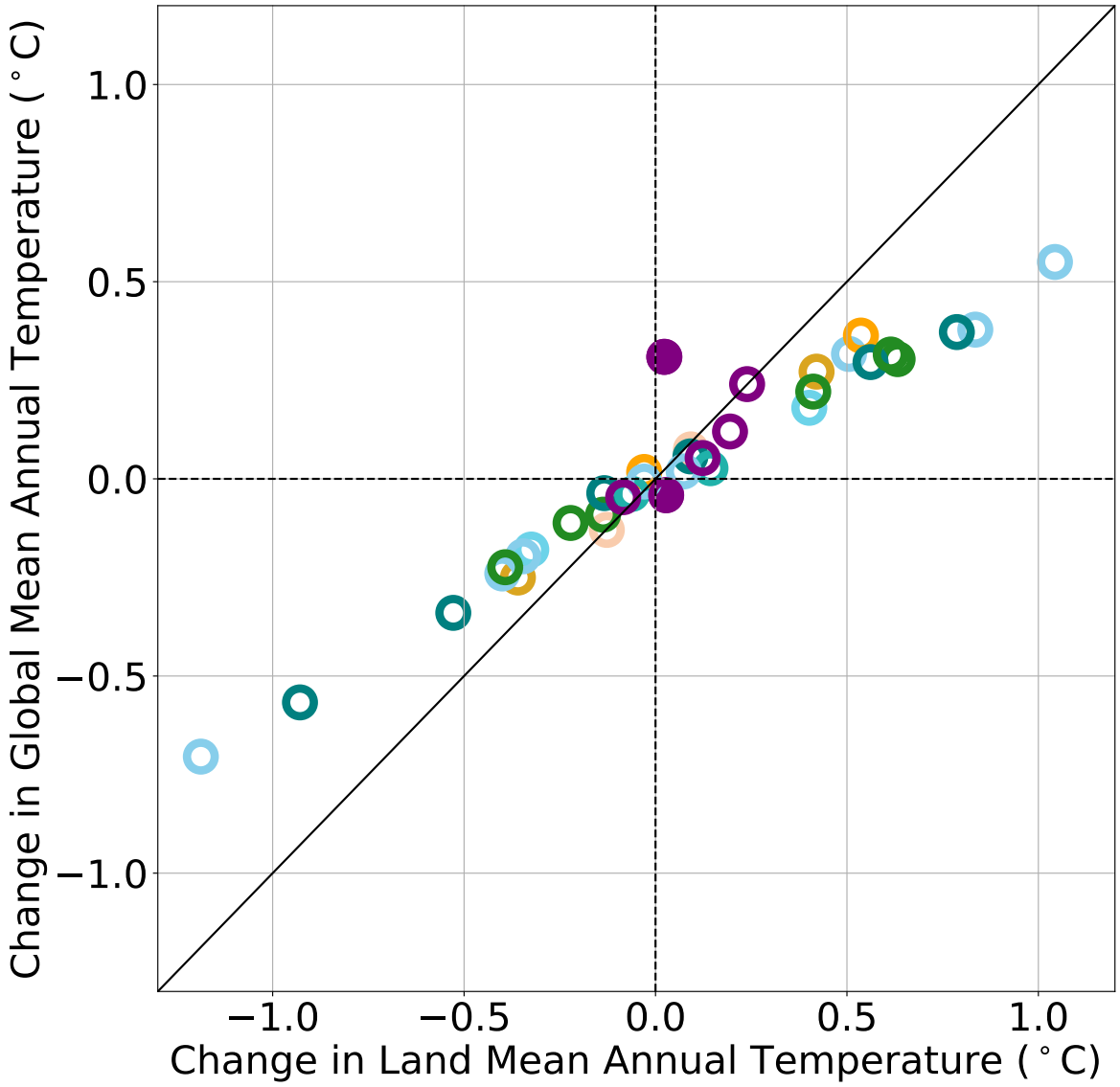

Figure B.5: Correlation between the change in annual mean land temperature and annual mean global temperature (including both land and ocean). Colors indicate parameter category as in Figure 3.1. Because the parameter `zetamaxstable` is an outlier in our PPE, it is denoted as the filled purple point.

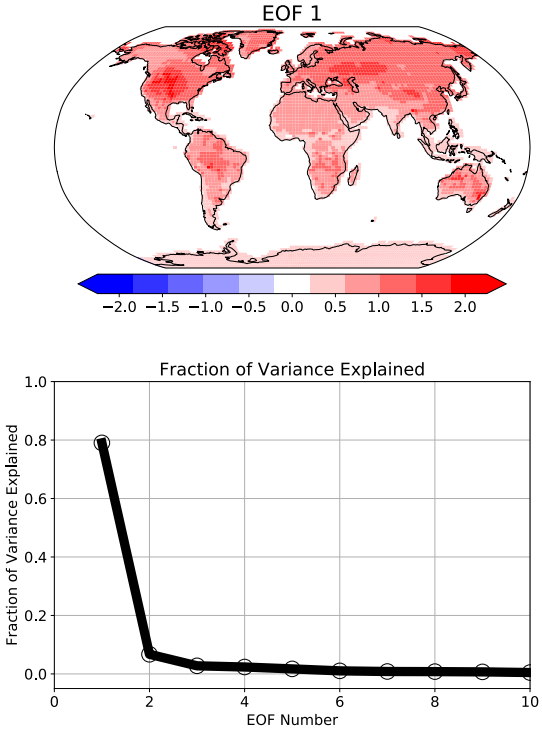

Figure B.6: EOF analysis of changes in land surface temperature across the PPE.

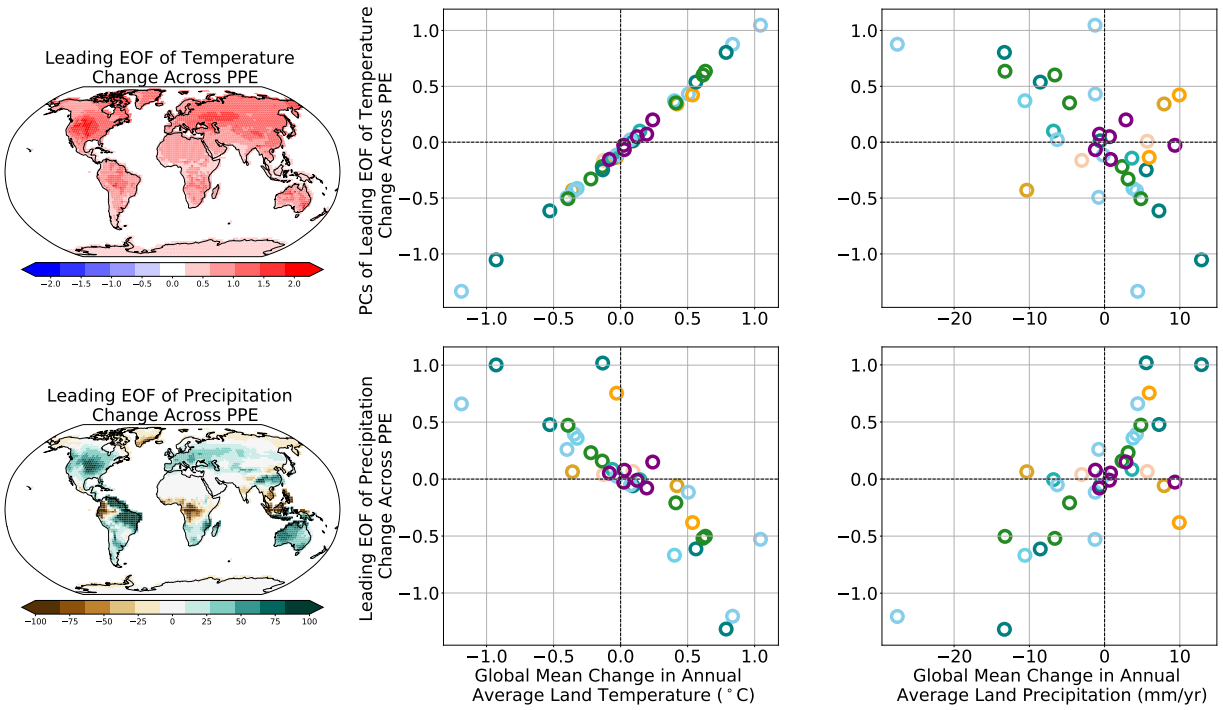

Figure B.7: Correlation between leading EOFs of annual average land and temperature changes and global mean annual average land temperature and precipitation changes across the PPE. Ensemble members are colored by parameter category, as in Figure 3.1.

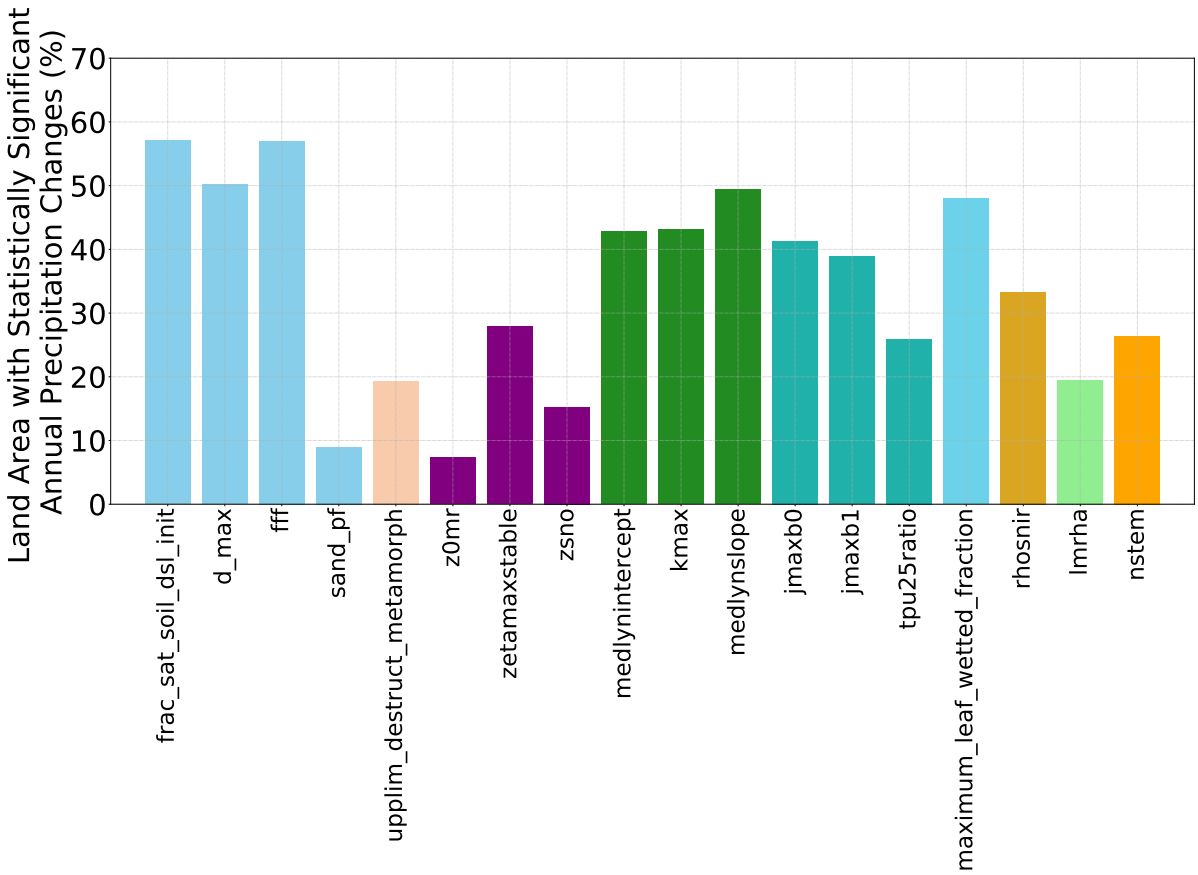

Figure B.8: Percentage of global land area that experiences statistically significant changes in annual mean precipitation due to perturbations in each parameter. For each land grid cell, we performed a two-tailed Student's t-test to test whether the parameter maximum simulation was different from the parameter minimum simulation.

Figure B.9: Maps of annual mean land precipitation changes for each ensemble member, compared to the reference case with default parameterizations. The percentage of land with statistically significant temperature changes are shown in parentheses, and * indicates field significance. For each grid cell, we performed a two-tailed Student's t-test to test whether the ensemble member mean (standard deviation calculated from the distribution from interannual variability in the ensemble member mean) was different from the default mean (standard deviation calculated from the distribution from interannual variability in the default mean). Hatching (black) indicates regions where the precipitation change was not significant at the 0.05 significance level. We test for field significance using Walker's test.

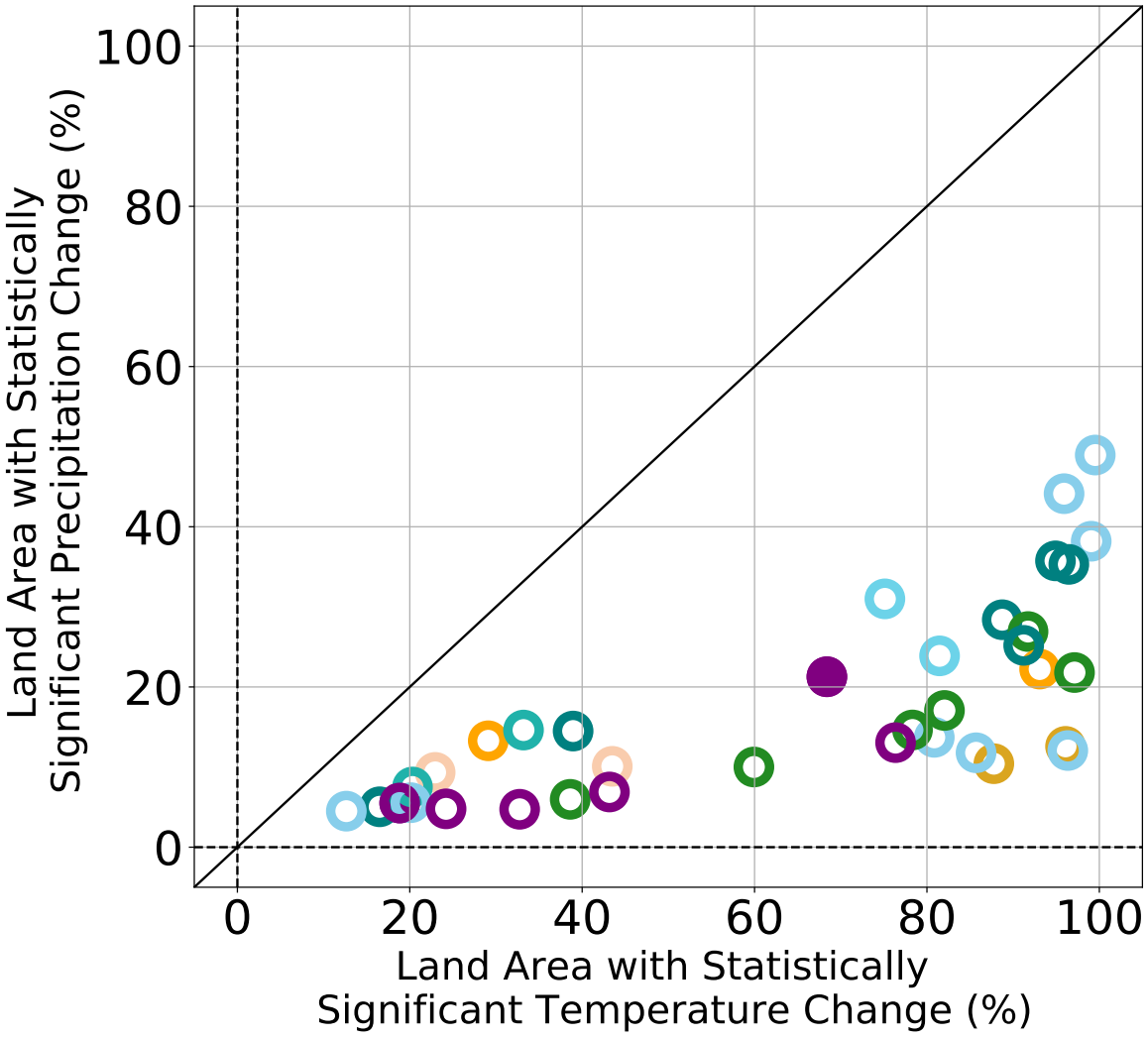

Figure B.10: Percentage of land area with statistically significant temperature vs. precipitation changes for each ensemble member in the PPE. Ensemble members are colored by parameter category, as in Figure 3.1. Zetamaxstable is indicated with a filled circle because it is a frequent outlier.

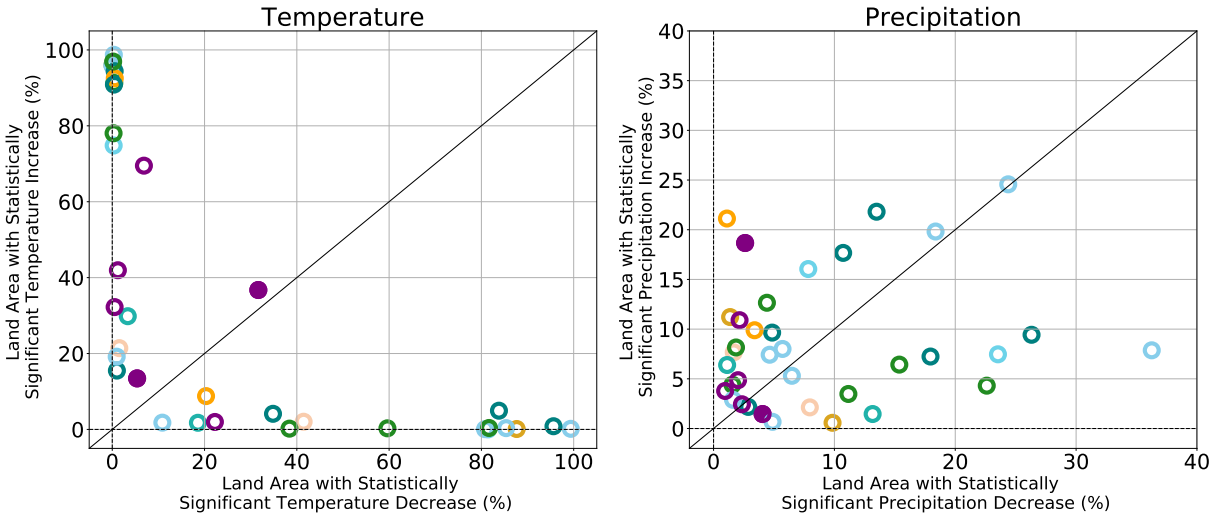

Figure B.11: Sign of change of statistically significant mean climate changes across the PPE. Percent of land area experiencing statistically significant decreases vs. increases in temperature (left) and precipitation (right) for each PPE ensemble member. Ensemble members are colored by parameter category, as in Figure 3.1. We note that one parameter (`zetamaxstable`) drove statistically significant temperature changes of opposite sign across 63% of land area, which canceled each other out in the global mean resulting in a minimal global mean land temperature change (Figure B.3) - this parameter is indicated with a filled circle because it is a frequent outlier.

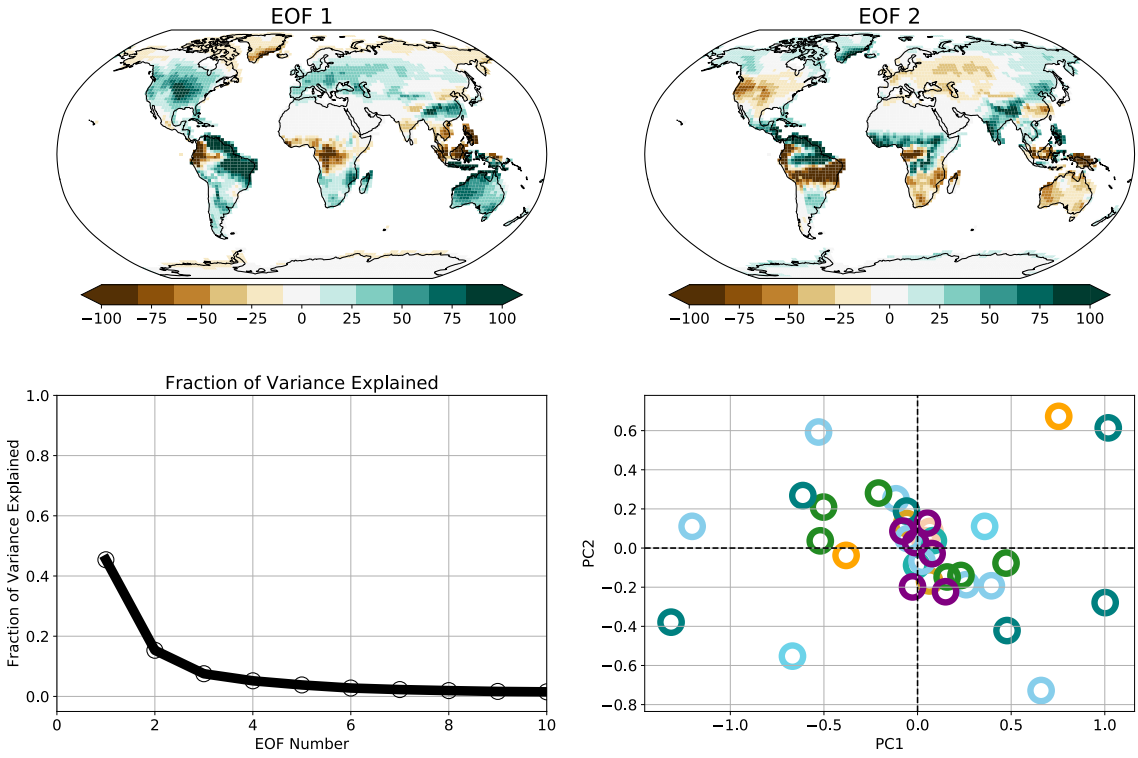

Figure B.12: EOF analysis of changes in land precipitation across the PPE.

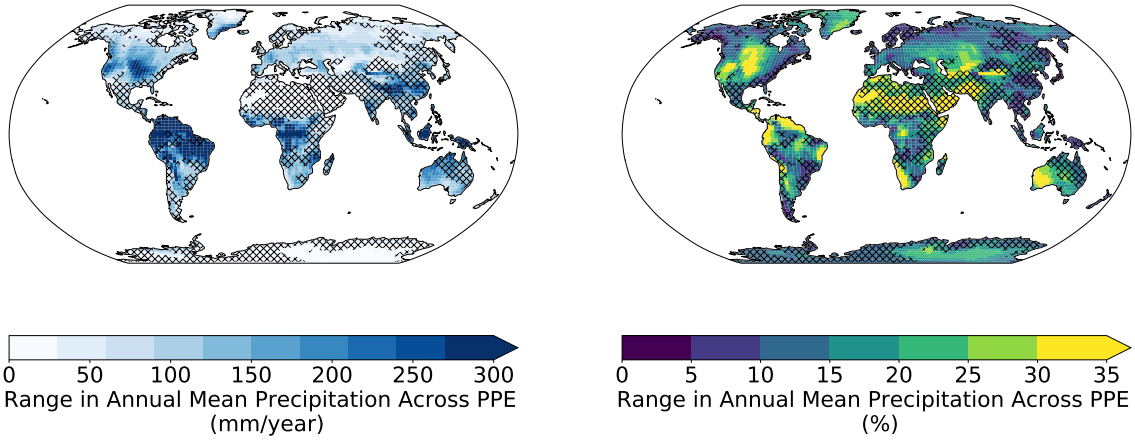

Figure B.13: Range in annual mean precipitation changes across the PPE, on an absolute basis (left) and as a percentage of the default precipitation (right), as repeated from Figure 3.3a. Hatching indicates regions where annual mean precipitation changes were not statistically significant for five or more ensemble members.

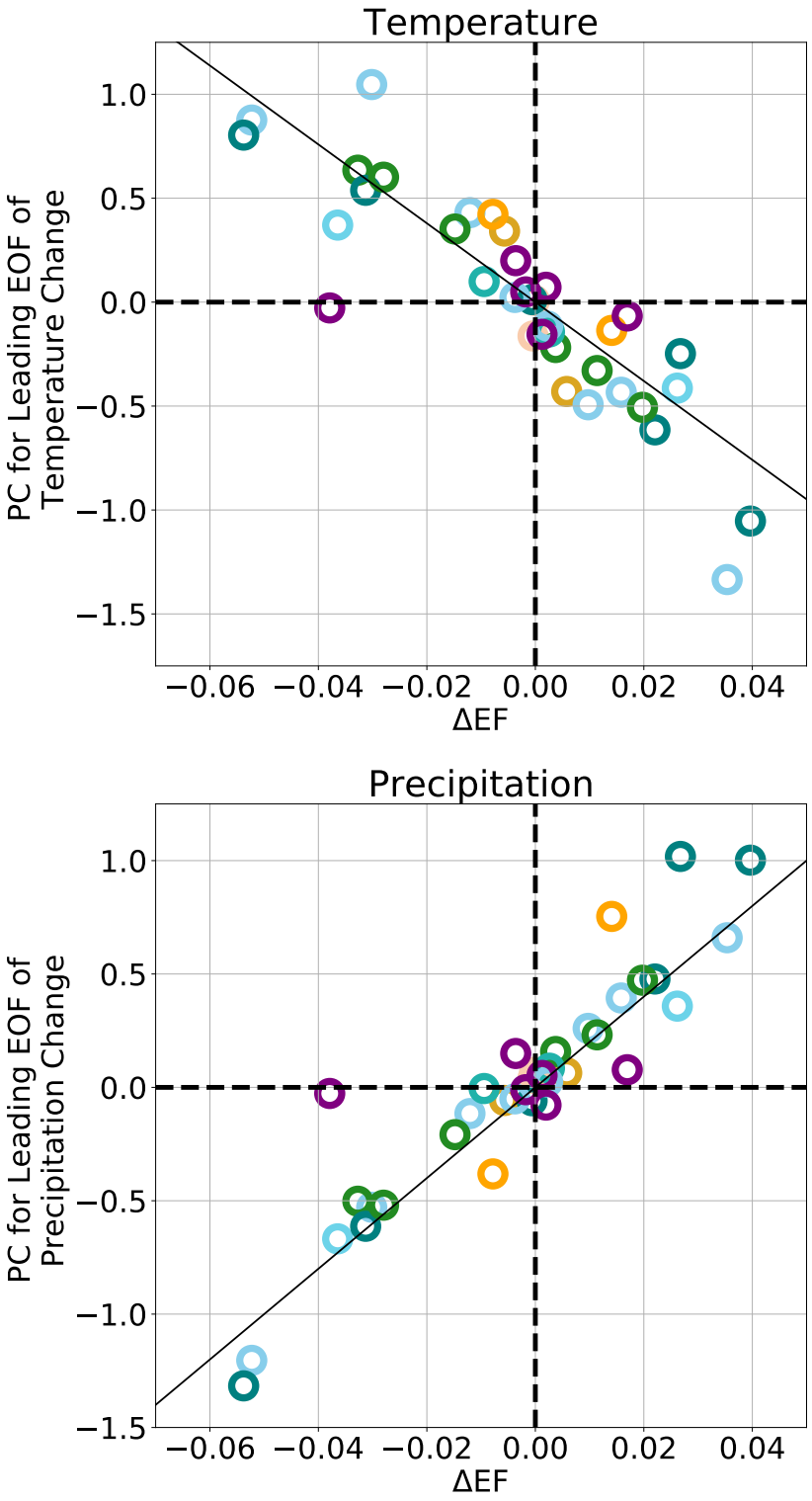

Figure B.14: Correlation between change in global mean evaporative fraction (EF) and first principal components of temperature (top) and precipitation (bottom) change across the PPE. Colors indicate parameter category as in Figure 3.1.

Parameter	Parameter description	Land Component	Parameter Category	Minimum Value	Default Value	Maximum Value	Unit	Range source	Reference
d_max	Parameter specifying the length scale of max dry surface layer thickness	Soil	Soil hydrology	10	15	60	mm	Literature review	Swenson and Lawrence (2014), van de Griend and Owe (1994), Goss and Madliger (2007), Smits et al. (2012)
frac_sat_soil_dsl_init	Fraction of saturated soil for moisture value at which dry surface layer initiates			0.5	0.8	1	unitless	Literature review	Swenson and Lawrence (2014)
fff	Decay factor for fractional saturated area			0.02	0.5	5	m^{-1}	Literature review	Niu et al. (2005), Hou et al. (2012), Fan and Miguez-Macho (2011), Fan et al. (2013)
sand_pf	Perturbation factor (via addition) for percent sand			-20	0	20	percent	Percentage perturbation	
z0mr	Ratio of momentum roughness length to canopy top height	Boundary layer	Boundary layer / Roughness length	0.033 to 0.072[a]	0.055 to 0.120[a]	0.077 to 0.168[a]	unitless	Literature review	Zeng and Wang (2007), Raupach (1994), Shaw and Pereira (1982)
zsno	Momentum roughness length for snow			0.00001	0.0024	0.07	m	Literature review	Chamberlain (1983), Manes et al. (2008), Gromke et al. (2011)
zetamaxstable	Max value zeta ("height" used in Monin-Obukhov theory) can go to under stable conditions.*			0.1	0.5	10	unitless	Expert judgment	
upplim_destruct_metamorph	Upper limit for snow densification through destructive metamorphism		Snow	100	175	250	kg/m^3	Literature review	van Kampenhout et al. (2017)
jmaxb0	Tthe baseline proportion of nitrogen allocated for electron transport	Vegetation	Photosynthesis	0.01	0.0311	0.05	J	Expert judgment	
jmaxb1	Determines the response of electron transport rate to light availability			0.05	0.17	0.25	unitless	Expert judgment	
tpu25ratio	Triose phosphate utilization at 25C (ratio of tpu25/vcmax25)			0.0835	0.167	0.501	unitless	Percentage perturbation	Lombardozzi et al., GRL (2018)
lmrha	Activation energy for leaf maintenance respiration (used in temperature acclimation of leaf maintenance respiration)		Temperature acclimation	-50%	46390	+50%	J/mol	Percentage perturbation	Bernacchi et al. (2001)
medlynslope	Medlyn slope of conductance-photosynthesis relationship		Stomatal conductance and plant water use	0.65 to 3.89[a]	1.62 to 5.79[a]	3.93 to 9.11[a]	μmol H_2O/ μmol CO_2	Literature review	Lin et al. (2015)
medlynintercept	Medlyn intercept of conductance-photosynthesis relationship			1	100	200000	μmol H_2O/(m^2/s)	Literature review	Duursma et al. (2018)
kmax	Plant segment maximum conductance			2.3e-10 to 1.5e-8[a]	1.3e-9 to 4.0e-8[a]	1.9e-9 to 2.3e-7[a]	mm H_2O (transpired)/ mm H_2O (water potential gradient)/sec	Literature review	Bonan et al. (2014), Chuang et al. (2006), Sperry et al. (1998), Sperry and Love (2015), Williams et al (1996), Kennedy et al. (2019)
rhosnir	Near-infrared stem reflectance		Plant optical properties	0.29 to 0.42[a]	0.36 to 0.53[a]	0.43 to 0.64[a]	unitless	Percentage perturbation	Majasalmi and Bright (2019)
maximum_leaf_wetted_fraction	Maximum fraction of leaf that may be wet prior to drip occuringoccurring		Canopy evaporation	0.01	0.05	0.5	unitless	Expert judgment	
nstem	Stem number; number of individuals per meter squared (similar to stocking number). Influences canopy height and biomass heat storage.		Canopy height / biomass heat storage	0.03	0.035 to 100[a]	0.5	number/m^2	Expert judgment	

Table B.1: Land parameters used in this study. [a]Parameter ranges vary depending on the plant functional type.

Quantity
Latent heat flux
Sensible heat flux
Water vapor flux
Zonal momentum flux
Meriodional momentum flux
Emitted longwave radiation
Direct beam visible albedo
Direct beam near-infrared albedo
Diffuse visible albedo
Diffuse near-infrared albedo
Absorbed solar radiation
Radiative temperature
Temperature at 2 meter height
Specific humidity at 2 meter height
Wind speed at 10 meter height
Snow water equivalent
Aerodynamic resistance
Friction velocity
Dust flux
Net ecosystem exchange*

Table B.2: Quantities that the land model passes to the atmosphere in CESM2. Note that net ecosystem exchange does not impact the atmosphere in our experimental design because our experimental design held atmospheric CO_2 concentrations fixed.

Parameters	Global Ranking	Biome Ranking									
		Tropical rain forest	Tropical seasonal forest/savanna	Temperate rain forest	Temperate seasonal forest	Woodland/ shrubland	Temperate grassland/ desert	Subtropical desert	Boreal forest	Tundra	Ice sheet
kmax	1	1	1	-	3	3	4	4	4	4	-
medlynslope	3	-	4	-	1	5		5	1	1	-
fff	2	-	2	-		1	1	1		2	-
medlynintercept	5	5	3	5	2	-	-	-	2		-
liq_canopy_storage_scalar	4	2	5	-	4	-	-	-	3		-
jmaxb0	-	-	-	4	-	-	-	-	5	3	-
jmaxb1	-	-	-	3	5	2	-	-	-	-	-
tpu25ratio	-	-	-	2	-	4	-	-	-	-	-
sand_pf	-	-	-		-	-	5	3	-	-	-
maximum_leaf_wetted_fraction	-	3	-	1	-	-	-	-	-	-	-
krmax	-	-	-	-	-	-	2	2	-	-	-
snw_rds_refrz	-	-	-	-	-	-	-	-	-	-	3
upplim_destruct_metamorph	-	-	-	-	-	-	-	-	-	-	4
slopebeta	-	-	-	-	-	-	-	-	-	5	-
zetamaxstable	-	-	-	-	-	-	-	-	-	-	1
zsno	-	-	-	-	-	-	-	-	-	-	2
d_max	-	-	-	-	-	-	3	-	-	-	-
psi50	-	4	-	-	-	-	-	-	-	-	-

Table B.3: Example of parameter rankings in terms of their impact on mean latent heat flux, globally and for Whittaker biomes. Rankings are only shown if the parameter was ranked in the top 5. Bolded parameters were included in our PPE.

Metric	CLM5 Variable	Metric Category	Measure	Globally	By Whittaker Biome
Annual Mean					
Mean albedo	Calculated quantity	Albedo and shortwave radiation	Mean	Yes	Yes
Mean absorbed shortwave radiation	FSA		Mean	Yes	Yes
Mean emitted longwave radiation	FIRE	Temperature and longwave radiation	Mean	Yes	Yes
Mean near-surface air temperature	TSA		Mean	Yes	Yes
Mean land skin temperature	TSKIN		Mean	Yes	Yes
Mean latent heat flux	EFLX_LH_TOT	Water and turbulent fluxes	Mean	Yes	Yes
Mean sensible heat flux	FSH		Mean	Yes	Yes
Mean near-surface specific humidity	Q2M		Mean	Yes	Yes
Mean zonal momentum flux	TAUX	Wind and roughness	Mean	Yes	Yes
Mean 10 meter wind speed	U10		Mean	Yes	Yes
LAC Area (DJF)	Calculated quantity*	Land-atmosphere coupling (LAC)	Mean	Yes	No
LAC Area (JJA)	Calculated quantity*		Mean	Yes	No
LAC Area (MAM)	Calculated quantity*		Mean	Yes	No
LAC Area (SON)	Calculated quantity*		Mean	Yes	No
Interannual Variability					
Mean albedo	Calculated quantity*	Albedo and shortwave radiation	IAV	Yes	Yes
Mean absorbed shortwave radiation	FSA		IAV	Yes	Yes
Mean emitted longwave radiation	FIRE	Temperature and longwave radiation	IAV	Yes	Yes
Mean near-surface air temperature	TSA		IAV	Yes	Yes
Mean land skin temperature	TSKIN		IAV	Yes	Yes
Mean latent heat flux	EFLX_LH_TOT	Water and turbulent fluxes	IAV	Yes	Yes
Mean sensible heat flux	FSH		IAV	Yes	Yes
Mean near-surface specific humidity	Q2M		IAV	Yes	Yes
Mean zonal momentum flux	TAUX	Wind and roughness	IAV	Yes	Yes
Mean 10 meter wind speed	U10		IAV	Yes	Yes

Table B.4: Metrics for evaluating parameter impact on land-to-atmosphere fluxes.

Parameters	Global Ranking	Biome Ranking									
		Tropical rain forest	Tropical seasonal forest/savanna	Temperate rain forest	Temperate seasonal forest	Woodland/ shrubland	Temperate grassland/ desert	Subtropical desert	Boreal forest	Tundra	Ice sheet
fff	1	-	1	-	-	1	-	4	-	-	-
zetamaxstable	2	-	-	-	-		4	-	1	1	1
jmaxb0	3	-	-	5	3	-	-	5	3	4	-
kmax	4	1	2	-	2	-	-	-	5	-	-
leafcn	5	-	-	-	5	-	-	-	-	-	-
jmaxb1	-	-	-	2	1	2	-	-	2	-	-
tpu25ratio	-	-	-	1	4	4	-	-	4	-	-
zsno	-	-	-	-	-	-	1	-	-	2	2
clay_pf	-	-	-	-	-	-	3	2	-	-	-
leaf_long	-	4	5	-	-	-			-	-	-
maximum_leaf_wetted_fraction	-	2	-	3	-	-			-	-	-
sand_pf	-	-	-	-	-	-	2	3	-	-	-
d_max	-	-	-	-	-	-	5	-	-	-	-
frac_sat_soil_dsl_init	-	-	3	-	-	-	-	-	-	-	-
FUN_fracfixers	-	-	-	-	-	3	-	-	-	-	-
krmax	-	-	4	-	-	-	-	-	-	-	-
liq_canopy_storage_scalar	-	3	-	-	-	-	-	-	-	-	-
lmrha	-	-	-	-	-	5	-	-	-	-	-
medlynintercept	-	-	-	-	-	-	-	-	-	5	-
medlynslope	-	-	-	-	-	-	-	-	-	3	-
psi50	-	5	-	-	-	-	-	-	-	-	-
snw_rds_refrz	-	-	-	-	-	-	-	-	-	-	4
tpuha	-	-	-	4	-	-	-	-	-	-	-
upplim_destruct_metamorph	-	-	-	-	-	-	-	-	-	-	5
xdrdt	-	-	-	-	-	-	-	-	-	-	3
zlnd	-	-	-	-	-	-	-	1	-	-	-

Table B.5: Rankings of parameters with the largest land surface temperature change in the land-only CLM5-PPE, globally and for Whittaker biomes. Rankings are only shown if the parameter was ranked in the top 5. Bolded parameters were included in our PPE, and parameters relating to soil hydrology, stomatal conductance and plant water use, and canopy evaporation are highlighted.

Appendix C

SUPPLEMENT FOR CHAPTER 4

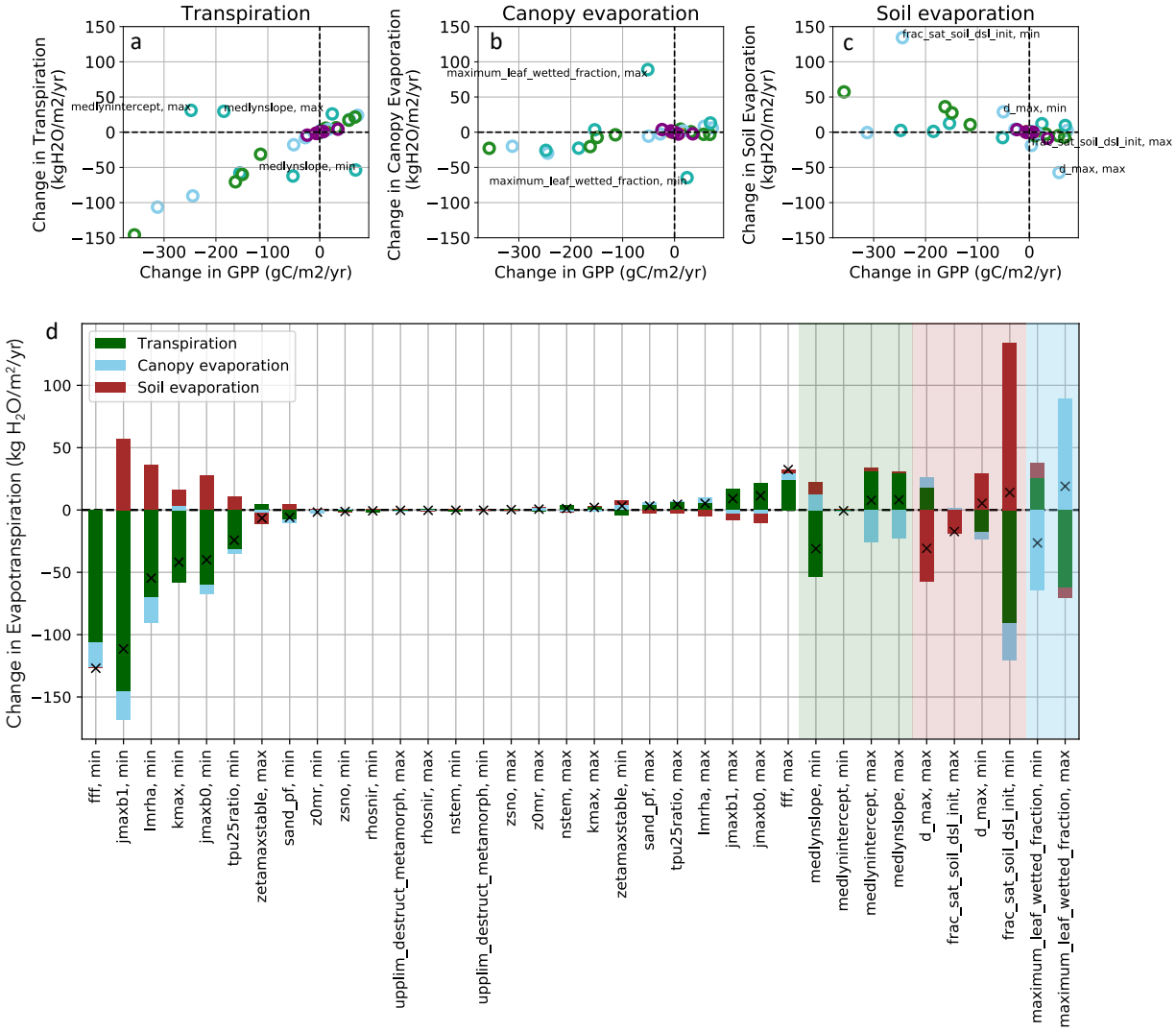

Figure C.1: Relationship between parameter perturbations and different components of the total evapotranspiration flux. Top row shows the relationship between land-only changes in GPP and land-only changes in transpiration (a), canopy evaporation (b), and soil evaporation (c). The bottom row indicates how parameter perturbations impact different components of evapotranspiration. Highlighted parameters on the right indicate stomatal conductance parameter perturbations (green), dry surface layer parameter perturbations (red), and perturbations which directly influence canopy evaporation rates (blue).

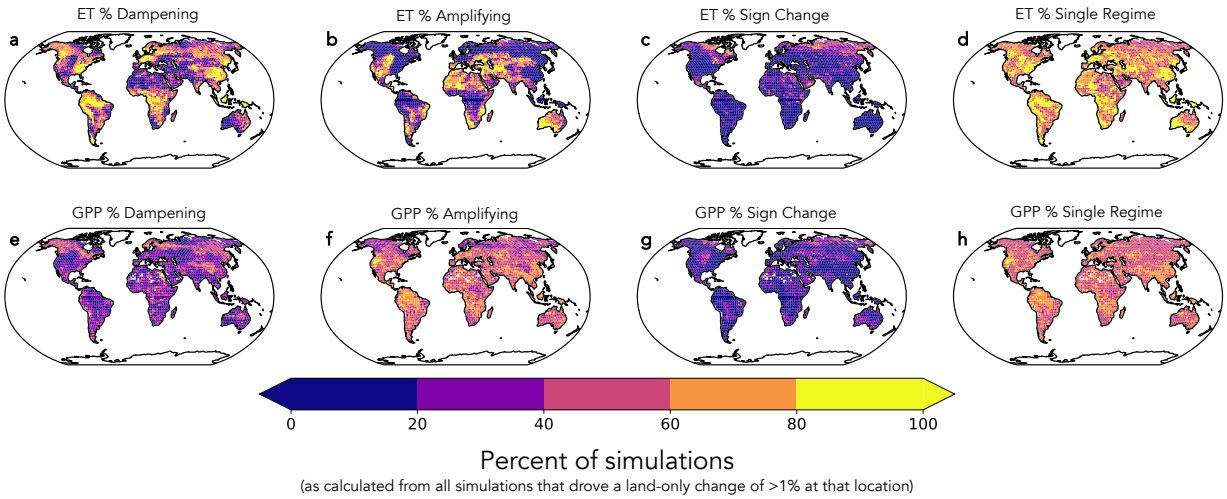

Figure C.2: Consistency in the sign of atmospheric feedbacks across the PPE, for ET (top row) and GPP (bottom row). For ET, there is spatial variation in whether atmospheric feedbacks dampen (a) or amplify (b) ET changes, but for a given location atmospheric feedbacks tend to have a consistent sign of change across the PPE. We define atmospheric feedbacks as being consistent when atmospheric feedbacks drive the same qualitative impact (i.e., dampening, amplifying, or driving a sign change) across more than 80% of the PPE. For ET, about 15% of the land surface experiences consistent dampening feedbacks (a), and 11% of the land experiences consistent amplifying feedbacks (b), leading to consistent signs of change for 26% of the land surface (d). For GPP, there is less spatial variation in whether atmospheric feedbacks dampen or amplify GPP changes, but at a given location atmospheric feedbacks are less consistent (i.e., atmospheric feedbacks are parameter dependent). Essentially none of the land surface experiences consistent dampening feedbacks, and less than 2% of land experiences consistent amplifying feedbacks.